The Hydrologic Function of Small Sinkholes in the Edwards Aquifer Recharge Zone

by

Adrien Lewis Lindley, BA

Thesis

Presented to the Faculty of the Graduate School of

The University of Texas at Austin

in Partial Fulfillment

of the Requirements

for the Degree of

Master of Science in Geological Sciences

The University of Texas at Austin

December 2005

The Hydrologic Function of Small Sinkholes in the Edwards Aquifer Recharge Zone

Approved by
Supervising Committee:

John M. Sharp Jr.

Susan D. Hovorka

Jay L. Banner

Dedication

This Masters Thesis is dedicated to my family. Their love, support, and constant questions have kept me motivated to complete this project.

Acknowledgements

This project was funded by the Texas Commission on Environmental Quality (TCEQ). Fieldwork for this project was greatly facilitated by assistance from Kevin Thuessen, Ph.D. and the City of Austin's Wildland Conservation Division, Lucas Cooksey of the Essex Corporation, George Veni of George Veni and Associates, Dr. Clyde Munster of Texas A&M University and Honey Creek State Natural Area. I thank my co-supervisors Dr. Susan D. Hovorka, Dr. John M. Sharp and my committee member Dr. Jay Banner for their support and guidance. I also thank the following individuals for their technical and logistical assistance: Robert Reedy (BEG), Cynthia Burton (Exploration Instruments), James Donnelly (CRC), and Steven Kelley (PRC).

December 2005

Abstract

The Hydrologic Function of Small Sinkholes in the Edwards Aquifer Recharge Zone

Adrien Lewis Lindley, M.S.

The University of Texas at Austin, 2005

Supervisor: John M. Sharp, Jr.

Thin soils on Cretaceous karst bedrock typify the Edwards aquifer recharge zone in central and south Texas U.S.A. Most of the recharge occurs in major streambeds in this region, but abundant evidence of active karstic dissolution suggests that some of the recharge is occurring in the uplands. The City of San Antonio uses the karstic Edwards aquifer as its main municipal water source, and is undergoing rapid development in the uplands of the aquifer recharge zone. What is the risk to water quality of development over typical small-scale yet abundant upland karst features? This project is designed to determine more precisely what constitutes a significant recharge feature in the context of state law by directly measuring infiltration rates of typical upland karst features.

The hydrologic function of the soil and bedrock system in small sinkholes, identified by their morphological characteristics, and background areas is determined by

large-scale constant head infiltration tests, microtopographic and soil thickness surveys, dye tracing and subsequent excavation of features, and imaging the subsurface with GPR.

Measurements made with a large-scale single ring infiltrometer compare typical upland karst features to paired control plots. The average infiltration per unit head for sinkholes is slightly higher than background in areas with similar soils (0.30 1/hr for sinkholes and 0.27 1/hr for background), though both are within the range for local soils. Results from infiltrometer experiments indicate the thin clay soils typical in the uplands dominates the infiltration process, yet recharge via these features under natural conditions is greater than background when ponding occurs due to their maintained microtopography. As the thin soils typical in the uplands of the Edwards aquifer recharge zone dominate the infiltration process in these small sinkholes, as shown by ring infiltrometer experiments, the risk of recharging poor quality water via these small features from developed areas sufficient to pose a threat to aquifer water quality is little greater than background.

Table of Contents

List of Tables

List of Figures

Chapter 1: Introduction

This chapter is a broad review of karst geomorphology and hydrology relevant to this study, an overview of the Edwards aquifer of south central Texas, and karst aquifer susceptibility to contamination via small karst features. Karst morphological and hydrological perspectives are useful to help place the following research on the Edwards recharge zone in the context of karst systems worldwide.

1.1. REVIEW OF KARST GEOMORPHOLOGY AND HYDROLOGY

The word *karst* is the German word for barren, stony ground, which has been derived from the Slovene word *Krs* or *kras* (Sweeting, 1972; Jennings, 1971; Field, 2002) and is defined by the U.S. Environmental Protection Agency as:

> A terrane, generally underlain by limestone or dolomite, in which the topography is chiefly formed by the dissolving of rock, and which may be characterized by sinkholes, sinking streams, closed depressions, subterranean drainage, and caves. The term *karst* unites specific morphological and hydrological features in soluble (mostly carbonate) rocks. Morphological features include karren, dolines (sinkholes), jamas, ponors, uvalas, poljes, caves, caverns, etc. Hydrologic features include basins of closed drainage, lost rivers, estavalles, vauclusian springs, submarine springs, more or less individualized underground streams and incongruity of surface and groundwater divides. *Karst* is understood to be the result of natural processes in and on the earth's crust cause[d] by solution and leaching of limestones, dolomites, gypsum, halite, and other soluble rocks…." (Field, 2002)

Karst has been adopted with a more broad definition in the scientific community. In the fields of geomorphology, geography, and hydrogeology, karst can take on three distinctly different meanings; 1) one that denotes a landscape with a unique set of landforms, 2) one that denotes a specific geographic area, and 3) one that denotes a unique drainage and circulation system. In geomorphology, *karst* is describes a landscape that has been formed by the process of dissolution. Within this karst landscape are suites of features both large and small that are developed by differential dissolution.

That is, that dissolution is not uniform across the landscape, but which occurs where heterogeneities in the host rock, drainage patterns, and local and regional structure increase the flow of water on, in, and through the host rock. Geographically, *Kras* refers to an area in Slovenia where much of the original scientific work related to karst was conducted. Karst, in the hydrological sense, indicates a drainage and circulation system that is generally unlike non-karst areas in that fracture, solution enhanced fracture, and conduit porosity provide preferential pathways for flow in an aquifer, recharge to the aquifer is fast and direct through features that connect the surface to the aquifer, and hydrologic systems are not necessarily defined by topography. The typical karst landforms found in the uplands and stream and creek bottoms of the Edwards aquifer recharge zone, where surface water enters the subterranean drainage network is shown in Figure 1.

Karst can be described as a group of independent yet interrelated elements that when combined together represent a unified whole. The elements, lithology, and morphology, are linked by erosional processes that are a function of hydrology aided by structural elements. The action of these processes upon lithology is called *karstification*, which is defined as:

> 1. The process of solution and infiltration by water, mainly chemical but also mechanical, whereby the surface features and subterranean drainage network of a karstland are developed to form a karst topography, including such surface features as, dolines, karren, and mogotes and such subsurface features as caves and shafts. An area currently or formerly undergoing karstification, and thus characterized by karst landforms, is said to be karstified. 2. The process by which karst is formed. The term has been given a wide range of meaning, from almost a synonym [of] corrosion of soluble rocks by water to a term comprising all processes responsible for the development of karst features including, besides corrosion, such phenomena as mechanical erosion, jointing, and faulting…." (Field, 2002)

Lithology is the practical beginning for the discussions of karst, because without it, there could be no karst.

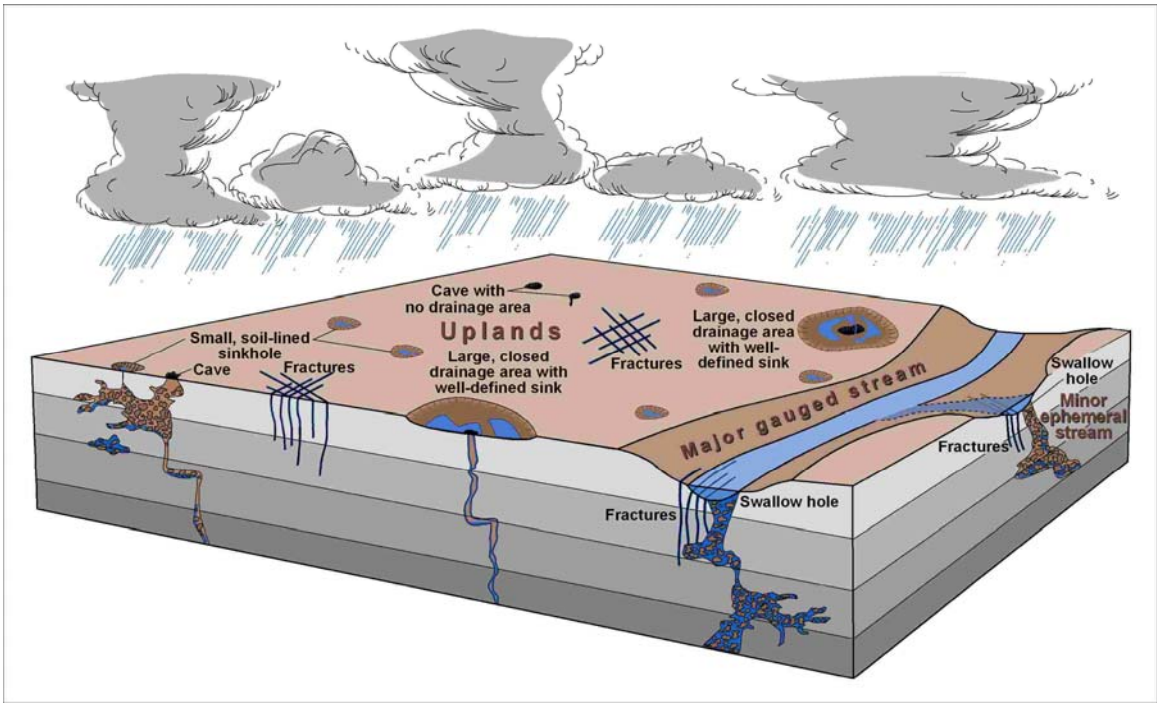

Figure 1. Typical karst features in the Edwards aquifer recharge zone include: solutionally enlarged fractures, small soil-lined sinkholes, large, closed drainage basins (microbasins), and caves with or without large drainage areas in the uplands and fractures and caves or swallow holes in river and creek beds.

1.1.1. The Lithology of Karst Rocks

Karst forms in soluble rocks. Karst features and the landforms associated with karst develop fully only in highly soluble rocks with few impurities. Limestones and dolomites are the most common examples of soluble rocks in which karst forms. The presence of impurities, notably clay minerals or silica, in soluble rocks can lead to an insoluble residue covering the surface or effectively clogging the incipient voids, which restricts further solutional development of the land surface (Klimchouk and Ford, 2000).

Carbonate rocks are generally the most likely to undergo karstification because of their mineral composition. Carbonate rocks are composed of at least 50 % carbonate minerals, commonly calcite ($CaCO_3$) in limestones or dolomite ($CaMg(CO_3)_2$) in dolostones, which are moderately soluble in water (Sweeting, 1972; Jennings, 1971, 1987). Thus, in order to have full karst development, the host rock must be a relatively pure form of a carbonate rock. The classification of carbonate rocks is given in Figure 2, with their susceptibility to karstification. It is estimated that at least 60% $CaCO_3$ in limestone is necessary to begin the process karstification, but in order to become a mature, fully developed karst landscape a limestone should be composed of at least 90% $CaCO_3$ (Corbel, 1957).

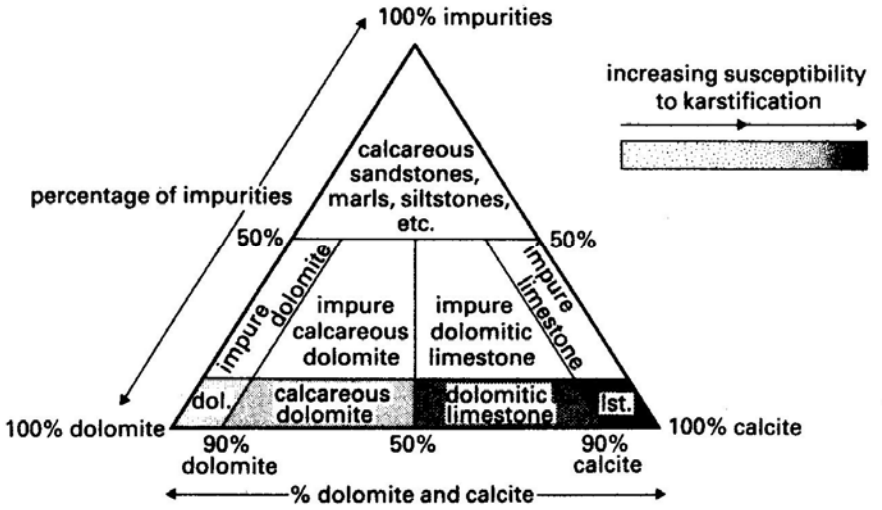

Figure 2. Karstifiable carbonate rock characteristics and classification (Drew, 1985).

1.1.2. Karst Processes

The primary process in the development and maturation of a karst landscape is solutional erosion while mechanical and fluvial processes take a secondary role in the development of karst landforms and features. For example, the creation of collapse

sinkholes occurs after the ceiling of a void or cave, previously created by the dissolution of the host rock, cannot maintain its structural integrity and falls into the open space. Other examples of karst processes include subsidence, sapping, freeze-thaw action, and biological weathering.

Karst is formed by the dissolution of soluble rocks, but the dissolution of the rocks is an ongoing process that has many factors that influence the rate at which preferential enlargement occurs. These factors include: the initial shape of the feature to be enlarged (aperture or conduit dimensions), chemical composition of the bedrock, CO_2 concentration, chemical composition of the water, amount of water flowing through the opening, temperature, and the type of system (open or closed) (Sweeting, 1972; Palmer, 2003). The dissolution of limestones and dolomites occurs when rainwater dissolves carbon dioxide in the air and soil zone forming a weak carbonic acid which follows the chemical reaction:

$$H_2O + CO_2 \Leftrightarrow H_2CO_3 \quad (1)$$

This weak carbonic acid infiltrates on and through the bedrock along joints and fractures and dissolves the calcite at the water-rock interface enlarging fractures and creating voids.

$$CaCO_3 + H_2CO_3 \Leftrightarrow Ca^{2+} + 2HCO_3^- \quad (2)$$

The amount of limestone that can be dissolved is related to the volume of water, the corosivity of water, mineralogy, grain size, purity of carbonate, and the contact area between water and rock. The amount of carbon dioxide dissolved in water is in turn controlled by the concentration of carbon dioxide in the soil and atmosphere and the temperature (Dreybrodt and Gabrovsek, 2002). Yet, things like plant roots, which supply water, maintain openings, and create high pCO_2 via microbial decay of roots, can be very

important. Soil and clay can assist dissolution as it supports microbes which raise the pCO_2 in the soil and enhance the surface area by creating depressions that pond water.

Figure 3 shows the growth rate of solution enlarged fractures as a function of discharge (Q) per meter of fracture height and flow length (L) assuming closed conditions, T = 10 deg. C, and P_{CO2} = .01 atm., while Figure 4 shows the approximate time required for a cave to development from fractures in limestone under different conditions. The growth rate of a cave is heavily dependent on the amount and chemistry of the water that facilitates the dissolution of rock. Enlargement rates may reach as high as 0.15 cm/yr or as low as 0.02 cm/yr (Palmer, 2003). Thus, caves and large-aperture conduits require a long time to develop from fractures to features which dominate flow in the system. The dissolution and preferential enlargement of fractures and joints creates the positive feedbacks necessary to develop a karst landscape.

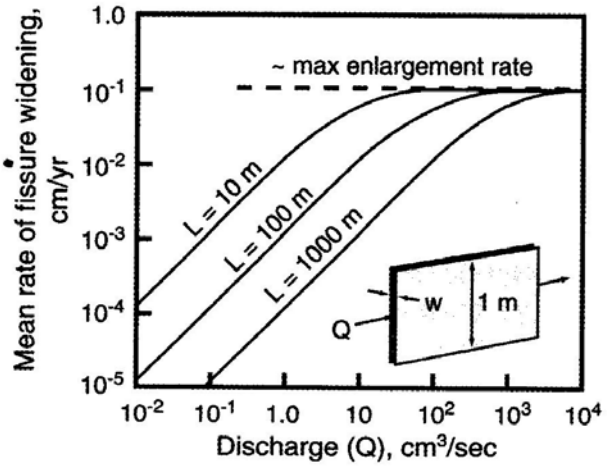

Figure 3. Mean enlargement of a fracture as a function of discharge and flow length (Palmer, 2002).

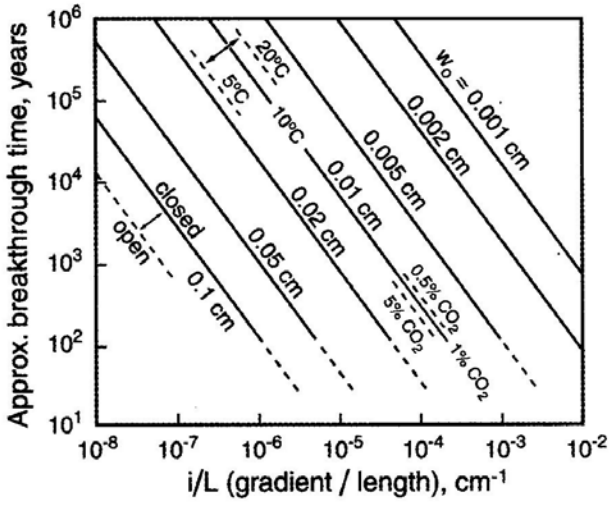

Figure 4. Approximate breakthrough times for cave inception from fractures (Palmer, 2002).

1.1.3. Karst Hydrology

Understanding the hydrology of karst requires an appreciation for the complex interactions of water between the surface and subsurface. Many aspects of the hydrological system in karst, like sinking streams, and karst aquifers' integration of surface water and ground water system dominated by triple porosity, are not present elsewhere.

In karst terrains, streams and rivers have the tendency to sink. That is, there are features in stream and riverbeds in karst areas that facilitate the rapid infiltration of surface waters into the subsurface drainage network. The length and connectedness of surface streams is an indicator of how mature a karst terrain has become. Relatively immature karst may contain long streams with well-connected tributaries while a very mature karst has a very well connected subsurface drainage network with little or no surface flow, thus few or no streams. The subsurface drainage network is composed of

solution modified fractures and conduits that facilitate the circulation of groundwaters very rapidly. A karst aquifer is defined in *A Lexicon of Cave and Karst Terminology* as:

> An aquifer in which the flow of water is or can be appreciable through one or more of the following: joints, faults, bedding-plane partings and cavities – any or all of which have been enlarged by dissolution (Field, 2002).

Karst aquifers have unique porosity characteristics that set them apart from other types of aquifers. Karst aquifers are composed of matrix porosity, fracture porosity, and conduit porosity. Matrix porosity is the pores found in unfractured bedrock. Matrix permeability is a function of the type and a characteristic of the bedrock, like grain size, roundedness, sorting, and is subject to diffuse flow. Fracture porosity includes all fractures created by mechanical processes within the bedrock as well as fractures such as bedding plane partings created by depositional or erosional processes. Fracture permeability is a function of aperture size and spacing, and is subject to non-Darcian flow, as is the last category, conduit permeability. Conduit porosity is any pipe-like void with a diameter larger than 1 cm. Conduit permeability is a function of the diameter and length of the conduit. These types of porosity form a triple porosity or triple permeability system (White, 2002; White, 2003). Though three types of porosity make up the aquifer, groundwater flow through the regional system is dominated by conduits if present (White, 2002; Halihan, *et al.*, 2000). The hydraulic conductivity of the system will be anisotropic if fractures or conduits have a preferred orientation (Kiraly, 2002).

Groundwater flow in karst aquifers is directly linked to the development of the landscape. Water is introduced to the system from the surface through features that make up the karst landscape. The surface features and the aquifer evolve concurrently as fractures and conduits are enlarged by preferential dissolution increasing the overall aperture of fractures and conduits as well as the overall connectivity of the system. Surface features are able to transmit more water to the subsurface as they mature. Thus,

the groundwater circulation system in karst aquifers is developed by the positive feedback from the dissolution within and at the surface of the host rock.

One of the main characteristics of karst aquifers is that conduits provide pathways for fast and direct recharge from the surface to the subsurface and discharge groundwater from the aquifer to the surface as springs. Waters that recharge a karst aquifer may come from four differing sources: allogenic recharge, diffuse infiltration, internal runoff, and overflow from perched aquifers (Figure 5). Allogenic recharge includes precipitation that falls on a contributing zone, or an area of higher elevation than the recharge zones, whose surface streams cross into the recharge zone and sink, recharging the aquifer via features in stream bottoms. Diffuse recharge includes precipitation that falls on the recharge zone, or area where the karst surface is present, and recharges the aquifer by infiltration through the soil and fractures or matrix of the underlying host rock. Internal runoff consists of storm waters that flow into closed depressions or microbasins, rather than surface streams, and enters the aquifer rapidly through open drains in sinkholes or caves. Overflow from perched aquifers, though not common in the Edwards, includes waters from a perched aquifer above a karst aquifer that recharge the karst aquifer through vertical shafts and solutionally enlarged fractures (White, 2002).

Ground water discharges a karst aquifer through springs at the surface. These springs may be open conduits or fractures that are driven by gravity or under pressure as artesian springs in confined settings. Ground water may also discharge the aquifer in the subsurface as flow to adjacent or underlying units.

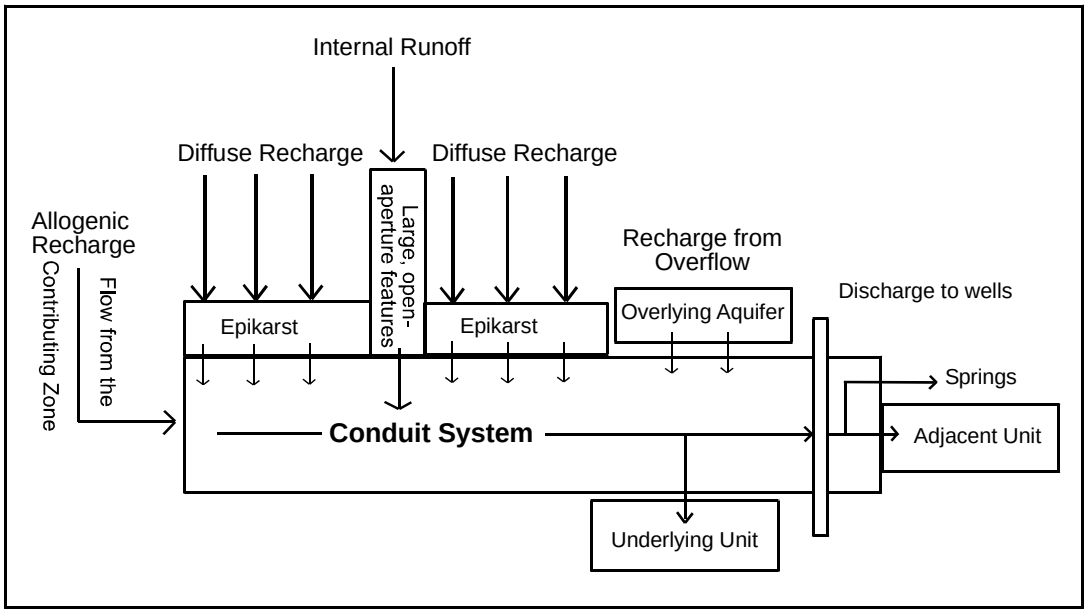

Figure 5. General conceptual model of a karst aquifer including four sources of recharge modified from White, 2003.

1.1.4. Karst Landforms

Sweeting (1972) classifies five main groups of karst landforms. These are:

1. Closed depressions of moderate dimensions (i.e. sinkholes or dolines and microbasins in the uplands and sinks or swallets in stream or riverbeds).
2. Superficial landforms (i.e. rill karst).
3. Landforms in limestone areas caused by fluvial processes (i.e. blind valleys).
4. Subterranean landforms (i.e. caves and cave deposits).
5. Large scale closed depressions of complex polygenetic origin (i.e. poljes).

One other landform must be included in order to discuss the comprehensive karst system, epikarst. These features, large and small, purely surficial and those that extend deep within the host rock combine to create a karst landscape. Sinkholes are discussed in more detail than the other types of karst landforms because they are the focus of this study;

however, the five other types of landforms will be discussed briefly. A closed depression is defined as:

> 1. Any karst hollow with internal drainage, including dolines, uvalas, poljes, cockpits and all variety of blind karst valleys, of both large and small scale. 2. A general term for any enclosed topographic basin having no external drainage, regardless of origin or size (Field, 2002).

The term sinkhole will be used to refer to closed depressions of moderate dimensions, while the term polje will be used to refer to closed depressions of large dimensions. Every closed depression whether of moderate or large dimension has three basic components; a drain, a solutionally modified zone in the host karst rock, and the presence of variable amounts of unconsolidated material that makes up the land surface (White, 1988). It should be noted that the term sinkhole is equivalent to doline; however, sinkhole is the more commonly used term in America. Sinkholes are the fundamental landform in karst landscapes, and as such play an important role in the development of the landscape (Jennings, 1985; Sweeting, 1972).

1.1.4.a Sinkholes or Dolines

Sinkholes have a variety of morphological types based on the ratio of diameter to depth first described by Jovan Cvijic including: bowl-shaped, funnel-shaped, and well-shaped (Cvijic, 1893). The bowl-shaped sinkholes are broad relatively shallow features where the ratio of diameter to depth is approximately 10:1. Funnel-shaped sinkholes have diameter/depth ratios around 3:1 and with steep slopes ranging between 30 and 40 degrees. Well-shaped sinkholes have ratios where the depth is much greater than their diameter, thus they look like wells (Cvijic, 1893; Sweeting, 1972), but are referred to as shafts more commonly in America.

In addition to their morphological types, sinkholes are further categorized into five types by their mode of development (Figure 6). The development of a sinkhole

begins with the dissolution of the underlying host rock, as preferential enlargement of fractures or conduits. If solution remains the dominant mode for enlarging the feature at the surface a solution sinkhole is formed. A collapse sinkhole forms when the solution of the host rock results in the formation and upward propagation of a larger void, eventually the roof collapses into the void and creates a visible feature at the surface. Collapse sinkholes, given time, will eventually take on the funnel- or bowl-shape once soil cover forms. Subsidence sinkholes form when solutionally enlarged fractures of a host rock continually sap overlying sediments into the enlarged fractures and the subterranean drainage network. Much like collapse sinkholes, the subjacent karst collapse sinkhole occurs when the non limestone roof of a void in a karst host rock fails. However, in this case the collapse in the karst host rock propagates upward through an overlaying non-karst rock and the resulting sinkhole is expressed at the surface of the non-karst rock. Alluvial streamsink sinkholes form where streams sink through alluvium into an underlying host rock with solutionally enlarged fractures or conduits. This type of sinkhole is much like a subsidence sinkhole, but instead of relying solely on continual piping to maintain the depression, the sinking stream also washes the alluvium into the subsurface (Jennings, 1971; Jennings, 1987).

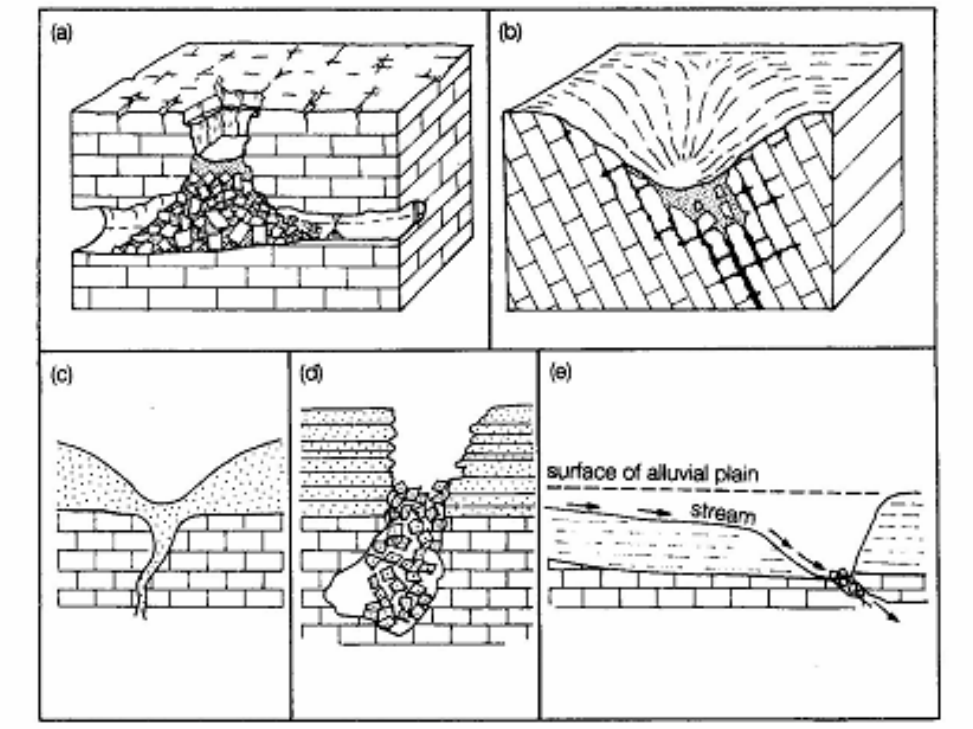

Figure 6. Five types of sinkholes including: (a) Collapse sinkhole; (b) Solution sinkhole; (c) Subsidence sinkhole; (d) Subjacent karst collapse sinkhole; (e) Alluvial streamsink sinkhole (Jennings, 1987).

Sinkholes with large drainage areas are more significant sources of recharge than those with small drainages. Thus, another characterization of sinkholes based on drainage size is used in this study. Small sinkholes are those with a small catchment area and bowl diameter of up to 4.5 meters. Medium sinkholes are those with a medium catchment area and bowl diameter of up to 15 meters. Internally drained microbasins will be used to refer to sinkholes with multiple-acre drainage areas.

Small sinkholes do provide more recharge than background because water ponds in them after rain events due to their microtopographic expression. When ponding occurs, there is an increase in head relative to areas with little relief, driving the infiltration process. Maintenance of this microtopographic expression is evidence that

karst processes are significant relative to other soil transport processes like sheet wash or eolian transport. Experience of cavers and people who conduct geologic assessments looking for cave habitat has documented that the removal of surface soils and rock from some small sinkholes will uncover openings to larger caves, shafts, and solution enlarged fractures. Other small sinkholes are found not to "go", that is, they fail to open up to a larger or open feature.

1.1.4.b Superficial landforms

Superficial landforms in karst are formed by the weathering of soluble rocks at the surface. These are generally small features, a few centimeters up to a meter, and may be found across the landscape etched into the bedrock. Though they may take on different appearances, they are all formed from the same basic process as any other landform in karst, the dissolution of bedrock. There are six factors that affect the size and distribution of superficial landforms including:

1. The chemical reaction that is primarily responsible for the dissolution of the bedrock.
2. The distribution of precipitation across the landscape.
3. Lithology and texture of the bedrock.
4. Orientation of the bedrock.
5. Soil or vegetative cover.
6. Climate.

1.1.4.c Landforms caused by fluvial processes

These are large-scale features in a karst setting that may have formed initially by fluvial processes, like valleys, but after a significant amount of time the drainage evolved

from predominantly horizontal to a more vertical karst drainage system. These include blind valleys and natural arches formed by lowering the base level of a stream or river.

1.1.4.d Subterranean landforms

Subterranean landforms are the result of solutional erosion of the karst drainage network or the deposition of solutes in the drainage network itself. Conduit porosity is the main type of subterranean landform, but the whole drainage network in a karst terrain including fractures should be included. Caves are naturally occurring conduit porosity that are large enough to be entered by humans. All manner of cave formations are included in the subterranean landform category including the erosional landforms that occur on cave walls and depositional landforms in caves like stalagtites and stalagmites. These caves serve an important role in upland recharge. Caves with little or no drainage areas are still important as potential input mechanisms for water quality issues, yet, as they do not provide large amounts of recharge, are not as sensitive as internally drained microbasins.

1.1.4.e Large scale closed depressions

Poljes are very large closed depressions (10s to 100s of square kilometers) that are; generally aligned to a major structural component, have flat bottoms, and may be internally drained or drained by streams. These features are more commonly found in areas where the karst landscape is mature.

1.1.4.f Epikarst

Epikarst is the zone of weathered carbonate rock below the soil zone that forms due to the enhanced solution of the uppermost part of the bedrock. Permeability within the epikarst is spatially variable and decreases with depth. Porosity in the epikarst is generally much greater than the underlying bedrock (Klimchouk, 2004). The epikarst

may effectively store water, transport water laterally, or leak water. This zone of rock undergoes the greatest amount of solution due to its proximity to the surface and the main source of CO_2. Climate, roots from trees and other plants, and karst processes responsible for the enlargement of fractures creates a more permeable zone above the host rock, but the permeability of this zone is very heterogeneous aerially and tends to diminish with depth, as the source of CO_2 becomes further away and solutional enlargement of fractures lessens (Williams, 2004; Williams, 1983; Klimchouk, 2004). This is the zone where infiltration occurs. Infiltration in the epikarst may be rapid and direct, where open fractures and vertical conduits occur at the surface, and concentrated, where these open fractures or conduits occur in the base of sinkholes or may occur more slowly, where fractures and conduits are plugged with soil, or where larger fractures terminate and create a bottle-neck effect. When this occurs, the epikarst may become saturated, effectively becoming a perched aquifer. Storage of water and the delayed infiltration to the conduit system below and lateral flow within the epikarst occurs. Water that is stored may discharged into open fractures that connect to the conduit system in the host rock or evaporated (Bakalowicz, 2004).

1.1.5. Evolution of Karst Features

The progress of the evolution of a karst landscape can be gauged by the drainage network. Immature karst terrains have not developed complex subterranean drainage networks and have few karst features. Therefore, they depend on surface drainage as well as subterranean drainage to transport water down gradient, thus they have a more connected river system. Mature karst terrains, however, have developed a complex internal drainage network, with many karst features that facilitate drainage, and thus have few surface streams or rivers. Similarly, the evolution of karst features can be gauged by the size of its catchment area. Thus, small sinkholes are relatively immature compared to

medium sinkholes. In terms of the evolution of the overall landscape, small sinkholes are incipient features, just beginning to become part of the drainage system.

1.2. THE EDWARDS AQUIFER

The Edwards aquifer is a prolific karst aquifer that supplies water to a population of 1.7 million people (Edwards Aquifer Authority, 2005), supports irrigated agriculture, and supplies spring flow to major springs that provide habitat to endangered species and flow to diverse downstream ecosystems and communities (Figure 7). Annual rainfall in the recharge zone of the Edwards aquifer ranges from 20 to 40 inches (50 to 100 cm) but is highly variable on both a seasonal and annual basis. The capacity of the Edwards aquifer to capture water during wet periods and store that water to sustain pumpage and spring flows through dry periods is a critical issue for the region. Risk of degradation of water quality or water quantity because of urbanization of the recharge zone is a management issue that should be receiving increased attention.

Understanding the karst nature of the Edwards aquifer is critical for protection of both water quality and quantity. The aquifer is characterized as having low amounts of run-off and high amounts of infiltration due to the lack of regular surface drainage patterns and relatively thin soils (Woodruff, 1984). Conduits dominate flow through karst aquifers (Halihan, *et al.*, 2000). Orders of magnitude difference in the hydraulic conductivity can at times mean that up to 90 % of the flow in a karst aquifer may be from conduits, where the matrix and other fractures make up the remaining 10% (White and White, 2001). Hovorka and others (1998) and Halihan and others (2000) documented a similar relationship for the Edwards aquifer. Halihan and others published data on permeability from matrix samples, fracture properties and core diameters; they also modeled the permeability of fractures and conduits and found that conduit permeability is orders of magnitude greater than both fractures and matrix, thus, conduits most likely

control flow in the Edwards aquifer (Figure 8). They also hypothesized that many wells intercept isolated voids that are unconnected with the regional conduit system and that well yields can be attributed to the intersection of fractures including bedding plane partings (Hovorka, *et. al.*, 1998).

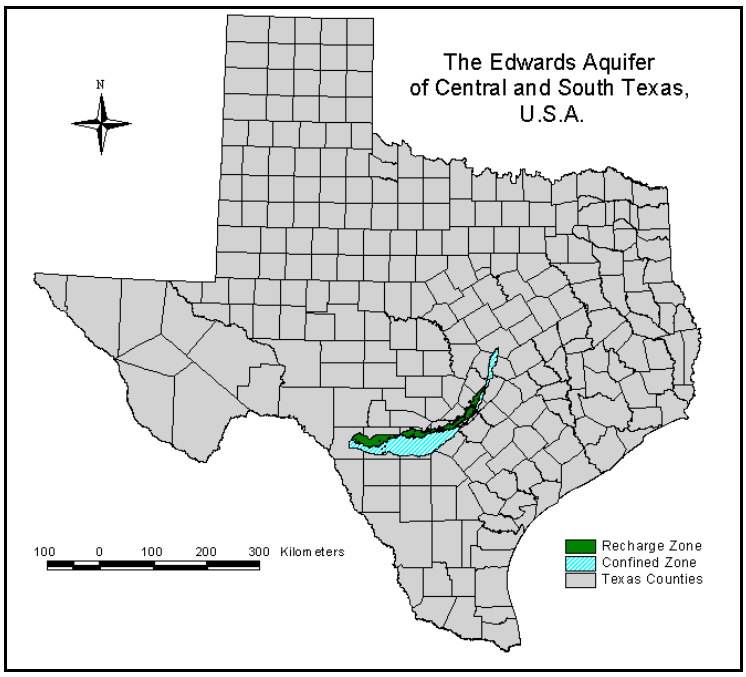

Figure 7. Map of the Edwards Aquifer.

With hydraulic conductivities of several orders of magnitude higher than the matrix or fractures, conduits provide a direct path to the subsurface for water or any contaminants contained in the water. Conduits support rapid flow within the aquifer and rapid discharge to springs. The median springflow discharge from 1934 to 2004 in the Edwards aquifer is an estimated 15 m^3/sec (383,900 acre-feet a year) (EAA, 2005). Well yields of as much as 40 thousand gallons per minute have been documented in the Edwards aquifer (Rettman, 1991).

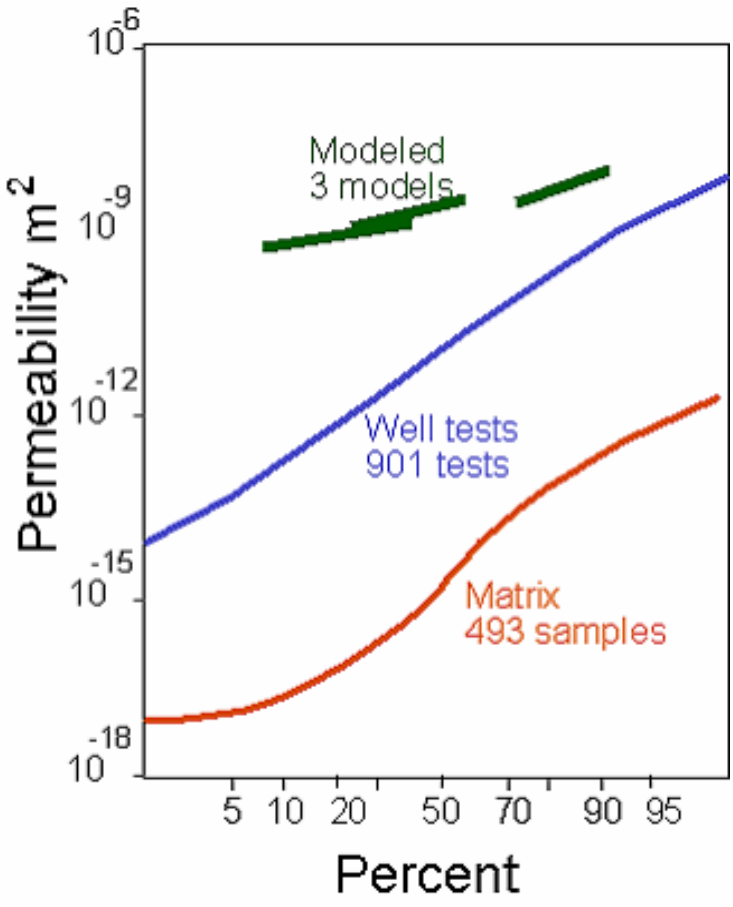

Figure 8. Modeled conduit flow in the Edwards aquifer is much higher than measured values reflecting the influence of large aperture, low incidence conduits (Halihan, *et. al.*, 2000).

The Edwards aquifer is composed of six aquifer segments separated by groundwater divides (Sharp, 1990), however, as field studies are limited to the San Antonio and Barton Springs segments, only these segments are discussed. The San Antonio segment of the Edwards aquifer is separated from the Barton Springs segment by a groundwater divide in Hays County. Flow trends to the northeast in the Barton Springs segment and discharges into Barton Springs. In the San Antonio segment, flow is generally east in counties west of San Antonio, then northeast, discharging in major springs like Comal and San Marcos Springs.

1.2.1. Geology of the Edwards Aquifer

The Edwards aquifer of south-central Texas is developed in the Lower Cretaceous Kainer and Person Formations of the Edwards Group along the Balcones Fault Zone. The Del Rio Formation overlies the Edwards and acts as the major confining unit, and the underlying Glen Rose Formation is the lower boundary of the Edwards aquifer and the uppermost unit of the Trinity aquifer (Mace, *et. al.*, 2000). The Edwards Group consists of generally thick bedded to massive limestones, commonly dolomitic, with minor beds of argillaceous limestone and calcareous shale (Hill, 1901). The Edwards aquifer includes eight informal hydrologic subdivisions (Maclay, and Small, 1976) with the Kainer and Person Formations divided into seven informal members (Rose, 1972) combined with the overlying Georgetown Formation (Figure 9).

Hydrologic subdivision VIII (Basal nodular member) generally consists of massive, shaly, nodular limestone and *miliolid* grainstone. Cavernous porosity in the Basal nodular member is localized to a few areas in Comal County. Hydrologic subdivision VII (Dolomitic member) is generally described as massively bedded, mudstone to limestone and crystalline limestone, with fracture porosity and permeability associated from local faulting. The cavernous porosity found within this hydrologic subdivision is generally related to structure and bedding plane fractures. Hydrologic subdivision VI (Kirschberg evaporite member) is the most porous and permeable subdivision of the Kainer Formation. Cavern and sinkhole development is extensive in the crystalline limestones and chalky mudstones that are the common lithologies of this subdivision. Hydrologic subdivision V (Grainstone member) is primarily composed of a tightly cemented *miliolid* grainstone. Though there is little fabric porosity and permeability, local fracture porosity and permeability associated with faulting foster the development of cavernous porosity within this subdivision. Hydrologic subdivision IV

(Regional dense member), a dense, argillaceous mudstone, denotes the lowest member of the Person Formation. The low porosity and permeability causes this member to be a locally confining unit within the Edwards aquifer. With lithologies that consists of bioturbated iron-stained beds separated by massive limestone beds of crystalline limestone and mudstone to grainstone, Hydrologic subdivision III (Leached and collapsed members, undivided) is one of the most porous and permeable subdivisions. The majority of the porosity and permeability associated with this subdivision comes from the collapsed zones resulting from the dissolution of evaporites and faulting. Hydrologic subdivision II (Cyclic and marine members, undivided) consists of mudstone to Packstone and *miliolid* grainstone with fossiliferous zones where vuggy and moldic porosity and permeability is common as well as fracture porosity and permeability associated with faulting. Hydrologic subdivision I (Georgetown Formation) consist mainly of a marly limestone, and have little porosity or permeability. The Del Rio Clay acts as the upper confining unit for the Edwards aquifer.

The Balcones Fault Zone separates the Edwards Plateau to the north and west from the Gulf Coastal Plain to the southeast, and is framed by a series of generally northeast trending, en echelon, high angle normal faults generally downthrown to the southeast (Small, *et. al.*, 1996). The aquifer is unconfined where the rocks crop out and becomes unconfined as younger rocks overlap the generally southeasterly dipping aquifer at depth (Hovorka *et. al.*, 1998).

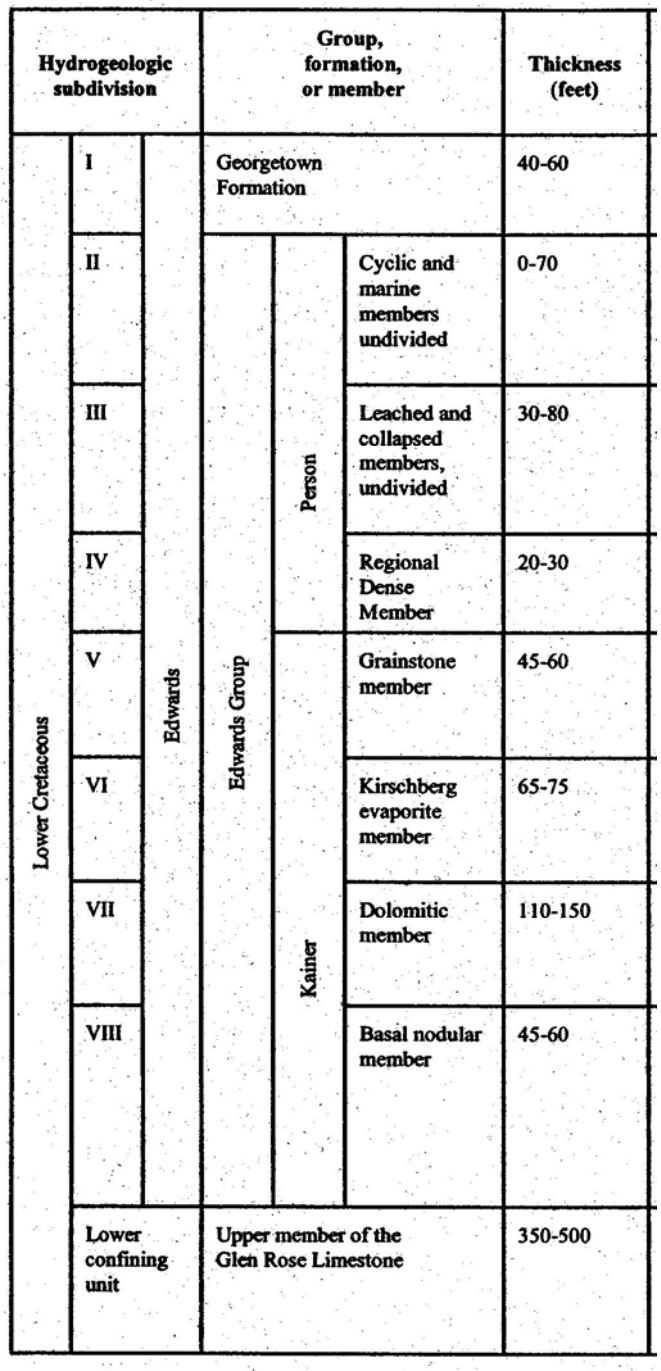

Hydrogeologic subdivision			Group, formation, or member			Thickness (feet)
Lower Cretaceous	I	Edwards	Georgetown Formation			40-60
	II		Edwards Group	Person	Cyclic and marine members undivided	0-70
	III				Leached and collapsed members, undivided	30-80
	IV				Regional Dense Member	20-30
	V			Kainer	Grainstone member	45-60
	VI				Kirschberg evaporite member	65-75
	VII				Dolomitic member	110-150
	VIII				Basal nodular member	45-60
	Lower confining unit		Upper member of the Glen Rose Limestone			350-500

Figure 9. Generalized stratigraphic column of the Edwards aquifer, from Small, *et. al.*, 1996.

1.2.2. The Balcones Fault Zone

The Edwards aquifer is developed along Balcones Fault Zone (BFZ), a regional zone of extension with a width of 50 kilometers (30 mi.). The top of the Edwards Group has been displaced downward a total of more than 1965 meters (6450 ft.) across the BFZ (Collins and Hovorka, 1997). Throws on individual faults are as much as 260 meters (850 ft.) and a down-to the coast displacement is prevalent, though grabens are common (Hovorka *et. al.*, 1998). Faults and associated fractures are high angle. Opening mode fractures associated with regional faults are parallel to the regional fault trend (Collins, 1987). Displacement on faults varies along the length of the faults. Displacement is transferred to adjacent fault strands, forming relay ramps, which may be cross-faulted or folded zones of greater structural complexity (Ferrell and Morris, 2003). Porosity of the Edwards aquifer is predominantly the result of Balcones faulting (Hovorka, *et. al.*, 1996). Recharge of the Edwards aquifer chiefly takes place along this zone of fractured and faulted rock where the permeable karstified rocks of the aquifer crop out.

Uplift on the Balcones Fault Zone has also created a regional topography, which gives the name Balcones to the principle escarpment. High-relief Edwards Plateau Glen Rose outcrop of the Edwards Group forms the recharge zone, which occurs at elevations of 490 meters (1600 ft.) in the northwest. The southern and eastern parts of the Edwards aquifer are overlain by weak, low transmissivity rocks, creating artesian conditions in the aquifer, and freshwater flow through a highly transimisive karst conduit systems extends to depths of more than 915 meters (3000 ft.) below sea level. Deep dissection along major eastward flowing rivers has created flow paths to low elevation. Karst piracy has diverted flow in the whole aquifer system from western highlands toward eastern spring discharge points (Woodruff and Abbott, 1986).

Regional orientation of lineaments studied on aerial photographs in the southern Edwards Plateau show lineaments related to two fractures sets, one of short incidence, up to 4.5 km, and one of long incidence, up to 160 km (Wermund, *et. al.*, 1978). Approximately 400 lineaments were identified in each of the almost 200 aerial photo mosaics of the Balcones Fault Zone and the Edwards Plateau. The Balcones Fault Zone is an area of extensive faulting with associated fractures. Caves in the Edwards and underlying Glen Rose in this region were found to have passage segments that are oriented in a direction similar to that of both short and long fracture sets. Veni (1994) studied the bearings of 40 joint-guided passage segments in 23 caves in the southwestern Edwards Plateau to determine the orientations more prone to development (Veni, 1994). Though two trends showed the greatest development, the values were not high enough to be considered statistically significant.

1.3. KARST SUSEPTIBILITY TO CONTAMINATION

The vulnerability of karst aquifers to contamination is higher than many other types of aquifers because the focused flow paths provide rapid and direct recharge to the aquifer. Matrix flow provides opportunities for sorption, retardation, biodegradation, and dilution of a contaminant. In groundwater recharged through the fast and direct flowpaths, the natural mitigation processes are reduced or absent. These flowpaths include large-aperture karst features like caves and sinkholes in the uplands and open fracture zones and swallets in river and streambeds. The most common karst feature in karst landscapes, including the Edwards aquifer recharge zone, are sinkholes.

In the Edwards recharge zone sinkholes are commonly subtle, soil-floored depressions that lack large-aperture open drains. Other types of small-aperture karst features that occur in the uplands include solution cavities and soil filled solutionally enlarged fractures. Many of these are small (less than 3 meters in diameter) and shallow

(less than 25 centimeters in depth) bowl-shaped sinkholes. The hydrologic function of small sinkholes was not well known prior to this study. Though these sinkholes have little topographic relief, they may indicate a larger, more complex, well developed flow system in the upper few meters of the soil and bedrock.

1.3.1. Recharge in the Uplands

The majority of recharge in the Edwards aquifer occurs via karst features in creek bottoms and streambeds. Water balance studies estimate that 85% of recharge occurs in creeks and streams in the Barton Springs segment of the aquifer (Slade, *et. al.*, 1986). However the remaining significant portion of the recharge is occurring at small drainages or upland karst features. A year-long water balance study for an internally drained microbasin in the Barton Springs segment showed that 42% of the precipitation that fell within the microbasin recharged the aquifer, 33.5% as diffuse recharge and 8% as discrete recharge. With internal drainage microbasins comprising 10% of the area of two subsegments of the Barton Springs segment and assuming all microbasins recharge 42% of precipitation, it was estimated that these features contribute the equivalent of 5% of the total discharge of Barton Springs (Hauwert, *et. al.*, 2005). Similarly, rainfall simulations over two caves in the San Antonio segment show that recharge via caves, while variable, may still account for a significant amount of recharge. One of the caves tested showed that nearly 4% of the total water applied to the cave footprint recharged through the cave, while the other cave tested showed that under natural conditions, a minimum of about 64% of the rain calculated to fall over it's footprint recharged into the cave (Gregory, *et. al.*, 2005).

Historically, caves have been poorly protected, used as dumps, filled or cemented shut, and used as drains for poor quality water. Caves serve an important role in upland recharge, and thus they pose a risk to water quality. Protection of caves with large

drainage basins have a clear role in the protection of water quality in karst aquifers. The quality of all surface water must be protected because of the immediate and unmitigated transfer of surface water to the aquifer. Protection of caves with small drainage basins is different in the volume of water that they normally contribute is small. Protection needs to reduce the risk that concentrated contaminant will be introduced directly into a cave or that large volumes of poor or questionable quality water be directed near a cave.

1.3.2. Urban Development on the Edwards Recharge Zone

The uplands of the Edwards aquifer recharge zone are currently undergoing development. Houses, streets, water and sewer lines associated with this development may introduce water quality risks to the aquifer due to the introduction and disbursement of contaminants in karst features. Figure 10 shows typical development in the uplands in which a housing development, Circle C Ranch, has been built on the recharge zone, in green, near a karst preserve, J17 Fortune Tract. This type of upland development is currently underway near the large urban areas of San Antonio, Austin, San Marcos, and New Braunfels on the Edwards aquifer recharge zone in central Texas. Urban development near karst features may present risks to water quality as discrete and diffuse recharge facilitates the transport of contaminants from houses, streets, and water and sewer lines to the aquifer. The research issue is to correctly understand the hydrologic features in order to correctly design effective BMP's.

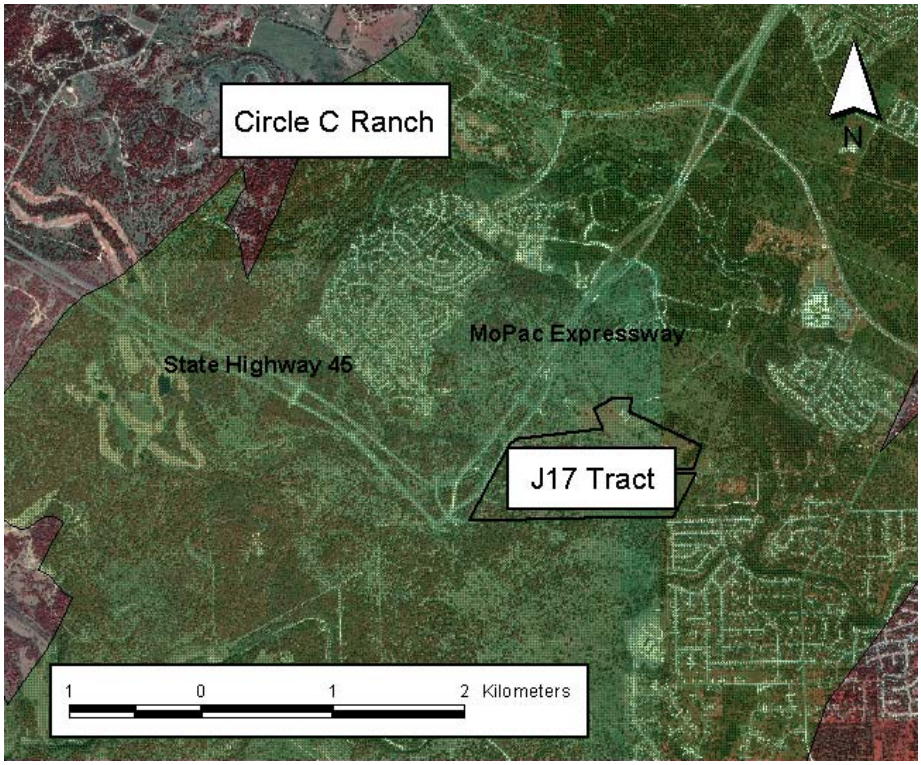

Figure 10. Typical development in the uplands of the Edwards aquifer recharge zone (green area). Note the proximity of developed areas to the karst preserve J17 Fortune Tract.

1.3.3. Protection of Recharge Features

Currently, Texas State law (Edwards Rules [Title 30 Texas Administrative Code (TAC) Chapter 213]) regulates activities having the potential for polluting the Edwards aquifer. A key part of implementation of the Edwards Rules is the requirement for the management of "sensitive features," which are defined as permeable geologic or manmade features located in the recharge zone or transition zone where the potential exists for hydraulic interconnectedness between the surface and the Edwards aquifer and where rapid infiltration to the subsurface may occur. The initial step in managing sensitive features is to identify them during visual inspection for geomorphic indicators. The Texas Commission on Environmental Quality (TCEQ) provides guidance to

geologists in the “Instructions for Geologists for the Geological Assessment of Features”, to locate sensitive features based on their geomorphology. The method of recharge protection described by the Edwards Rules uses geomorphologic characteristics to infer the most likely areas of the landscape that are likely to contain subsurface karst conduits that focus flow. Based on the geologic assessment of features, developers propose a plan for implementing “best management practices” (BMP’s) to mitigate any negative impacts caused by the development on or around sensitive features. Sinkholes have the potential for interconnectedness between the surface and the Edwards aquifer because of their karst origin. Previously small sinkholes have been regarded as possibly sensitive to contamination due to this potential for interconnectedness. An appropriate BMP has not been defined because the function of small sinkholes was unclear prior to this study. It is the purpose of this thesis to delineate the function of these features in the context of their potential for water quality contamination during development.

Chapter 2: Methods

Small sinkholes in the uplands of the Edwards aquifer recharge zone, regardless of their dimensions or state of their drains, should have a higher recharge rate than the surrounding area, due to the vertical permeability characteristic of all sinkholes, namely, the permeability caused by fractures and conduits. The geomorphic indicators of karst features, depressions, in the recharge zone would indicate areas of soil sapping and preferred dissolution. Testing the infiltration characteristics of features and non-feature areas, using a large-scale ring infiltrometer, compares the permeability of the background with that of the karst features. If the sinkholes have higher than background infiltration characteristics, then they are indicating a higher vertical permeability than the surrounding area. If these features indicate similar or lower infiltration characteristics than background, then at the present stage in their development, these features lack the high vertical permeability or the fractures or conduits that make up this zone are effectively clogged by naturally occurring soils. The head normalized infiltration rate is observed at features of varying microtopographic expression and at control plots with little topographic relief and no geomorphic indicators of karst.

2.1. FIELD SITES

Four field sites were included in this study representing the Barton Springs and San Antonio segments of the Edwards aquifer and the Contributing zone. These sites include: J-17 Fortune Tract, Rutherford Ranch, Honey Creek Natural State Area, and Camp Bullis (Figure 11). A few selected sinkholes at each site were tested for their hydrologic properties using a ring infiltrometer. Rutherford Ranch and the J-17 Tract are part of the Water Quality Protection Lands Program managed by the City of Austin Water Utility.

J-17 is located in southwestern Travis County and Rutherford Ranch is located in northern Hays County. Outcrops at both locations are Kainer and Person Formation. Five upland sinkholes were tested at the J-17 tract with four background plots. One recently excavated solution cavity was also tested at the J-17 Tract. Four upland sinkholes and their associated control plots were tested at Rutherford Ranch. Both the J-17 tract and Rutherford Ranch are situated within the Barton Segment of the Edwards aquifer.

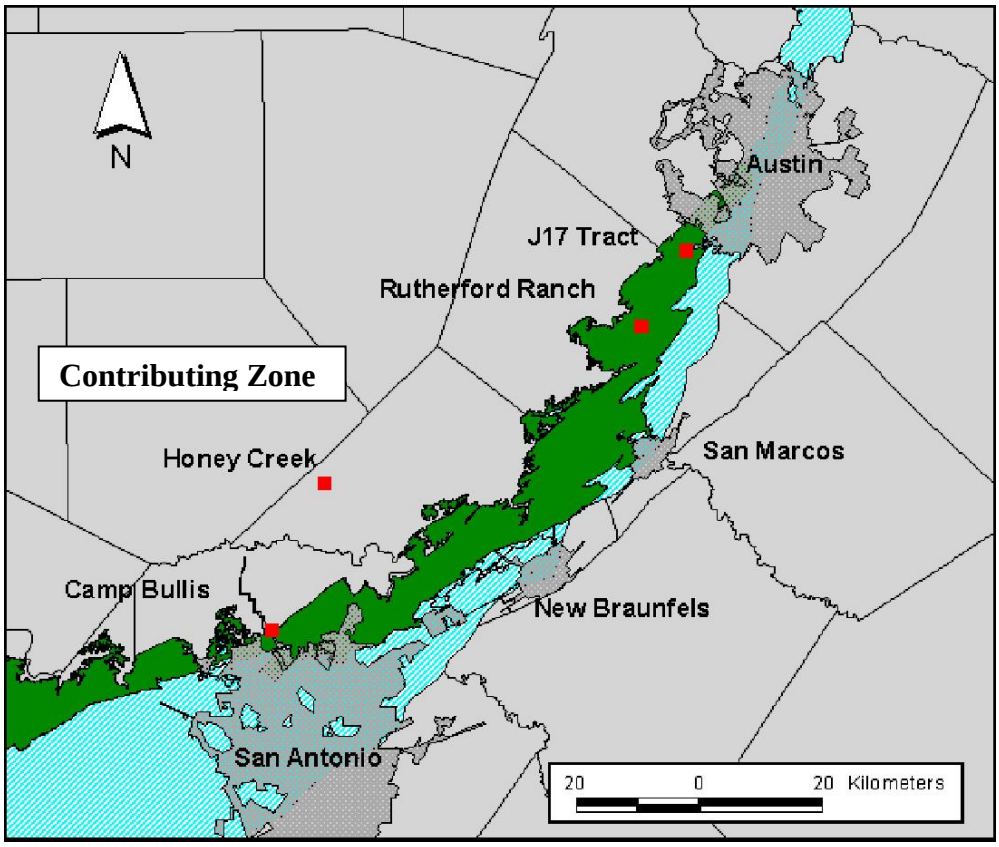

Figure 11. Site location map, green indicates the Edwards aquifer recharge zone, blue indicates confined zone areas north of the recharge zone are know as the contributing zone. The J17 tract and Rutherford Ranch are located within the Barton Springs segment of the Edwards aquifer, while Camp Bullis is located in the San Antonio segment. Honey Creek Natural State Area is located within the contributing zone.

Honey Creek Natural State Area is located along the border of Comal and Kendall Counties adjacent to the Guadalupe River State Park. One sinkhole, one control plot, and the area around a juniper tree were tested. Although not in the Edwards aquifer recharge zone, studies at the Honey Creek Natural State Area were conducted in order to assess possible scale effects by comparing ring infiltrometry results with data from a nearby large-scale rainfall simulation infiltration project conducted by the Biological and Agricultural Engineering Department at Texas A&M.

Camp Bullis is a 120 square kilometer military base located north of San Antonio in Bexar County. Edwards Formation limestones crop out in an area of approximately 7 square kilometers in the southeastern portion of the base, and are located within the San Antonio segment of the Edwards aquifer. These are lower Edwards members. One sinkhole and one control plot were tested. At each of the sites included in the study there are numerous large and small aperture karst features. The most common large aperture karst features encountered at the sites are caves. Most of these caves have little or no drainage area, though a few with large (multi-acre) closed drainage areas in the uplands or caves located in the streambeds do occur; which probably facilitate a significant amount of recharge to the aquifer. Small aperture karst features, like subtle sinkholes and fracture zones are ubiquitous across the Edwards recharge zone. Though they do not have the drainage areas of some of the caves, that they exist in such numbers may mean that collectively they provide a modicum of recharge both in the uplands and the streambeds alike.

The dominant soil types at the field sites, Speck stony clay loam (SsC) and the Rumple-Comfort association (RUD), are described in the Travis County and Comal and Hays County Soil Surveys as having a permeability range of 0.1524 – 0.508 cm/hr (or 0.06 – 0.20 in/hr). The Soil Conservation Service estimates these permeability ranges

based on the structure and porosity of the soil. Typically these soils are thin, generally 35 to 50 cm, with 35% to 85% rock fragments (Werchan, *et. al.*, 1974). The Speck stony clay loam is described as having slow saturated transmissivity, or slow infiltration rates when wetted. Permeability for the Rumple-Comfort association is described as moderately slow in the Rumple and slow in the Comfort, yet is well drained, with a medium amount of surface runoff (Batte, 1984). Soils at the Honey Creek site are typically part of the Real-Comfort-Doss complex. Tarpley clay is the dominant soil type at the Camp Bullis site. The Real-Comfort-Doss complex saturated hydraulic conductivity is an estimated 0.36 cm/hr using the Natural Resources Conservation Service web soil survey and the Tarpley clay saturated hydraulic conductivity is an estimated 0.972 cm/hr (NRCS, 2005).

2.2. IDENTIFICATION OF SINKHOLES

Geologic assessments for the J17 Fortune tract and Rutherford Ranch were consulted prior to field inspection to locate previously identified karst features. Site managers assisted in locating these features during field visits and walking surveys. Follow up surveys of potential sites were conducted to identify potential features for study. These follow up surveys were accomplished by walking transects across the property in areas likely to contain karst features. Candidate features are identified by their bowl shape, though in many cases they are difficult to see due to vegetation. In some cases, sinkholes were discovered when they were walked into, and the shape and extent of the depression was determined by feel. Potential features were inspected more closely for organics and charcoal in the soil, indicators of flow into the depression to determine whether they were in fact karst features rather than the product of previous land management (i.e., caused by livestock or other human activities). Each candidate feature has a paired control plot that is selected based on proximity to the feature and lack

of any visible sign of rapid infiltration that may indicate a karst feature. Features and their associated control plots were given a feature identification number that included an abbreviation of the site name, feature type, and number. For example, RRSH4 indicates the site, Rutherford Ranch, the feature type, sinkhole, and identifying number 4. Basic descriptive characteristics of the candidate features were cataloged including their location, obtained via GPS (Table 1), dimensions, diameter and depth, soil cover, and setting.

Candidate features are identified using their geomorphic characteristics as a guide. These more subtle features of the karst landscape do not have an obvious hydrologic function or clearly accept large volumes of water. A ring infiltrometer is used to determine the infiltration rate of the soil and bedrock system, under saturated conditions, that these features occupy in order to draw some conclusions about their role in facilitating the flow of water to the subsurface. The microtopography and soil thickness of these subtle sinkholes are used to help better describe features tested. Landowner permission and access for a water truck limited the number and location of features tested. The water truck used to transport the large volumes of water necessary to conduct the experiments was required to stay on or near roads to ensure that it would not damage the area due to its heavy load, but a 27 meter hose allowed features to be tested that were away from the road or in areas of thick vegetation.

The five sinkholes studied at the J-17 Tract (Figure 12) are small soil-lined features with little topographic relief. J17SH1, J17SH2, and J17SH6 and their control plots are developed in the Person Formation, while J17SH3 and J17SH4 and their associated control plots and J17SC1 are developed in the Kainer Formation. The features tested at the J17 Fortune tract are generally in grassy areas with small shrubs, prickly pear cacti, small mesquite, ashe juniper, and oak trees. A contrast in the vegetation initially

prompted a closer inspection of the area where J17SH1 was discovered. J17SH1 is approximately 1.8 meters by 1.5 meters, with a depth of 10 centimeters (6 feet by 5 feet, with a depth of 4 inches). It is elongated in to the northwest and is one of three sinkholes that form a complex that trends N38W. No evidence of rapid recharge, i.e. vegetation bent towards the sinkhole or an abundance of leaf litter, was observed upon initial inspection of the feature. The soil in and around J17SH1 consists mainly of a grayish brown clay loam with some organic detritus. J17SH2 is 1.5 meters in diameter and 25.4 cm deep (5 feet in diameter and 10 inches deep). A large prickly-pear cactus growing in the sinkhole was subsequently removed so infiltration tests could be conducted with few impediments. The loose clay loam soil has an abundance of organic detritus, and there was no direct evidence of flow into the sinkhole. Few rounded, fist-sized cobbles were found at the surface of the sinkhole and around the feature in the immediate subsurface. J17SH3 is 1.8 meters by 1.5 meters and 15.24 centimeters deep (6 by 5 feet and 6 inches deep), with soil consisting of clay loam and organic detritus. Fist-sized, rounded cobbles were observed around the rim and base of the bowl at the surface and in the immediate subsurface. J17SH4 is 1.5 by 1.37 meters and 20.32 centimeters deep (5 by 4.5 feet and 8 inches deep). It is elongated in the NNE direction. J17SC1 is a solution cavity with an opening that is 1.37 by 0.91 meters (4.5 by 3 feet), elongated along a N55W trend. Initially, this solution cavity was completely filled with a silty clay loam soil. At the time water was applied to the feature, it had been excavated to a depth of 1.22 meters (4 feet) and resembled a cylindrical shaft. Further excavations have increased its depth to approximately 1.83 meters (6 feet), and have revealed a more horizontal component as the cavity widens on the east side. J17SH6 is 2.13 by 1.37 meters (7 by 4.5 feet), elongated in the east-west direction, and is 15.88 centimeters (6.25 inches) deep. Several

large rocks are present at the surface around the rim of the bowl. No open drain or any evidence of rapid flow to the sinkhole was detected.

Four sinkholes and their associated control plots were studied at Rutherford Ranch (Figure 13). RRSH1, RRSH3, and RRSH4 are developed in the Grainstone Member of the Kainer Formation, Edwards Group limestone, while RRSH2 is developed in the Leached and Collapsed Member of the Person Formation, Edwards Group limestone. RRSH1 is a broad, 2.44 by 2.59 meter (8 by 8.5 foot) shallow, 14.6 centimeter (5.75 inch) deep, sinkhole that was initially identified by a contrast in vegetation. Within the sinkhole, low grasses and lush green plants were common and desiccated algae were observed, while the surrounding area consisted mainly of waist-high plants and less lush grasses and no algae. Two larger features are located approximately 20 meters southeast of RRSH1, both distinguished by the vegetative contrast. RRSH2 is a relatively large sinkhole with a diameter of approximately 7.5 meters (25 feet). A large prickly pear cactus was removed from the sinkhole to facilitate the initial survey and infiltration tests. The base of the bowl contains an obvious drain filled with fist-sized angular cobbles. A three-foot-long soil probe was inserted into the drain to a depth of 0.6 meters (2 feet). Leaf litter accumulated near the drain and vegetation bent in the direction of the drain indicate rapid flow into the feature. It was previously identified in a 1999 Geologic Assessment by SWCA, Inc., Environmental Consultants and given the identification S-13, however, it will be referred as RRSH2 in this report. RRSH3 and RRSH4 are two of a complex of four sinkholes that trend WNW. RRSH3 is 2.29 by 1.83 meters (7.5 by 6 feet) and 17.78 centimeters (7 inches) deep and has fist-sized cobbles in the base of its bowl. RRSH4 is 2.13 by 1.68 meters (7 by 5.5 feet) and 15.24 centimeters (6 inches) deep with weathered rocks at the surface and in the

subsurface. Soil for both of these features is dominated by clay loam with some organic detritus.

Features studied at Honey Creek State Natural Area are located in Figure 14. HCSH1 is 2.13 by 1.22 meters (7 by 4 feet) and 15.24 centimeters (6 inches) deep. It is elongated to the NNE along a fracture zone that trends in the same direction and has several well developed solution cavities and many solution enlarged fractures. There were several 5 to 10 centimeter diameter rocks near the base of the bowl and the dominantly clay loam soil is between 5 and 20 centimeters thick over solid bedrock. HCJP1 is the area enclosed by the ring that surrounds a 6-meter tall ashe juniper. A mat of juniper leaf litter 10 centimeters thick surrounds the tree above the loose very dry clay loam soil. Roots and large rocks are common in the subsurface.

One sinkhole and its associated control plot were tested at Camp Bullis (Figure 15). This sinkhole was identified previously by Joe Ivy and George Veni in 1993 and was named 11B-83. It is 1.98 meters (6.5 feet) in diameter and 20.32 centimeters (8 inches) deep. This sinkhole is referred to as CBSH1 for consistency. The soil is dominantly a clay loam with chert fragments. CBSH1 is located in a thicket of ashe juniper and small oak trees.

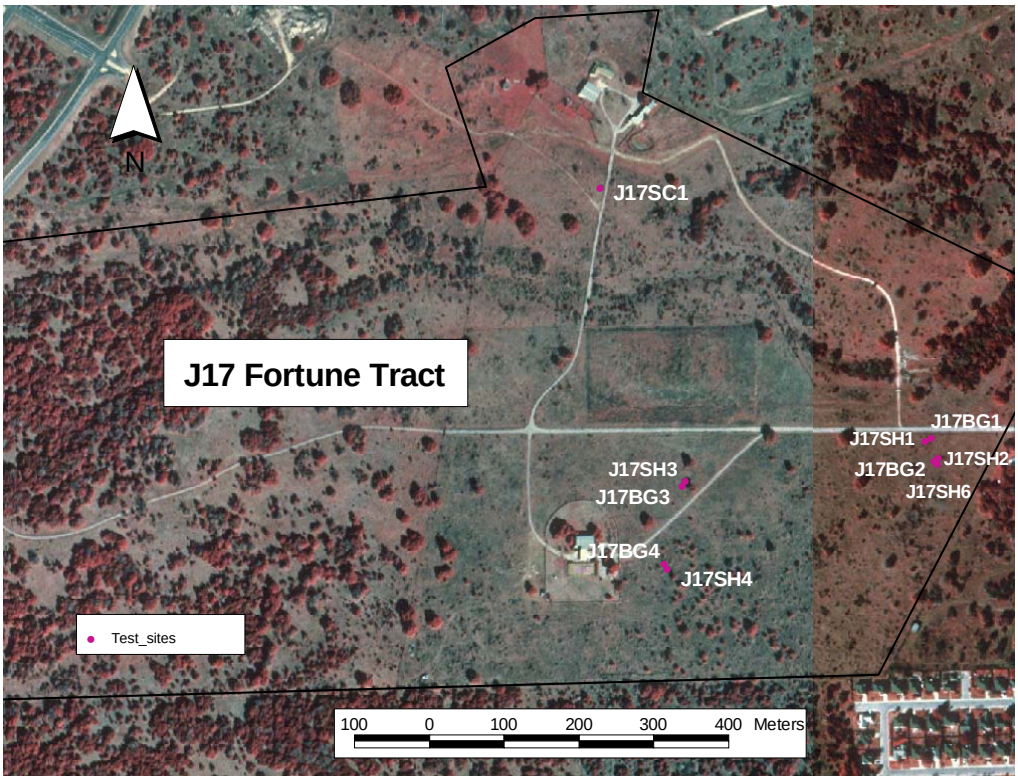

Figure 12. Map of J17 Fortune Tract and locations of tested features.

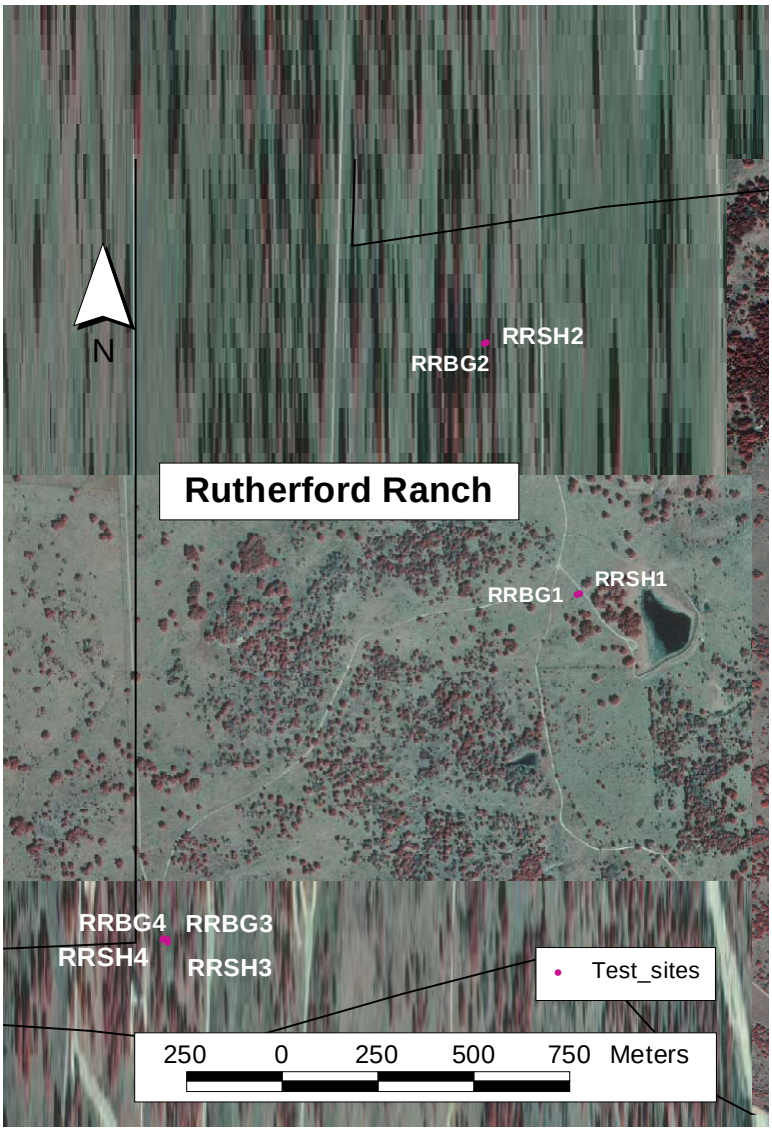

Figure 13. Map of Rutherford Ranch and locations of selected features.

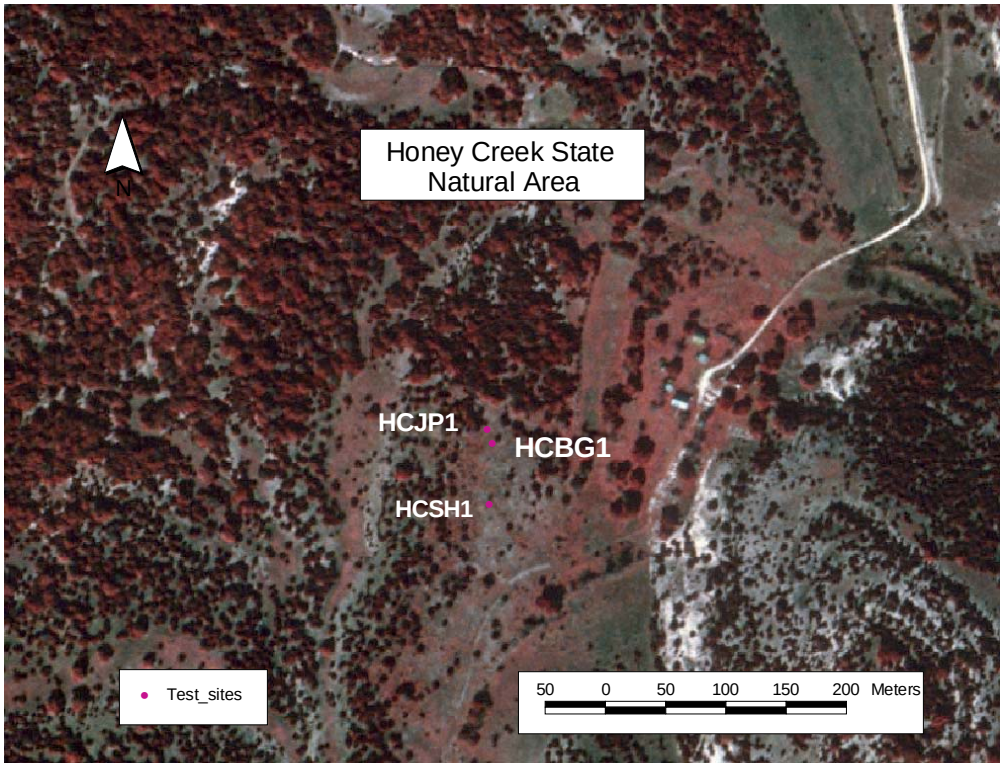

Figure 14. Map of Honey Creek State Natural Area and locations of features tested.

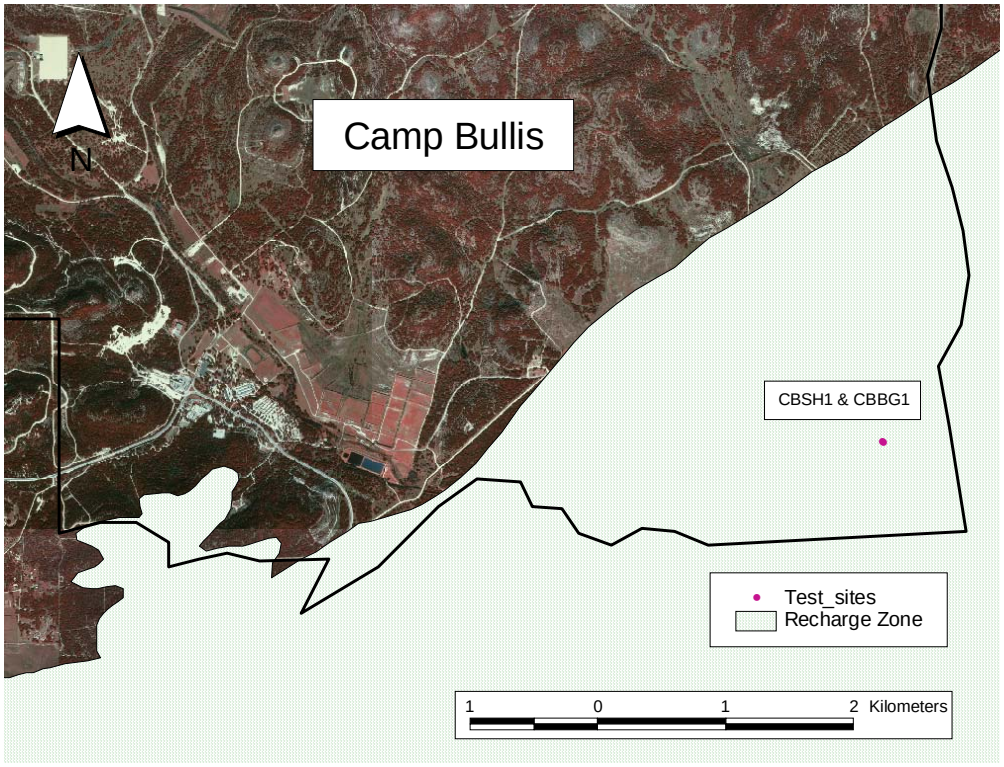

Figure 15. Map of Camp Bullis and locations of tested features.

Table 1. Location information for features tested. Eastings and northings are in meters for UTM zone 14.

Feature Name	*Easting*	*Northing*	*Feature Type*
J17SH1	608822	3338805	Sinkhole
J17BG1	608831	3338809	Background
J17SH2	608840	3338783	Sinkhole
J17BG2	608835	3338779	Background
J17SH3	608477	3338634	Sinkhole
J17BG3	608473	3338640	Background
J17SH4	608501	3338752	Sinkhole
J17BG4	608498	3338745	Background
J17SH6	608839	3338775	Sinkhole
J17SC1	608387	3339144	Solution Cavity
RRSH1	601639	3326183	Sinkhole
RRBG1	601631	3326179	Background
RRSH2	601393	3326872	Sinkhole
RRBG2	601389	3326868	Background
RRSH3	600549	3325234	Sinkhole
RRBG3	600553	3325235	Background
RRSH4	600562	3325226	Sinkhole
RRBG4	600563	3325234	Background
HCSH1	549805	3300732	Sinkhole
HCBG1	549807	3300782	Background
HCJP1	549803	3300793	Juniper Plot
CBSH1	545993	3278308	Sinkhole
CBBG1	545984	3278317	Background

2.3. HYDROLOGICAL EXAMINATION OF SINKHOLES

A ring infiltrometer is a device used to measure the infiltration rate directly of soil in a small area. Infiltration is a complex process that may be spatially as well as temporally variable. Single and double ring infiltrometers are two types of infiltrometers both consisting of a cylinder constructed of impermeable material (i.e. metal) which is driven into the ground in order to ensure that water applied infiltrates the area enclosed. Single ring infiltrometers include only one cylinder, while double ring infiltrometers include two different sized rings.

Constant head and falling head are the two main methods used to determine the infiltration rates using ring infiltrometry. Falling head tests involve measuring the amount of time required for a volume of water applied to an area to infiltrate. In a constant head test, the amount of water required to maintain a set water level is recorded as well as the time of application. The volume of water added to maintain a constant water level, and the time are recorded in a constant head test, while in a falling head test the time required for a volume of water to infiltrate, thus an initial head and final head, is recorded.

In unsaturated soils, capillary pressure and gravity both influence the movement of water applied to an area enclosed by a ring infiltrometer. This causes the wetting front to move vertically downward as well as laterally (Dingman, 2002). When water is applied to the area enclosed by both rings, the area between the larger and smaller ring acts as a buffer, so the infiltration rate measured in the smaller inner ring describes the vertical component rather than infiltration due to capillary action horizontally. In a single ring infiltrometer, lateral leakage will occur, but the effects are minimized by increasing the size of the ponded area. Thus, using a large-scale ring reduces the error expected from horizontal flow.

Ring infiltrometers are used to measure infiltration in a wide variety of situations. Under normal circumstances, ring infiltrometers are used to determine the infiltration parameters in soils for effective soil, water, and crop management not to determine the infiltration characteristics of large areas. One reason for the more common use of small ring infiltrometers is that they are small. This allows easy transport in the field and requires small amounts of water to conduct each test. The logistical problems associated with transporting the large volumes of water required to conduct large-scale ring

infiltrometry experiments to field sites is one of the reasons sinkholes have not been studied extensively with this technique.

Guelph permeameters can also be used to determine the *in-situ* unsaturated hydraulic conductivity in soils. This type of instrument also uses the constant head method to determine infiltration characteristics. It is easily transported and operated by one person in the field and requires a small amount of water. The downside to using this type of permeameter is that the area where water is applied to the unsaturated soil is small. Accordingly, it is likely that many of the expected heterogeneities in the soil and bedrock in a sinkhole cannot be observed with this technique. For this reason a large-scale single ring infiltrometer was used rather than a Guelph permeameter.

Ring infiltrometers are devices used to determine the infiltration rate of an area enclosed by an impermeable boundary. A metal ring is placed around an area of interest; which may include a sinkhole, defined by topography (Figure 16). The ring is inserted into the ground to minimize lateral leakage, and is accomplished by digging a trench to match the circumference of the ring and packing it with bentonite or other relatively impermeable material. Water is then added either to maintain a constant head, or allowed to fall in order to obtain an infiltration rate for the area enclosed by the ring. There are a few differences between using a ring infiltrometer for testing soils versus karst features. First, the infiltration rate of the sinkhole is limited by the capacity of any surface soil to transmit water to the zone of high vertical permeability (i.e., any soil that covers a drain in a sinkhole may effectively clog the preferred pathway and the infiltration rate for the feature will be the same as that of the soil). Second, though the infiltrometer measures an average infiltration rate for everything contained within the ring, heterogeneities within the soil and bedrock can dominate flow. To determine the function of sinkholes, it is necessary to test non-karst control plots to determine whether or not the heterogeneities

found in the topographic depressions of sinkholes are unique to the sinkholes or if they are common all over the landscape, and to determine the soil infiltration to look for higher rates as a result of high vertical permeability. Therefore, comparing the infiltration per unit head (1/hr) for sinkholes with that of control plots will lead to a relative understanding of infiltration in each scenario.

Infiltration is the process by which water enters the subsurface. Thus, the infiltration rate is the time required for a volume of water to enter the subsurface. Sinkhole infiltration is the process by which water enters the subsurface via features of a sinkhole (i.e., fractures or conduits) and can be defined as a rate, by the time required for a volume of water to enter the subsurface through these features. Infiltration is a function of the initial volumetric water content of the soil (volume of water in the soil/volume of soil) thus, to ensure that the sinkhole infiltration rate is being accurately measured, the soil must be saturated, and the maximum rate of infiltration of the soil (infiltration capacity) exceeded. When sinkholes are not present, and the water input rate exceeds the infiltration capacity, ponding occurs. Where sinkholes are present, and the water input rate exceeds the infiltration capacity of the soil, infiltration via features associated with sinkholes occurs, and the rate of infiltration can be measured. Four factors that must be quantified in order to determine the sinkhole infiltration capacity include: the volume of water added $\boldsymbol{V}$ (L^3), the time required for infiltration to occur $\boldsymbol{t}$, the area on which the water is added $\boldsymbol{A}$ (L^2), and the depth of ponding, or head $\boldsymbol{h}$ (L).

These four factors were quantified as part of a constant head ring infiltrometer test. After the ring is installed water is added to the enclosed area and allowed to pond. Water is continually added to the area in the ring to maintain a continuous level of water within the ring, or constant head, on the feature of interest. A paddlewheel flow meter (Omega model #1521) is used to determine the rate (V/t) that water is added to the ring,

which is controlled by manually opening or closing a ball valve. The flow meter is connected to a datalogger that is programmed to record the volume of water introduced to the ring and the time at 10-liter intervals every 5 seconds. The area on which water is applied is the area of the ring, which is π times the square of the radius of the ring (L^2). Thus, by dividing the volume per time by the area, a sinkhole infiltration rate is achieved (L/t):

$$IR = \frac{V_{water}}{A_{ponded} * T} \quad (3)$$

To normalize the infiltration rates of the various sinkholes, the rates are divided by their respective heads.

It is necessary to conduct experiments that sense the entire feature as defined by topography to account for all of the local heterogeneities in the soil and bedrock of the feature. Conducting large-scale ring infiltrometer experiments determines the hydrologic properties of the whole system of soil and bedrock within the ring. This is necessary to determine the function of karst features because fractures, conduits, or preferential flowpaths can be concealed by the overlying soil and may cover broad areas. Thus, a 2.75-meter or 3.65-meter (9-foot or 12-foot) diameter ring is used to ensure that the whole feature is being tested. Experiments are generally several hours in duration, which limits the impact caused by disturbances in the soil where the ring is inserted as well as the effects of lateral leakage, resulting in a more accurate infiltration rate for the area tested.

Two different set ups are used to conduct the ring infiltrometer experiments. Both systems are designed to ensure constant head on the feature/area of interest; the only difference is in how the water is supplied to the ring. The first setup uses a 6800-liter (1800-gallon) capacity water truck as the water supply reservoir, while the second involves pumping water from a 3800-liter (1000-gallon) collapsible water tank to an

elevated 200-liter (55-gallon) drum. Water supplied from either of these two reservoirs is ultimately gravity fed through a flow control section, where the paddle wheel flow meter is affixed, and into the ring. The flow control section is required to reduce turbulence and maintain laminar flow both up and down gradient from the paddle wheel, and is a 3-meter (10-foot) length of 5-centimeter (2-inch) diameter PVC up gradient and an 45.7-centimeter (18-inch) length of 5-centimeter (2-inch) diameter PVC down gradient from the flow meter.

Figure 16. Site set-up at the sinkhole J17SH2 is an example of typical ring infiltrometer installation.

2.4. MORPHOLOGICAL EXAMINATION OF SINKHOLES

Microtopography and soil thickness surveys were conducted for tested sinkholes and soil thickness surveys were conducted for control plots in order to better characterize the epikarst system at each location. These surveys were conducted by laying out a grid with a one-foot by one-foot spacing and taking elevation and soil depth measurements at the intersections of rows and columns within the grid. String wrapped around four posts that mark the boundaries of the grid were leveled using a line level, creating a datum from which topographic information could be measured. Soil thickness measurements were obtained by measuring the depth a soil probe could be pushed into the soil along the one-foot intervals of the grid. The soil probe is a "T" shaped, one-meter long steel rod, 1.25 centimeters in diameter which can be pushed into the soil with minimal effort. Microtopography and soil thickness measurements were transferred to a spreadsheet as Z coordinates with X and Y coordinates obtained from their respective positions in the grid. This information is then imported to Surfer 7.0 (www.goldensoftware.com), a software package that displays topography as a three dimensional wire frame surface and creates contour maps of the soil thickness that is then draped over the three dimensional surface. Vertical exaggeration depicted on wireframes is internally controlled by the Surfer 7.0 software package, and is generally x2.5 or x5.

2.5. EXAMINATION OF THE SUBSURFACE

The examination of the subsurface is necessary to ground truth the observations from the surface. The subsurface is examined using ground penetrating radar, dye tracing and excavating features, as well as grain size analyses for soils. One concern that these tests allay is the origin of features. It is difficult to determine the origins of these features be they karst or the product of past land management by surficial observation. Thus, using GPR and excavating features can confirm karst origin. Dye tracing allows

preferred flow paths in the soils be identified. Grain size analyses help determine the nature of soils.

2.5.1. Ground Penetrating Radar (GPR)

The use of GPR has been used extensively in areas of karst to detect major structural and solutional features in the subsurface. Bedrock, cave, medium and large sinkhole detection, and mapping studies have proven GPR a quick and inexpensive method for determining the degree and extent of karstification in the subsurface (Chamberlain, *et. al.*, 2000; Collins, *et. al.*, 1994; Barr, 1993; Benson and Yuhr, 1987). GPR surveys across sinkholes and control plots at the J17 tract were conducted during wet and dry conditions, to explore the geometry of the soil and bedrock as well as the distribution of water during artificial recharge. GPR data are collected for J17SH6 24 hours after water was applied. A SIR3000 GPR transmitter and 200Hz antenna are dragged over the surface of features and along perpendicular transects using the geology scan function. The data obtained from the GPR surveys are processed using two software packages: Seismic Processing Workshop and RADAN, which allowed the data to be viewed graphically.

2.5.2. Dye Tracing

The introduction of dye to the subsurface allows preferential flowpaths to be identified after subsequent excavations. Dye was allowed to infiltrate two sinkholes at the J17 Tract - J17SH2 and J17SH6. Initially, 200 gallons of water were used to wet the feature of interest. FD&C Blue No. 1 (referred to as dye) is a FDA certified colorant commonly used as a food coloring. One and a half pounds of powered dye was mixed in a 100-gallon water tank with an attached agitator. Once mixed completely, the dye was pumped into the ring and allowed to infiltrate with an additional 200 gallons of water to

help flush the dye into the soil. The excavation of dyed features entailed the removal of soil and loose rock down to the bedrock in the area previously enclosed by the ring. These subsequent excavations of these sinkholes allow the identification of preferential flowpaths where the blue dye is most visible.

2.5.3. Hydrometer Tests

The percent clay content of the soils at selected sinkholes and control plots was determined. Soil samples were collected at several sinkholes and control plots to determine the percent clay content grain-size analysis. A 151H is used to determine the grain size distribution of soil samples

Chapter 3: Results and Conclusions

3.1. RESULTS

The goal of these experiments was to determine the hydrological function of the soil and bedrock system of small sinkholes in the Edwards aquifer recharge zone. This included: determining the infiltration per unit head (1/hr) for sinkholes and non-karst control plots; ascertaining flowpaths for infiltrating waters in sinkholes, imaging the subsurface to establish whether these features were part of a more complex system, and catalog the geomorphological characteristics. A few assumptions were made about the nature of sinkholes and single ring infiltrometers to simplify the experiments. The first assumption is that the region of highest vertical permeability in a sinkhole is located in the lowest part of the sinkhole bowl. The expectation is that there are solutionally enlarged fractures or conduits across the bedrock surface throughout the recharge zone, but sinkholes will form only in areas where these features are concentrated, and where the maximum transport of sediments and solutes occur, the greater the topographic relief. The second assumption is that the vertical permeability is equal to or greater than the horizontal permeability in the subsurface, and that lateral leakage under the ring is minimized with the use of bentonite. In an assessment of recharge in arid environments, Scanlon, *et. al.* (1999) concluded that, despite being clay filled, small subtle topographic depressions are the locus of high mean water fluxes based on mean chloride concentrations and high water potentials found in these features.

3.1.1. Infiltration Measurements

The results for ring infiltrometery for ten small sinkholes and their associated control plots using the ring infiltrometery method are presented in Table 2. J17SH2 and J17SH6 share a control plot due to their close proximity to one another. The miscellaneous feature results and their associated control plots tested using the ring infiltrometer method, including one medium sinkhole, one solution cavity, two excavated small sinkholes, and one juniper plot are presented in Table 3. Head values are not included for the miscellaneous features because; either a constant head could not be maintained, as in the medium sinkhole, excavated solution cavity, and juniper plot, or only enough water was used to cover the surface of the bedrock as in the excavated sinkholes.

Table 2. Ring infiltrometry results. Infiltration rates normalized for depth of ponding.

Feature name	*feature type*	*Head (cm)*	*infiltration per (cm) unit of head (1/hr)*
J17BG1	Background	12.70	0.31
J17BG2	Background	10.16	0.24
J17BG3	Background	12.70	0.06
J17BG4	Background	10.16	0.21
RRBG1	Background	10.16	0.40
RRBG2	Background	10.16	0.18
RRBG3	Background	10.16	0.43
RRBG4	Background	10.16	0.25
HCBG1	Background	12.70	0.19
CBBG1	Background	9.53	0.89
J17SH1	Sinkhole	13.97	0.06
J17SH2	Sinkhole	30.48	0.15
J17SH3	Sinkhole	20.32	0.11
J17SH4	Sinkhole	22.23	0.20
J17SH6	Sinkhole	20.32	0.35
RRSH1	Sinkhole	16.51	0.08
RRSH3	Sinkhole	19.05	0.24
RRSH4	Sinkhole	20.32	0.29
HCSH1	Sinkhole	17.78	0.44
CBSH1	Sinkhole	17.78	0.35

Table 3. Ring infiltrometry results of miscellaneous features.

Feature name	***Feature type***	***Average infiltration rate (cm/hr)***
J17SH2	exc. Sinkhole	0.16
J17SH6	exc. Sinkhole	0.42
RRSH2	med. Sinkhole	5.69
J17SC1	solution Cavity	3.44
HCJP1	juniper plot	6.31

3.1.2. Morphological

Sinkhole microtopography and soil thickness maps are presented in Appendix A. Soil contour maps created from soil thickness surveys has been draped over the three-dimensional wireframes to show the distribution of soils relative to elevation. Statistical information collected on each feature includes the average depth and average soil depth for sinkholes (Table 4), and the average soil depth for control plots (Table 5). The maximum topographic relief and the average depth of each sinkhole were used to calculate the infiltration per unit of head (1/hr). The average depth was not calculated for J17SH6 because it was excavated prior to the microtopographic and soil thickness survey and CBSH1 because it was partially excavated prior to hydrologic testing.

Table 4. Physical characteristics of sinkholes obtained by microtopographical and soil thickness surveys. Note: sinkhole J17SH6 was not surveyed.

	dimensions						
Feature Name	x (m)	y (m)	z (cm)	Average Soil Thickness (cm)	Average Depth (cm)	max length/max depth	Ratio (length:depth)
J17SH1	1.83	1.52	13.335	9.18	6.18	29.61	30 : 1
J17SH2	1.52	1.52	21.59	10.87	6.88	22.09	22 : 1
J17SH3	1.83	1.52	17.15	10.26	5.95	30.76	31 : 1
J17SH4	1.52	1.37	17.15	10.61	9.31	16.33	16 : 1
J17SH6	2.13	1.37	15.88			13.41	13 : 1
RRSH1	2.59	2.44	19.05	32.92	11.29	22.94	23 : 1
RRSH2	7.62	7.62	43.18	11.96	14.15	53.85	54 : 1
RRSH3	2.29	1.83	24.13	14.18	14.95	15.32	15 : 1
RRSH4	2.13	1.68	19.69	24.15	6.99	30.47	30 : 1
CBSH1	1.98	1.98	55.88	19.48	25.74	7.69	8 : 1
HCSH1	2.13	1.22	16.38	11.03	4.43	48.08	48 : 1

Table 5. Control plot average soil thickness obtained from soil surveys and statistical analysis in Surfer 7.0.

Feature Name	Average Soil Thickness
J17BG1	12.28
J17BG2	13.72
J17BG3	19.85
J17BG4	17.55
RRBG1	22.48
RRBG2	10.92
RRBG3	17.78
RRBG4	31.07
CBBG1	8.19
HCBG1	4.67

3.1.3. Geophysical

Processed radar profiles from one sinkhole at the J17 Tract are presented in Figure 9. All other sinkhole and control plot transects are presented in Appendix B. In each radar profile, the vertical scale is a time scale, and the horizontal scale is distance along the surface. Using the RADAN software package, profiles were surface normalized, color transforms were applied, and the range gain was set to one. The Seismic Processing Workstation software package was used to only to display the data with simple red and blue color transform.

Many of the perpendicular transects run over each of the sinkholes at the J17 Fortune tract failed to indicate an anomaly that may indicate the presence of a void, with the exception of the north to south transect for J17SH1, shown in Figure 17. In this transect, the center of the sinkhole is located at the 20 ft. tick mark, and the surface expression of the sinkhole extends three feet to either side of the center. The color transform selected using the RADAN software package shows areas of high dielectric contrast where white and gray are adjacent to one another. The high contrast shown in

this transect signifies an abrupt change in the material in the subsurface which may indicate the presence of a void.

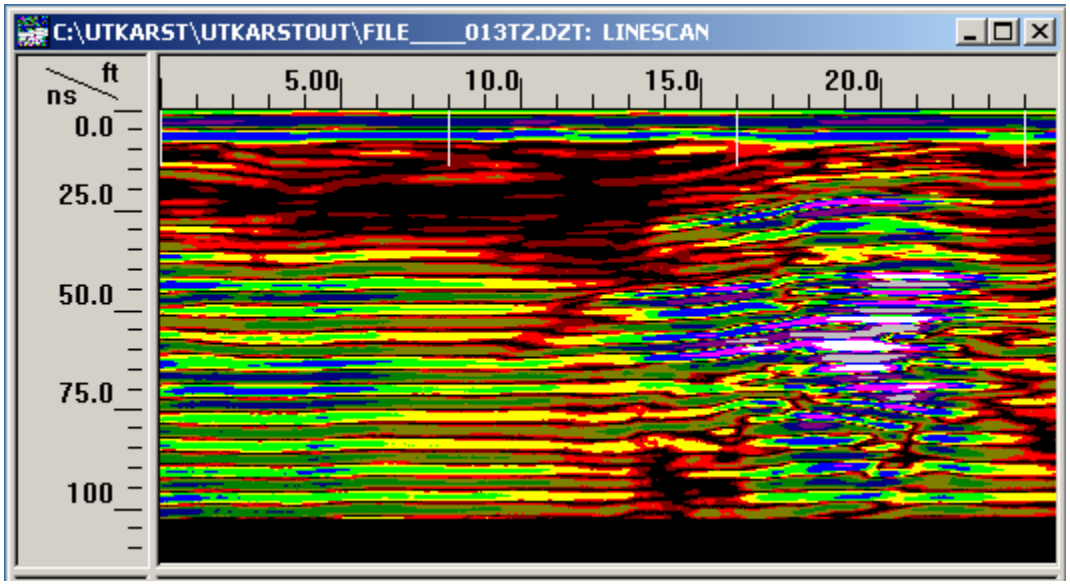

Figure 17. Image of the subsurface beneath J17SH1 obtained using GPR under dry conditions. Center of sinkhole is 20 ft. from left. High contrast in the dielectric is represented by white and gray, which may indicate a soil/air interface, indicating possible void.

3.1.4. Sources of Error

Error arises when the average topographic relief from surveys (square) is applied to the circular area of the ring. This results in a slightly lower estimation of the amount of head applied to the feature enclosed within the ring, thus a slightly higher infiltration rate is calculated when the average head is used. This is likely less erroneous than using the maximum depth of a sinkhole as the amount of head applied to the feature. Leakage under the ring is always a source of error when using ring infiltrometers as is the development of preferred flowpaths along the interface between the ring and soil, which is why double ring infiltrometers are used to create a buffer zone around the inner area of

interest. Error associated with lateral leakage is function of the ratio between the area enclosed by the ring and the circumference of the ring. For example; a typical small ring infiltrometer 30 cm in diameter has an area of 706.5 cm^2, and a circumference of 94.2 cm, thus a ratio of 7.5:1, while a large ring infiltrometer 2.74 meters in diameter has an area of 58934.7 cm^2 and a circumference of 860.4 cm, thus a ratio of 69:1. Lateral leakage out of the ring does occur, but the effect of which is greatly reduced with an increase in the size of the ring.

3.2. DISCUSSION

The first analysis of the infiltration data assumes that the deepest point in a sinkhole is the area with highest permeability. Consequently, the results show that many of the control plots have a somewhat higher infiltration per unit head (1/hr) than their associated sinkholes when the variation in topography is ignored and the maximum depth of ponding is assumed as the deepest point in the depression from which head is measured. The average infiltration per unit head for tested sinkholes at the J17 Fortune tract, using the maximum sinkhole depth is 0.13 1/hr, just below the permeability range (0.15 – 0.50) for the Speck stony clay loam (Werchan, *et. al.*, 1974), but was 0.24 1/hr when using the average depth of ponding. The average infiltration per unit head for background plots at J17 is within the soil's range with a value of 0.205 1/hr. Similarly, average infiltration per unit head values for sinkholes at Rutherford Ranch, 0.203 1/hr using maximum depth and 0.37 1/hr using average depth, are within the Rumple-Comfort association range of 0.15 – 0.50, as is the average background infiltration per unit head of 0.278 1/hr. The results from Table 2 have been plotted in Figure 18 comparing the infiltration per unit head (1/hr) of small sinkholes with paired control plots. The one to one line that bisects the graph separates the pairs of features as those in which sinkhole infiltration is higher than control plot, above the line, from those in which the infiltration

of the control plot is higher than its paired sinkhole, lower than the line. The different symbols, diamond, square, triangle, and circle, represent the different field sites.

The plotted results in Figure 18 do not indicate any pattern in the paired sinkhole and control plot infiltration rates related to location or geology. Sinkholes and control plots are similar in that either one can have a relatively higher infiltration rates than the other but both are variable. Overall, infiltration rates are low and generally within the range of the soil.

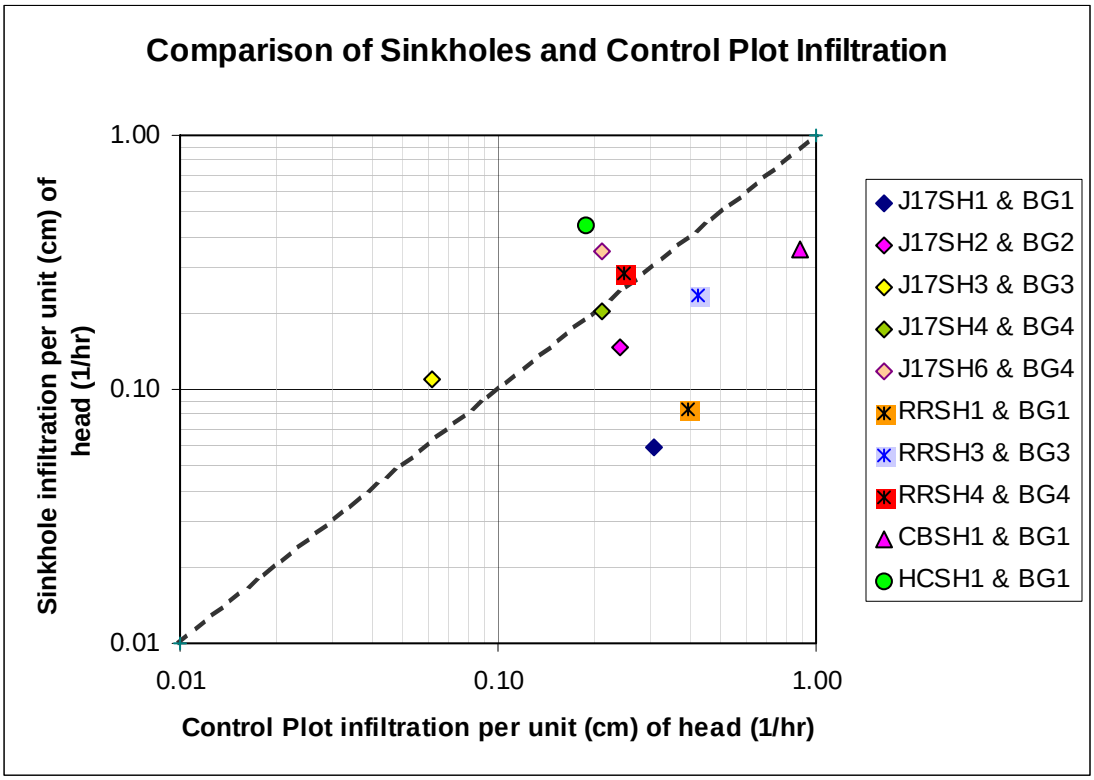

Figure 18. Infiltrometry results using maximum depth as applied head.

However, this may not represent infiltration under natural conditions. Under natural conditions, water will pond in the small soil-lined sinkholes. The variable topography between the flat lying land and the bowl of the sinkhole generates a

continuum of head values within the bowl. For this reason, the average depth for a sinkhole is may be used to determine more natural representative infiltration characteristics (Figure 19). The average depth is calculated using data collected from the Microtopographic survey and Surfer 7.0 (Table 6).

Table 6. Infiltration rates obtained using maximum and average depth of sinkholes.

feature name	*head applied using maximum depth*	*head applied using average depth*	*(max depth) infiltration per unit head (1/hr)*	*(average depth) infiltration per unit head (1/hr)*
J17SH1	13.97	6.815	0.06	0.12
J17SH2	30.48	15.77	0.15	0.28
J17SH3	20.32	9.12	0.11	0.25
J17SH4	22.23	14.39	0.2	0.31
RRSH1	16.51	13.19	0.08	0.11
RRSH3	19.05	19.05	0.24	0.24
RRSH4	20.32	7.62	0.29	0.76
HCSH1	17.78	5.83	0.44	1.35

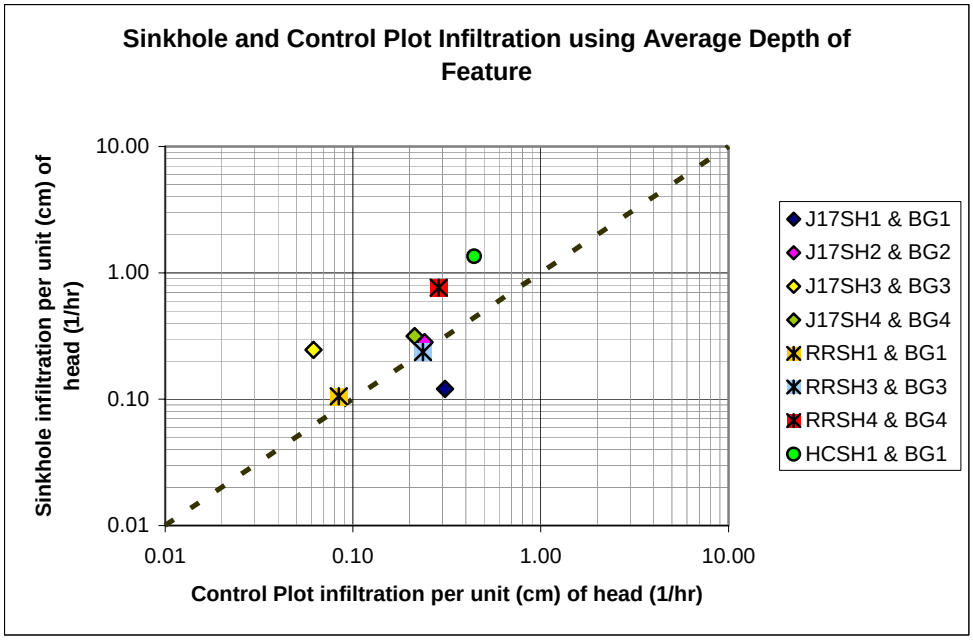

Figure19. Infiltrometry results using average depth as applied head.

Using the average depth of sinkholes as the base elevation to calculate the amount of head applied shows a more systemic distribution of infiltration values. The sinkhole infiltration is slightly higher than paired control plots when head is normalized this way.

Miscellaneous features tested had infiltration rates higher than their control plots (Figure 20) and the one-to-one line is not displayed on the graph. It is important to note that the solution cavity (J17SC1, light blue square) tested had been partially excavated prior to ponding water on the feature. It is likely that the infiltration per unit head (1/hr) would be slightly lower if the feature had been tested prior to excavation, and it is also likely that the infiltration per unit head (1/hr) would be higher if a cave is revealed after further excavations. Similarly, the medium sinkhole (RRSH2, pink dot) tested had a drain choked with small rocks and plant debris when tested. After a limited amount of excavation, a large open fracture was revealed and it is unlikely that water could be ponded over the feature using the ring infiltrometer method.

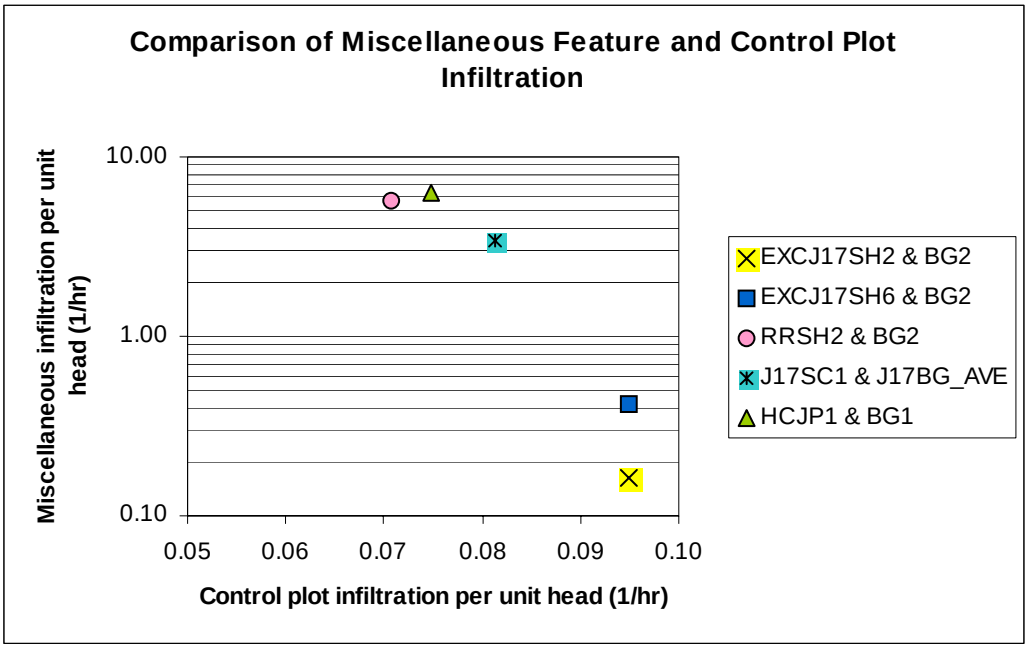

Figure 20. Miscellaneous feature infiltrometry results.

It is likely that these features experience cycles of soil-dominated infiltration when plugged and rapid infiltration when the plug is removed by natural processes, like soil sapping, only to become plugged once again when a choke develops further down in the drainage network. These are immature incipient features that will eventually become larger more significant features.

Although not in the Edwards recharge zone, features at Honey Creek Natural State area were tested. Rainfall simulation studies conducted by Clyde Munster of Texas A&M and his students indicated that recharge rates were significantly higher than the permeability range for the soils in the area (Taucer, *et. al.*, 2005, Gregory, 2005). Small sinkholes, solution cavities, and caves are common in the area. If soil is the factor that dominates the infiltration of small sinkholes in a karst terrain, then a similar relationship should be visible in the rainfall simulations. Rainfall simulations were conducted over a 7 by 14 meter area that contained several ashe juniper trees. The infiltration rates obtained by varying the intensity of simulated rain events over the juniper test plot ranged between 1 and 9.25 cm/hr (Gregory, L., personal communication, 2005). These values are orders of magnitude higher than those obtained with the ring infiltrometer, thus it was deemed necessary to determine the reason for the large discrepancy. A small sinkhole, 60 meters away, and control plot, 15 meters away, was tested using the ring infiltrometer to compare the infiltration characteristics obtained by the two methods. The resulting infiltration per unit head (1/hr) obtained for the sinkhole (0.44) and control plot (0.19) is comparatively low. Using the ring infiltrometer on an area that contained an ashe juniper tree revealed the source of the discrepancies. The infiltration rate obtained for the juniper plot using the ring infiltrometer method included a maximum value of over 10 cm/hr during the initial addition of water and an average sustained value, after the initial wetting of 6.31 cm/hr. Severe lateral leakage was observed 20 minutes after the

experiment was initiated. Water began upwelling several feet outside of the juniper plot around the ring. This is the ponded water flowing through preferential flow paths created by the tree roots in the shallow subsurface.

Under natural conditions, small sinkholes pond water during rain events (Figure 21). As ponding occurs, the increase in head from ponding increases the infiltration per unit head (1/hr), allowing a larger volume of water to infiltrate to the subsurface. As there is little runoff and ponding rarely occurs at non-depressed areas, areas of little relief do not benefit from this increase in head. Thus, maintained microtopography indicates an area where recharge is relatively larger than non-depressed areas.

Figure 21. Naturally occurring ponding in a sinkhole during a rain event at the J17 Fortune tract.

Figure 22. Dye tracing at J17SH2 indicate flowpaths along roots and the interface between soil and rocks in the subsurface.

Dye tracing experiments and subsequent excavations of sinkholes served three purposes. First, observations of dye in the soil and on the bedrock provided clues as to what the dominant types of flowpaths exist in the near surface. Dye was observed mainly along plant roots small, grass roots, and large, cacti and small brush, and along the interface between rocks and soil in the subsurface (figure 22). Along the surface of the bedrock, dye was observed along fractures and around solutionally enlarged fractures and conduits. Second, due to initial infiltration rates from ring infiltrometer tests, concerns arose that the depressions observed were not in fact karst features, but were the product of previous land management. Excavating sinkholes in order to look for the zone of high vertical permeability or drains allayed these concerns because fractures and solutionally enlarged vertical conduits were observed (Figure 23). Third, excavating these two

sinkholes allowed further infiltration tests to be conducted with the soil removed. The resulting infiltration per unit head (1/hr) is only slightly higher than when soil is present (J17SH2 – J17SH exc. and J17SH6 – J17SH6 exc., Tables 2 and 3), which indicates drains are plugged by soil in the subsurface. This may also indicate that active soil piping is occurring.

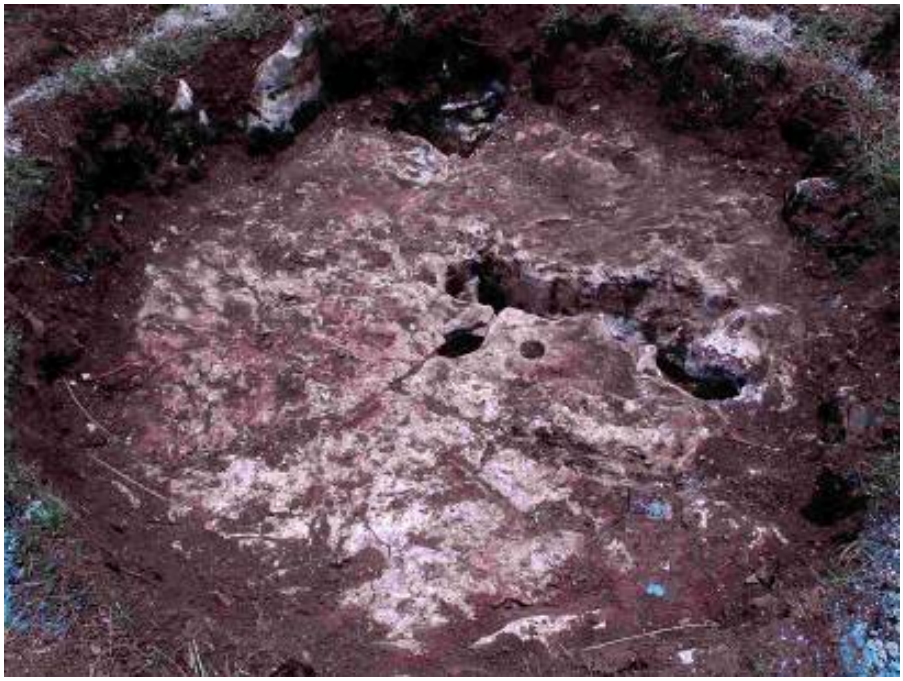

Figure 23. Excavating small sinkholes (J17SH2 shown) reveals solutionally enlarged fractures and conduits that provide pathways for preferential flow into the subterranean drainage network beneath small sinkholes in the Edwards Aquifer recharge zone.

Ground penetrating radar results were somewhat mixed. One void is interpreted for the GPR data, and though there may be some evidence of karst features in the subsurface, much of the data shows banded areas where the radar signal has been dramatically attenuated. This attenuation of signal may be due to saturated conditions in the subsurface or the clay content in the soil. The sinkhole imaged wet (J17SH6, appendix B) did indicate an anomalous region in the subsurface, though the contrast is

somewhat less than the interpreted void at J17SH2, this may be due to water filling the void. Signals travel slower in water than in air, thus a void filled with water may not show as much contrast as an empty void. Images of several other sinkholes show bands that seem to bow up. This is probably due to dragging the antenna through the sinkhole. When the antenna is on the sloped sides of the sinkhole, more time is required for the signal to reach the same unit than when the antenna is perpendicular.

Maintenance of numerous small sinkholes suggests that active karst processes such as soil sapping are focused by karst and epikarst development. Experience of local karst experts suggest that the excavation of these subtle features will lead to the discovery of more extensive karst features, including some potentially enterable caves, yet GPR over tested features indicate few voids in the subsurface. This lack of voids imaged by GPR may indicate a GPR sensitivity issue in that voids may be deeper than what is imaged using the current equipment and methods, or that voids may be too small to be detected. It is also possible that one large void detected out of five sinkholes imaged is a plausible expected ratio of large voids to surface expressions of karst.

The results of this study should not be overextended to include all aspects of the karst landscape. Three of the features tested using the methods described above show orders of magnitude higher infiltration than background. One, a medium sized sinkhole, that when excavated, revealed a large open conduit that was partially blocked near the surface. Another, a partially excavated large solution cavity, or well-shaped sinkhole, that after further excavation, showed a more horizontal component and overall enlargement, which may eventually come to be considered a proper cave. In addition, many well known and well documented karst features exist in the uplands of the Edwards aquifer recharge zone that have significant communication with the subterranean drainage network, including the aquifer, and have a high potential for recharge that are

both beyond the scope of this project and impossible to test using the methods described herein. And the area surrounding an ashe juniper tree had the highest infiltration rate of all the features studied. However, much of the water applied was quickly discharged from the subsurface around the tree, this indicates a more complex drainage system, with different types of vegetation providing recharge to the near subsurface via fractures and conduits created by the development of their root structure.

3.3. CONCLUSIONS

Small sinkholes are ubiquitous in the uplands of the Edwards aquifer recharge zone where much of the urban development is currently taking place. These incipient features are examples of the early steps in the evolution of karst terrains. In several study areas, these features exist near well-developed caves. This suggests that they are in the early stages of development on their way to becoming a larger more mature feature or they are features whose drainage is being pirated by the large aperture well connected subterranean drainage network and are being incorporated by a larger more mature feature.

Experiments show that soil dominates the infiltration process at these features. Tests conducted at four field sites including the use of a large-scale ring infiltrometer, the application of dye into soil-lined sinkholes and their subsequent excavation, and GPR demonstrate that the few centimeters of clay loam soil dominate infiltration of the soil/bedrock system. The numbers show that infiltration at these features is sensitive to the amount of head assumed. The best assumption for head relied on using feature average depth. Using this assumption, infiltration at sinkholes was only slightly higher than the background plots. Under natural conditions, these small, soil-lined sinkholes do not provide rapid recharge to the aquifer, they provide recharge somewhat more quickly than background, and recharge is more sustained when ponding occurs. Though

preferred flowpaths exist in the subsurface, these fractures and conduits are apparently plugged by the naturally occurring clay soils common in the uplands of the recharge zone.

Subtle karst features are significant for recharge because of their maintained microtopography. When ponding occurs, the increase in head allows a larger volume of water to infiltrate than areas where no ponding occurs.

Appendix A

Appendix A is the graphical representation of the microtopography for each sinkhole tested. All figures in appendix were created using the graphics software Surfer 7.0. Contour maps created show the soil thickness obtained from soil thickness surveys and draped over wireframes depicting sinkhole microtopography indicate the distribution of soils over karst features. Contour maps for control plots are also included. All wireframes, contour maps, and color scales are in centimeters. Each sinkhole has three images. The first is a wireframe of the microtopography. The areas in red indicate areas of greatest depth. The second is a contour map of the soil thickness. These contour maps show the areas where soil is thickest in white. The third image is the soil thickness contour map draped on top of the wireframe, which shows the soil thickness relative to the bowl. The scales are different in each wireframe for each sinkhole and in each soil thickness contour map for each sinkhole and control plot. For control plots, only a soil thickness contour map is created.

SINKHOLES

J17SH1

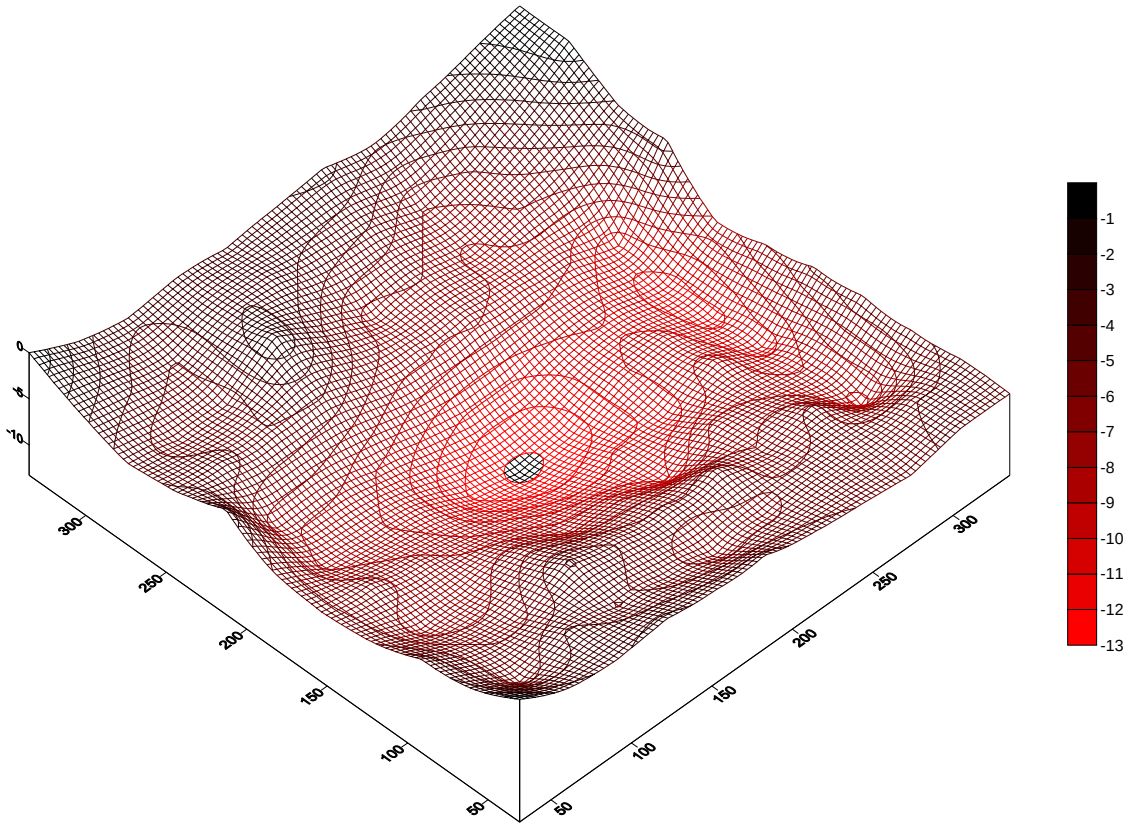
0
-1
-2
-3
-4
-5
-6
-7
-8
-9
-10
-11
-12
-13
300
250
200
150
100
50

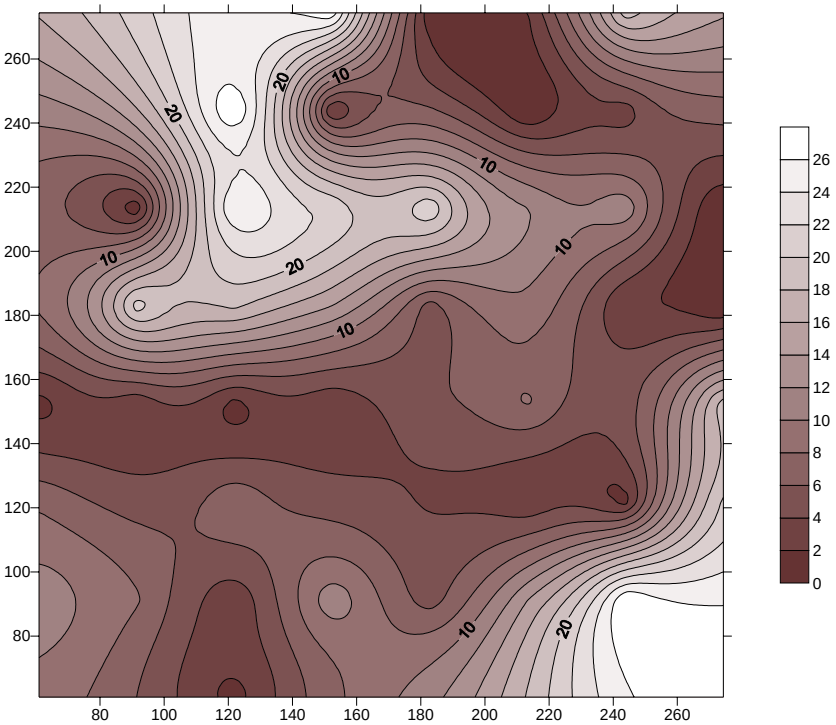
260
240
220
200
180
160
140
120
100
80
10
20
26
24
22
20
18
16
14
12
10
8
6
4
2
0

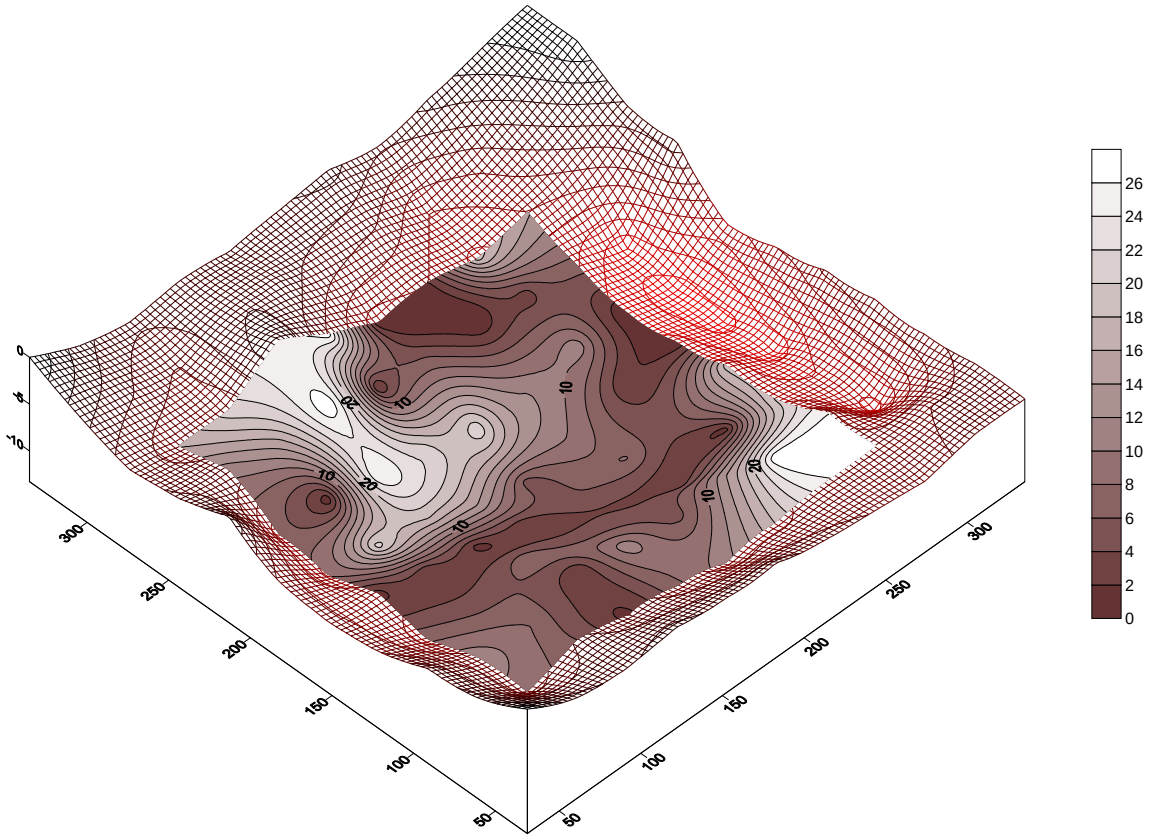
0
4
8
50
100
150
200
250
300
10
20
26
24
22
20
18
16
14
12
10
8
6
4
2
0

J17SH2

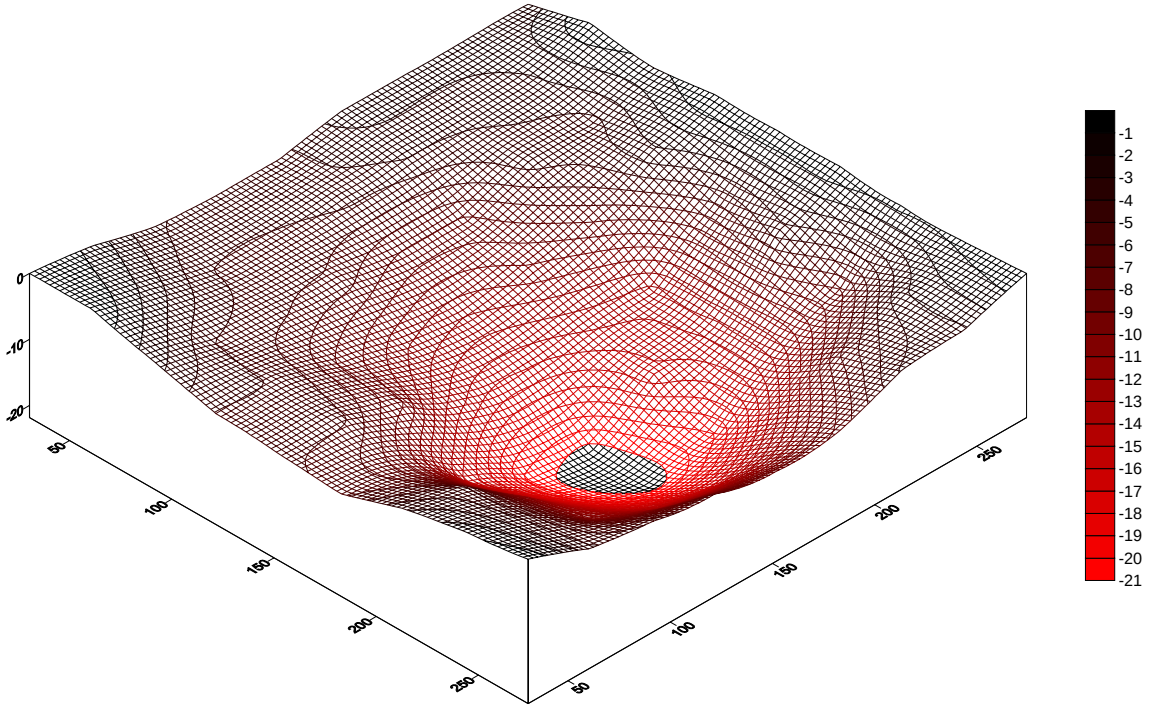
0
-10
-20
50
100
150
200
250
-1
-2
-3
-4
-5
-6
-7
-8
-9
-10
-11
-12
-13
-14
-15
-16
-17
-18
-19
-20
-21

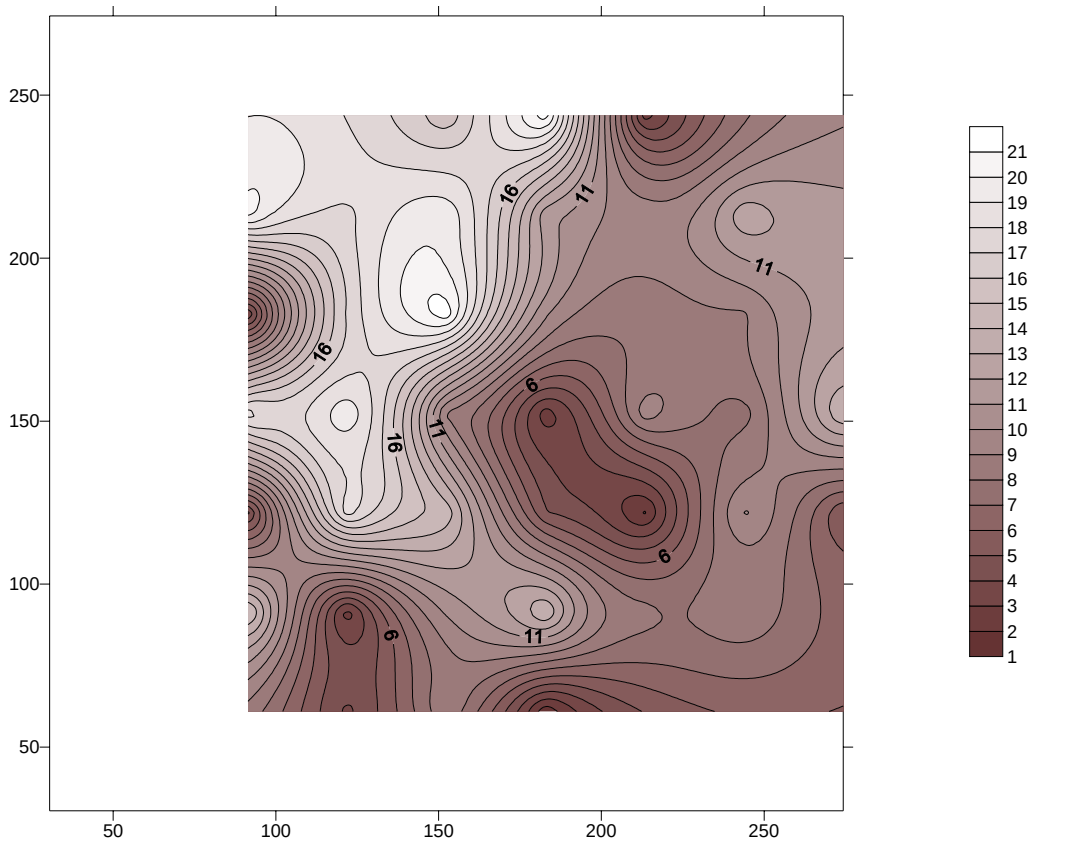
250
200
150
100
50
50
100
150
200
250
16
11
11
16
6
16
11
6
6
11
21
20
19
18
17
16
15
14
13
12
11
10
9
8
7
6
5
4
3
2
1

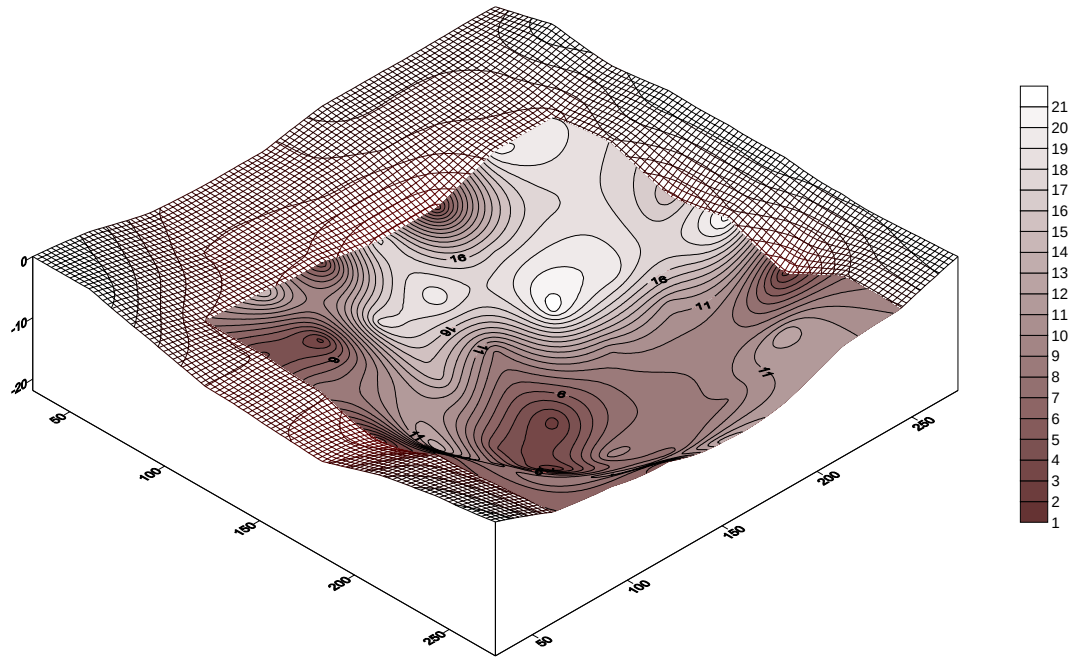
0
-10
-20
50
100
150
200
250
16
16
11
11
6
6
11
11
21
20
19
18
17
16
15
14
13
12
11
10
9
8
7
6
5
4
3
2
1

J17SH3

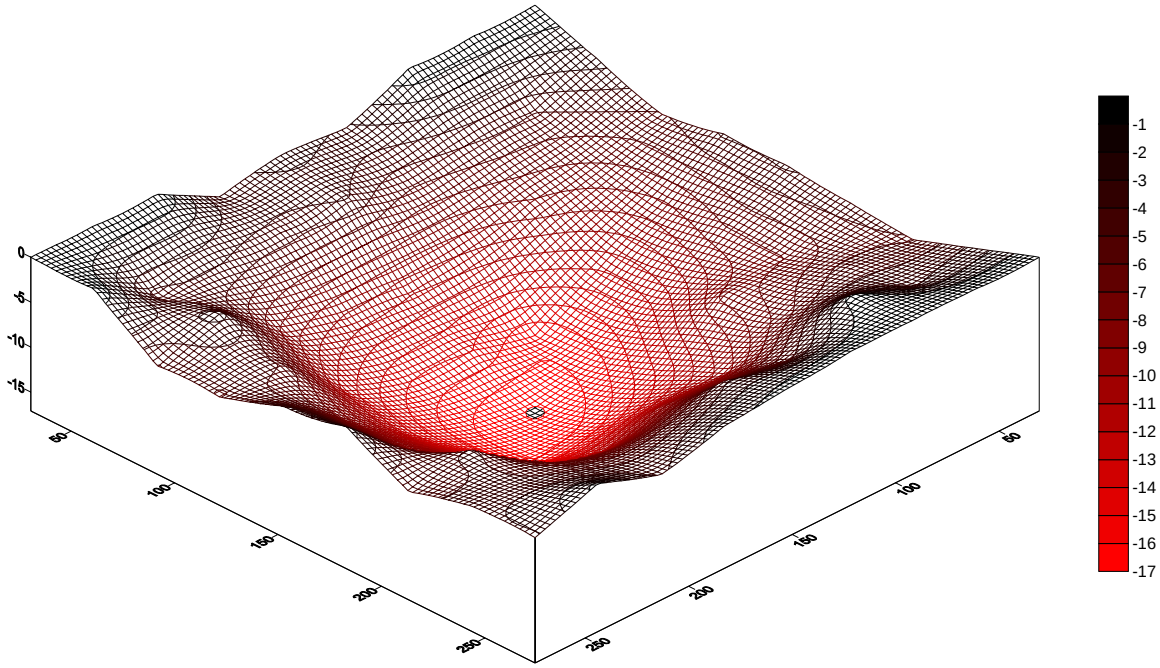

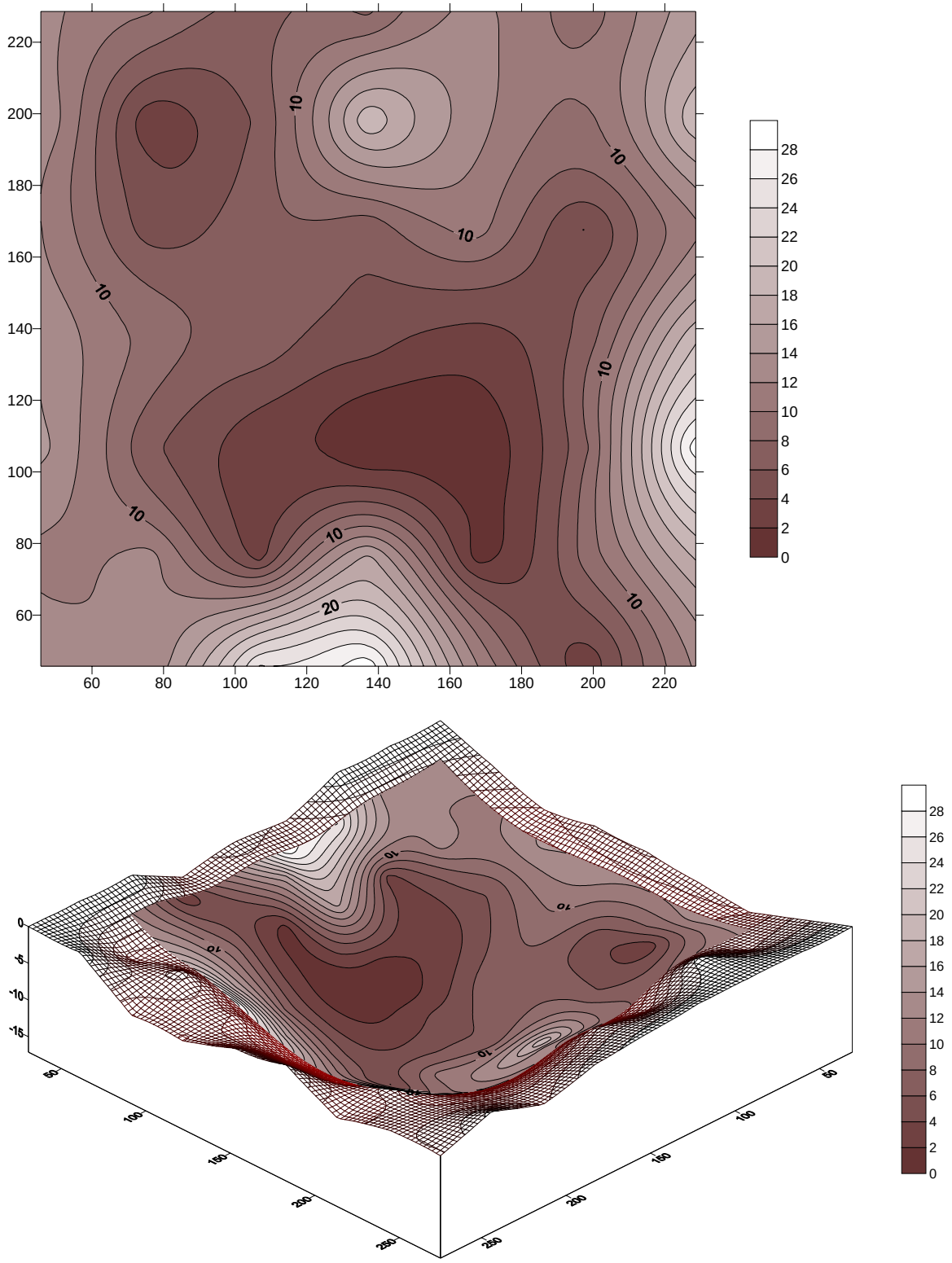
220
200
180
160
140
120
100
80
60
60
80
100
120
140
160
180
200
220
10
10
10
10
10
10
10
20
28
26
24
22
20
18
16
14
12
10
8
6
4
2
0

J17SH4

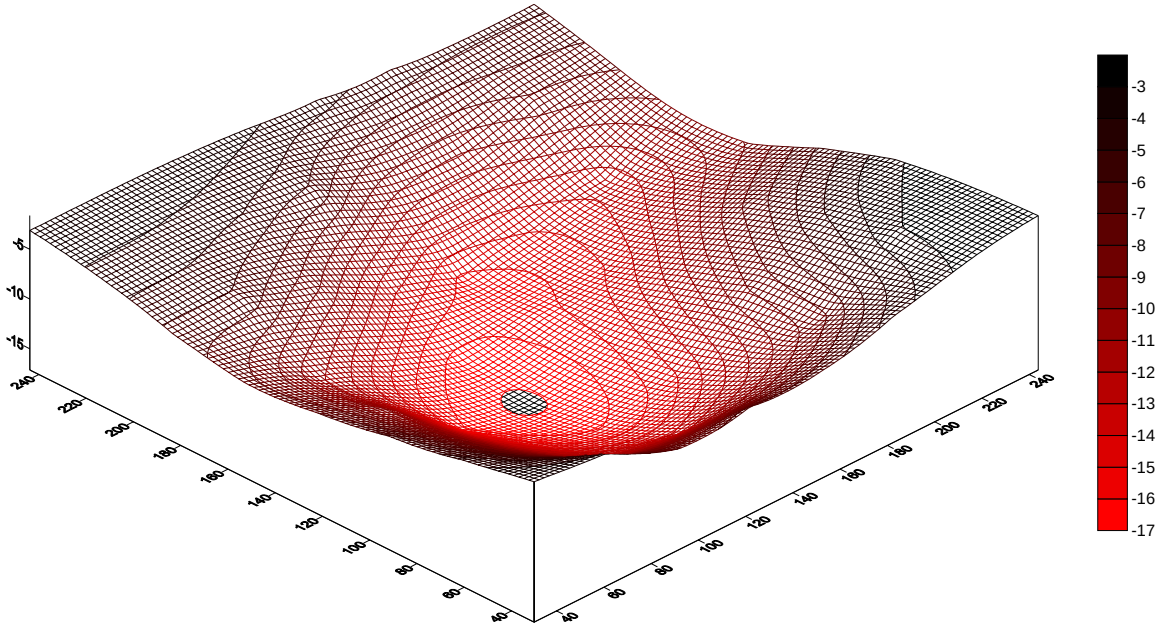
-3
-4
-5
-6
-7
-8
-9
-10
-11
-12
-13
-14
-15
-16
-17

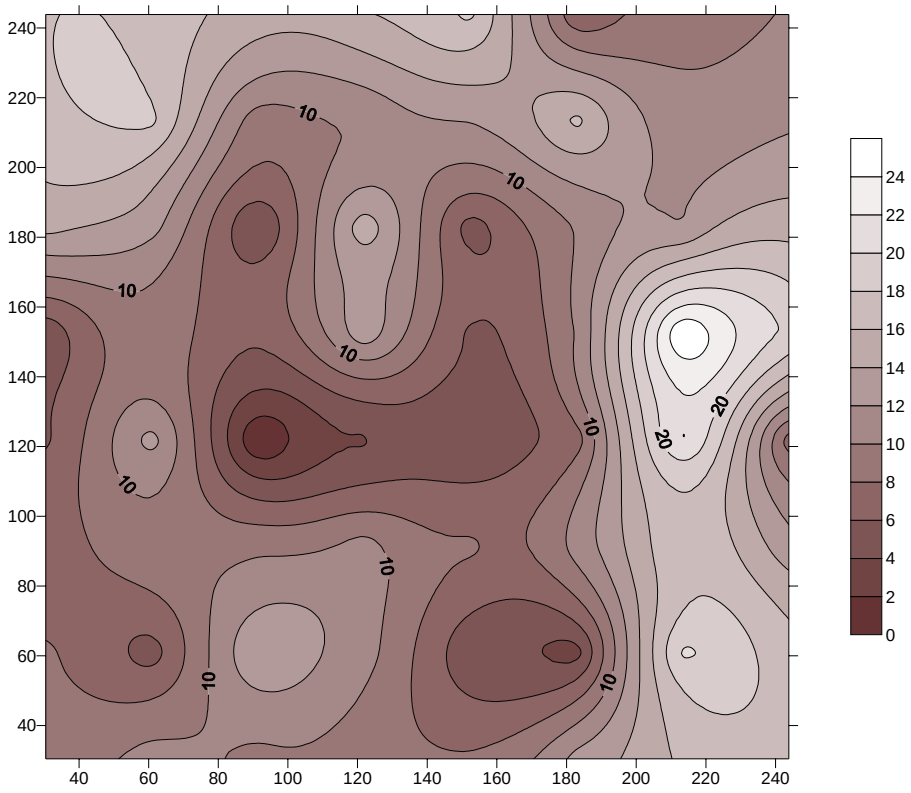
240
220
200
180
160
140
120
100
80
60
40
10
20
24
22
20
18
16
14
12
10
8
6
4
2
0

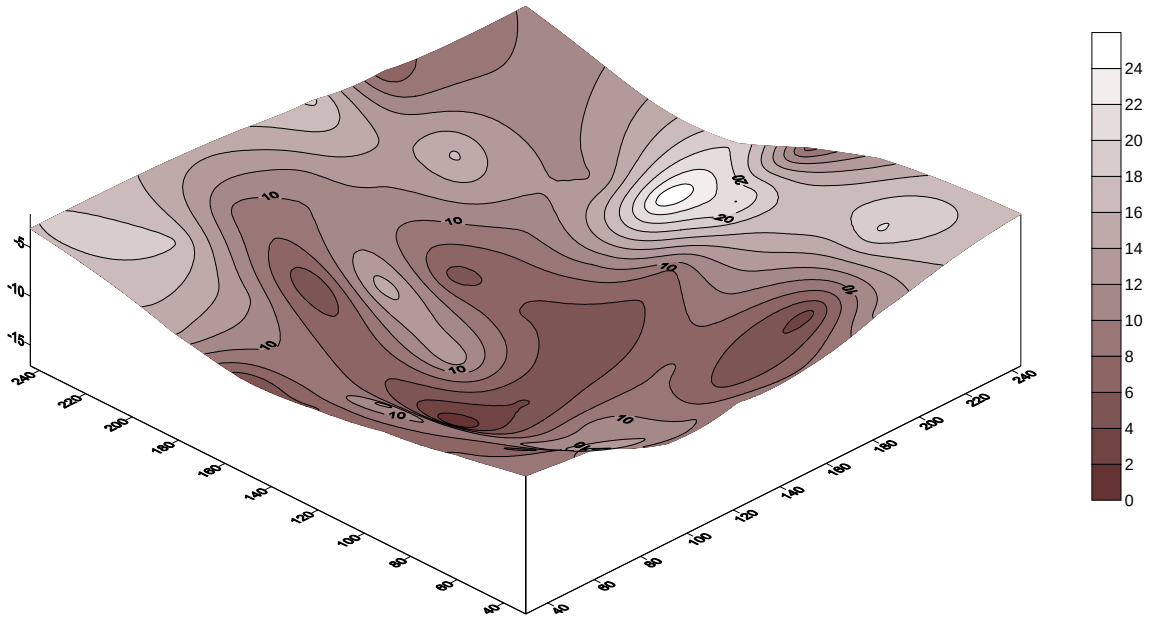
24
22
20
18
16
14
12
10
8
6
4
2
0
240
220
200
180
160
140
120
100
80
60
40

RRSH1

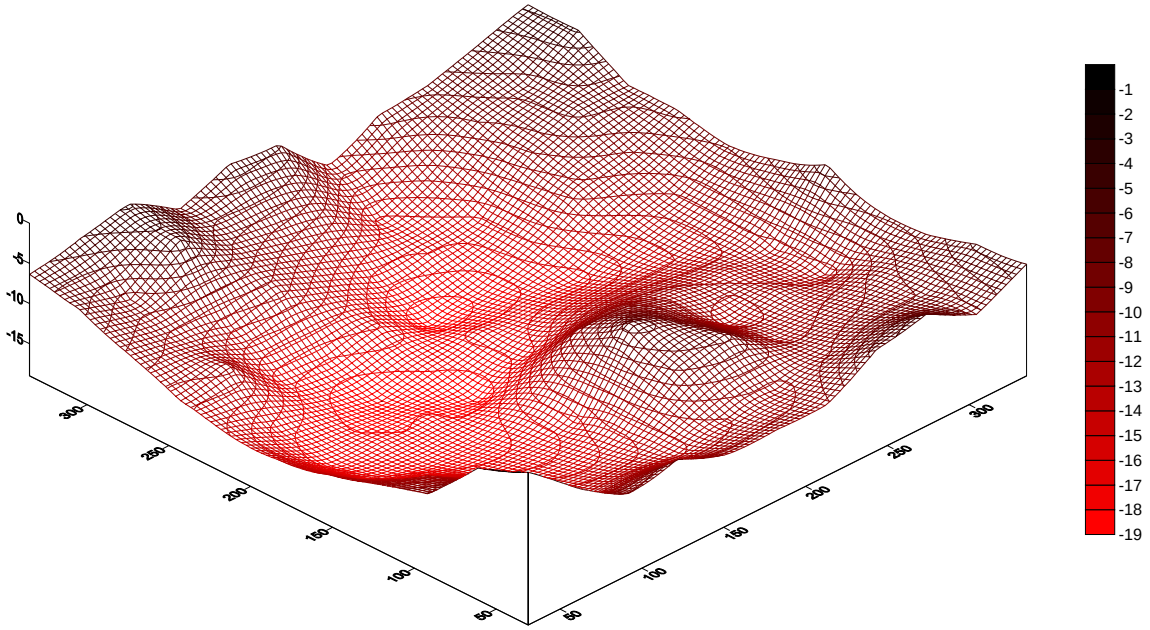
0
-5
-10
-15
300
250
200
150
100
50
-1
-2
-3
-4
-5
-6
-7
-8
-9
-10
-11
-12
-13
-14
-15
-16
-17
-18
-19

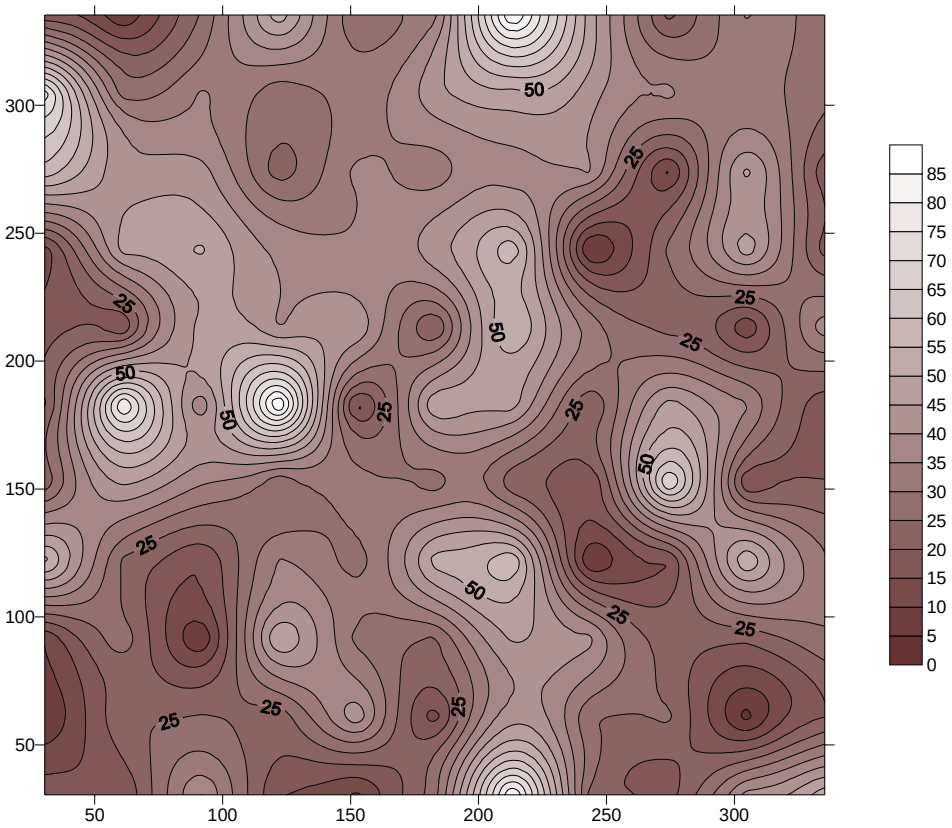
300
250
200
150
100
50
50
100
150
200
250
300
85
80
75
70
65
60
55
50
45
40
35
30
25
20
15
10
5
0

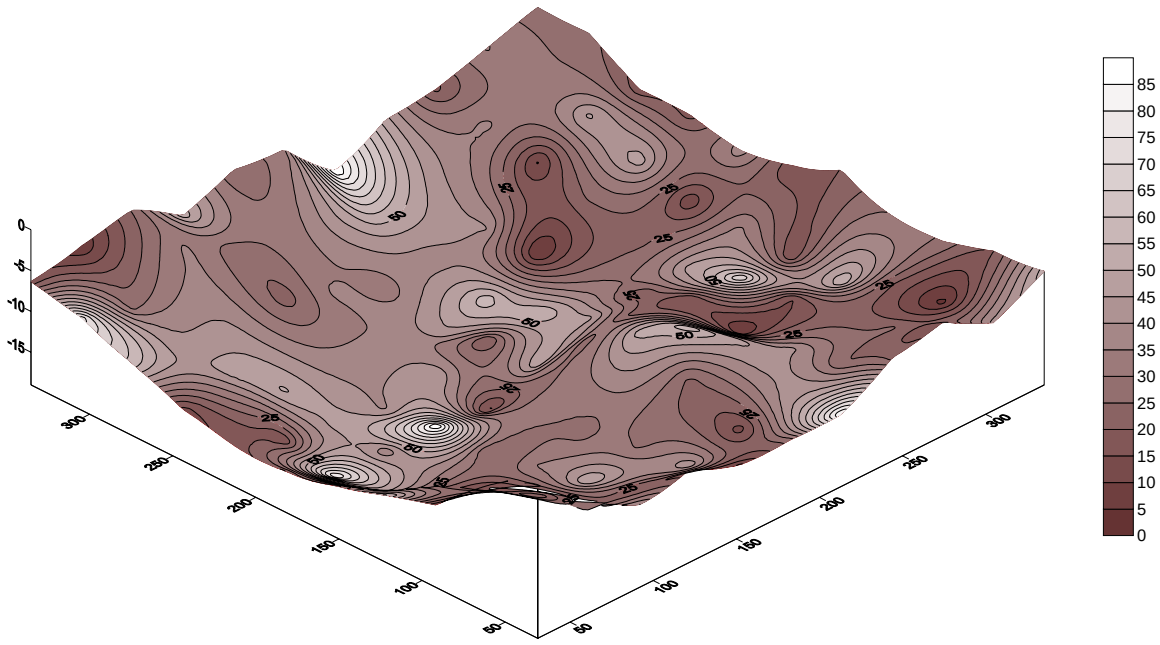
0
-5
-10
-15
300
250
200
150
100
50
50
100
150
200
250
300
85
80
75
70
65
60
55
50
45
40
35
30
25
20
15
10
5
0

J17SH2

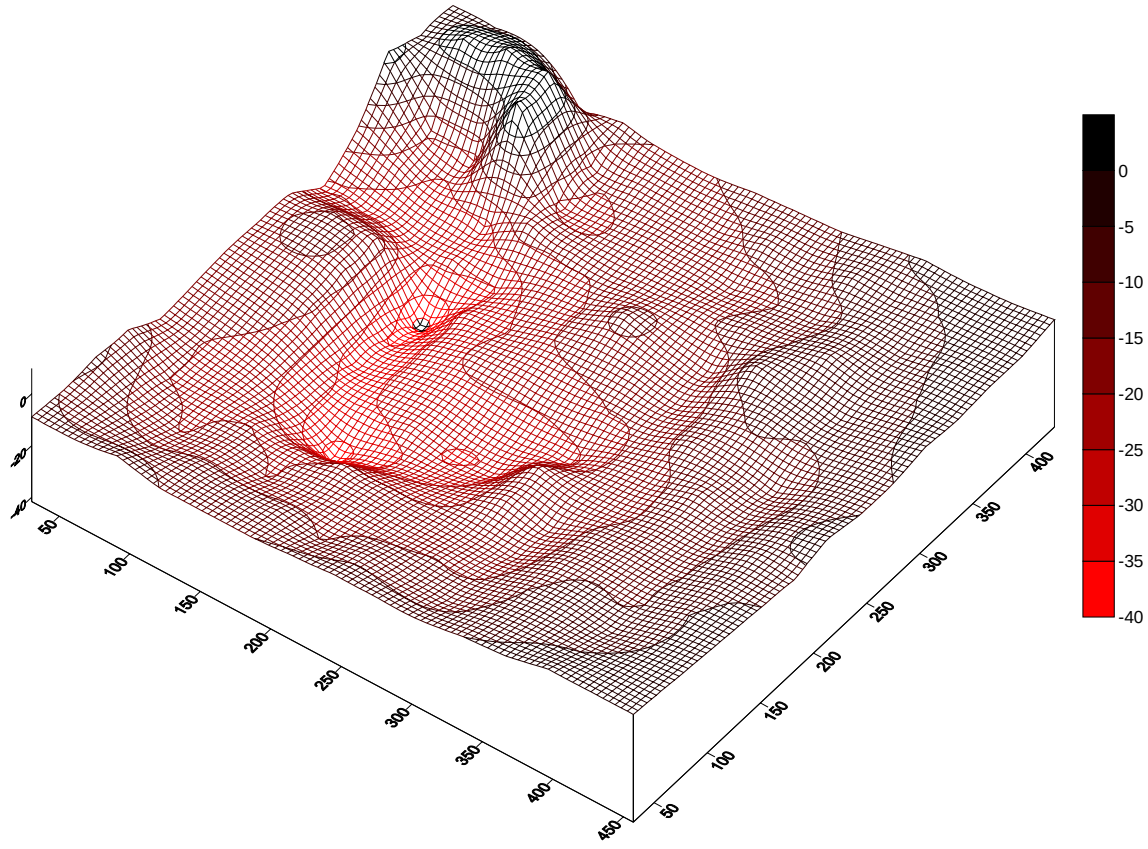

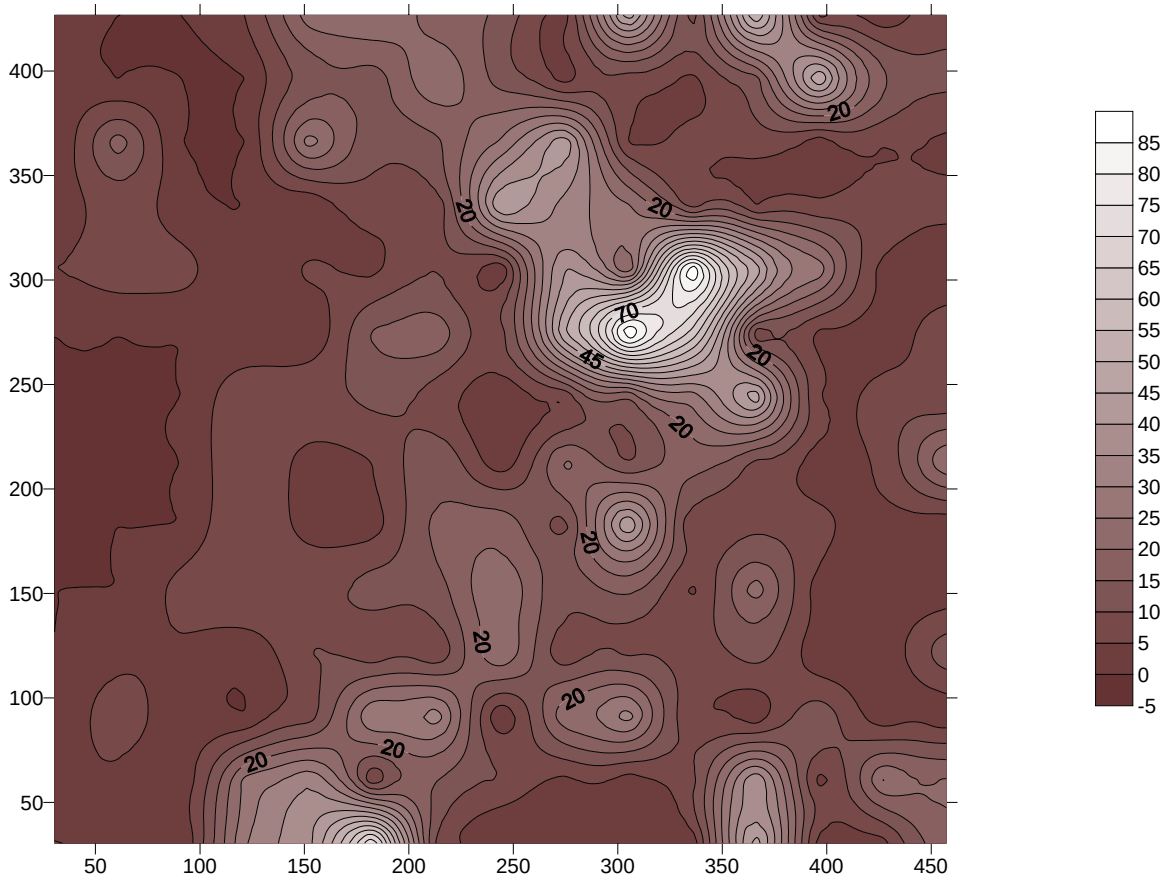
400
350
300
250
200
150
100
50
50
100
150
200
250
300
350
400
450
20
20
20
70
45
20
20
20
20
20
20
85
80
75
70
65
60
55
50
45
40
35
30
25
20
15
10
5
0
-5

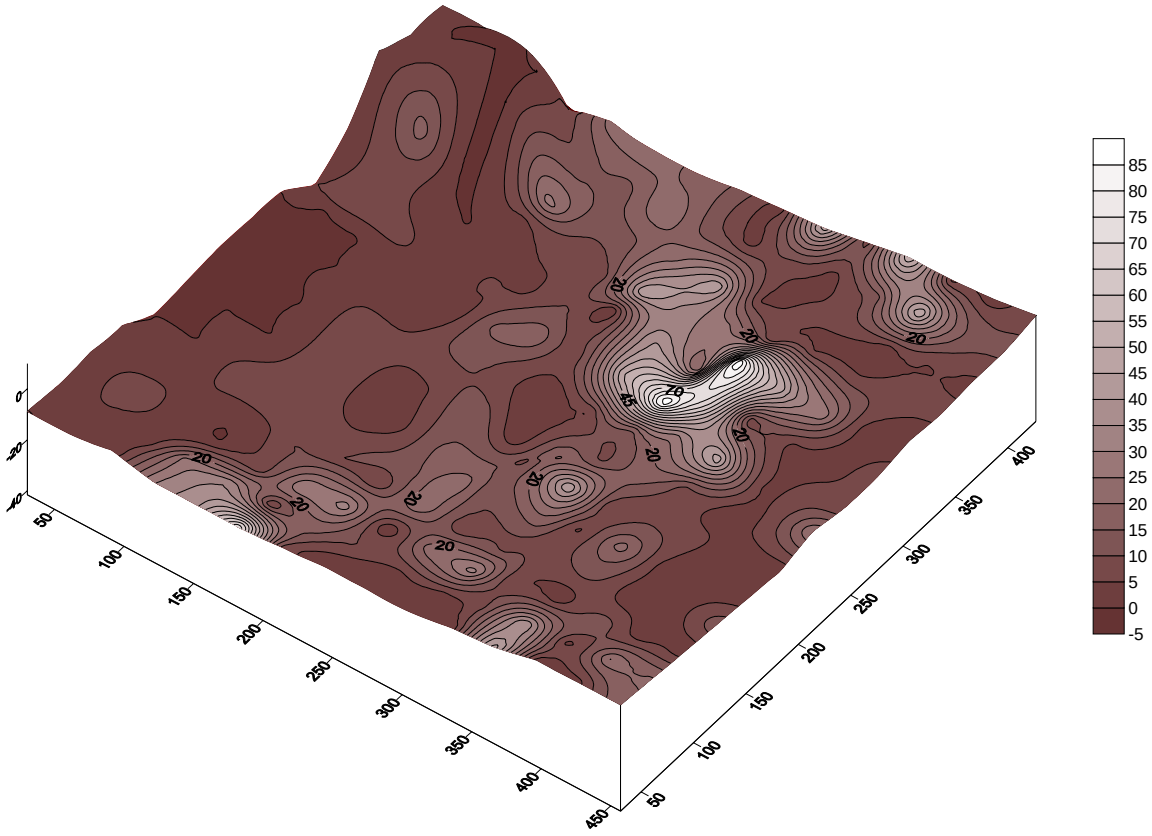
85
80
75
70
65
60
55
50
45
40
35
30
25
20
15
10
5
0
-5
0
-20
-40
50
100
150
200
250
300
350
400
450
50
100
150
200
250
300
350
400
20
45
70

RRSH3

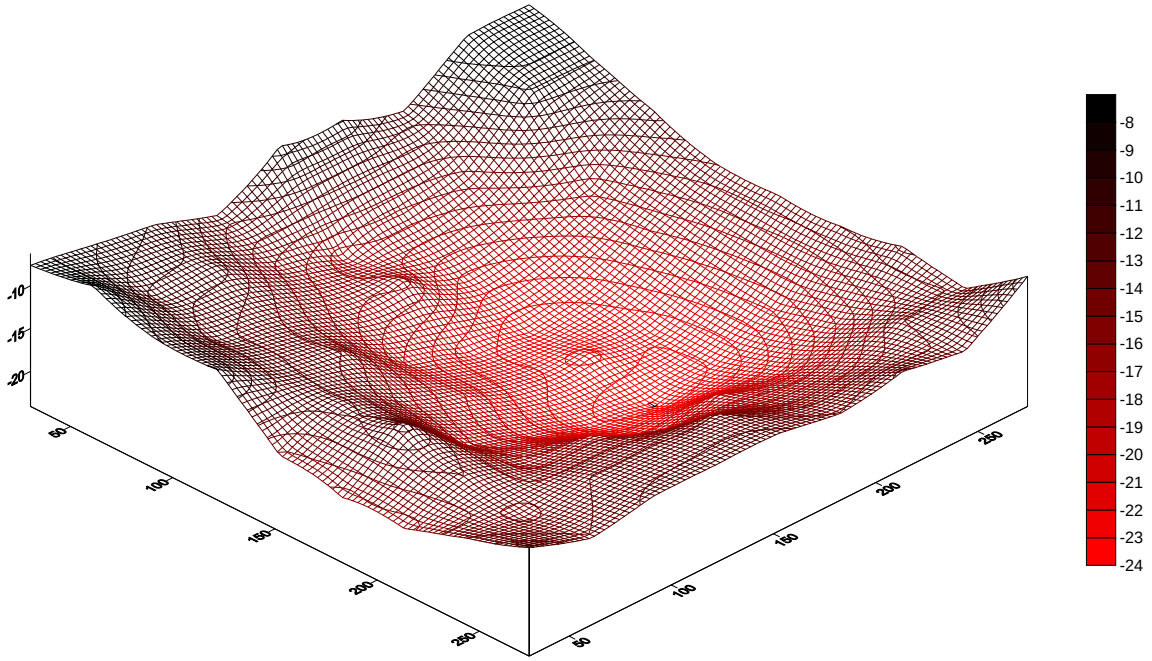
-8
-9
-10
-11
-12
-13
-14
-15
-16
-17
-18
-19
-20
-21
-22
-23
-24

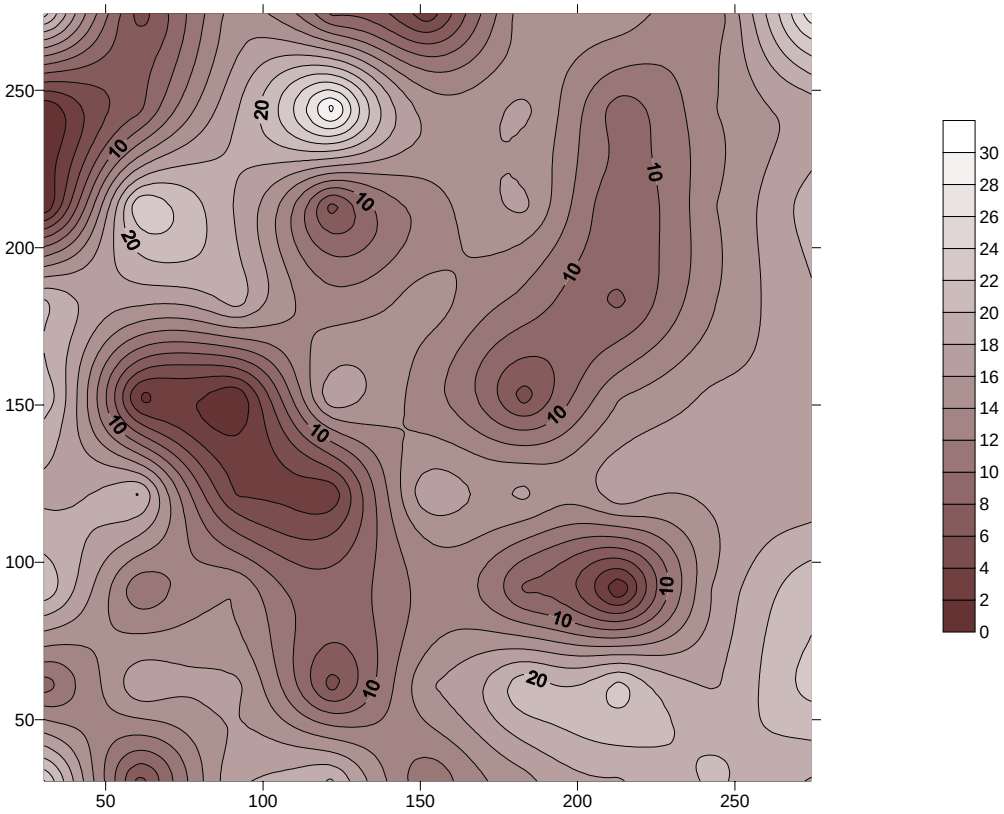
250
200
150
100
50
50
100
150
200
250
30
28
26
24
22
20
18
16
14
12
10
8
6
4
2
0

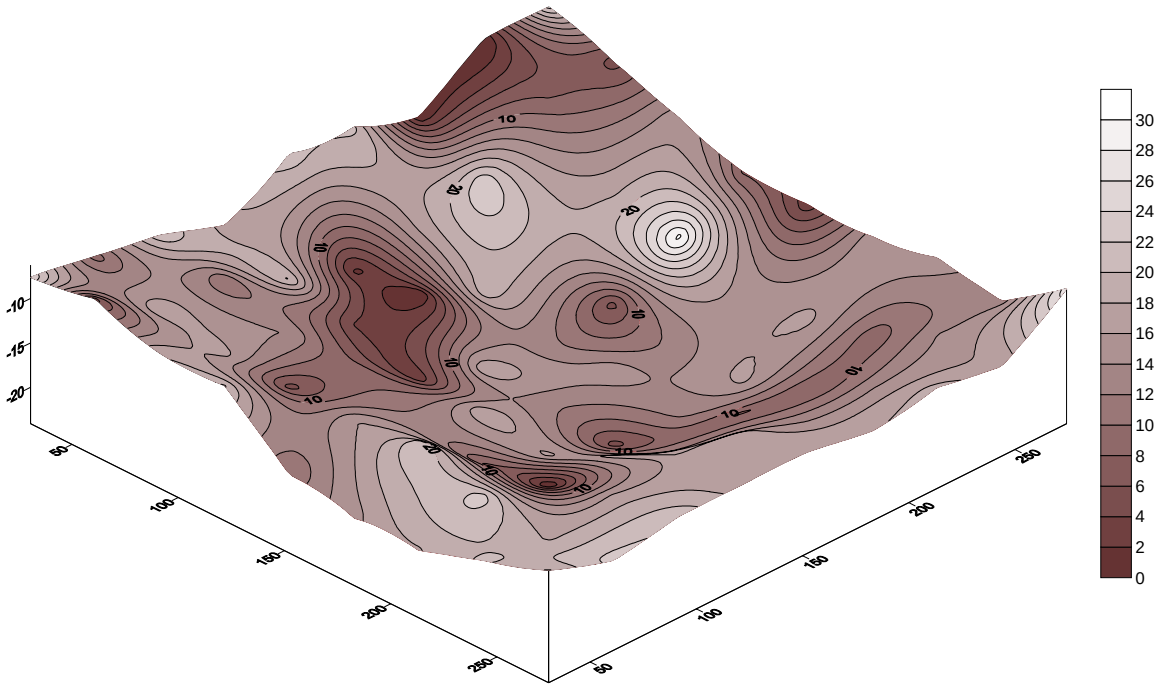
-10
-15
-20
50
100
150
200
250
30
28
26
24
22
20
18
16
14
12
10
8
6
4
2
0

RRSH4

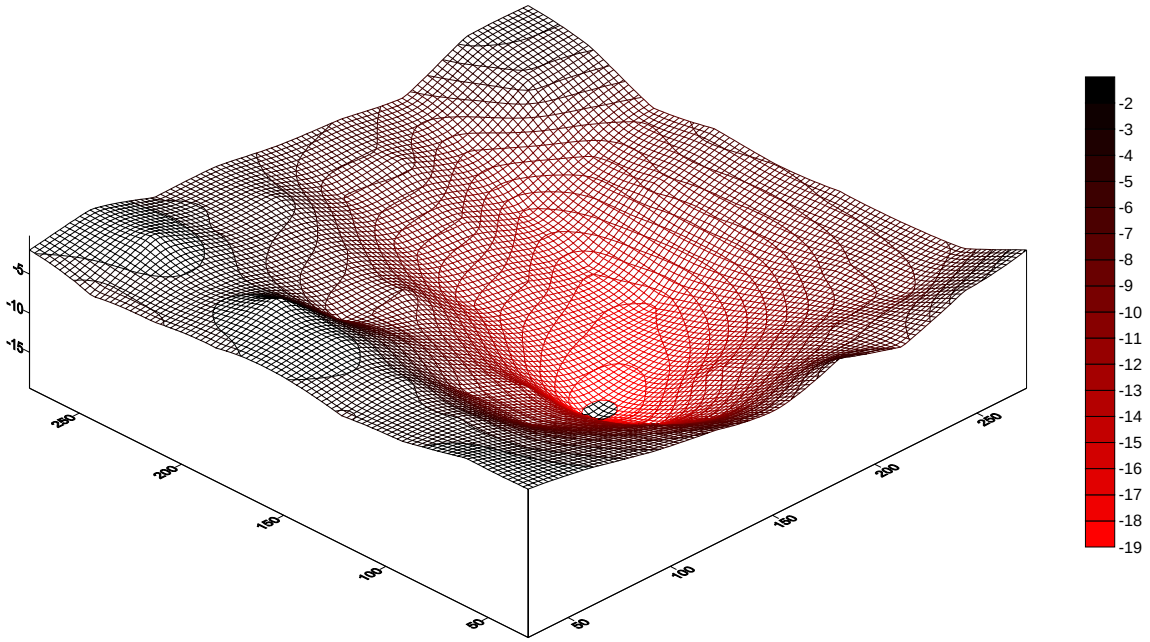
-2
-3
-4
-5
-6
-7
-8
-9
-10
-11
-12
-13
-14
-15
-16
-17
-18
-19

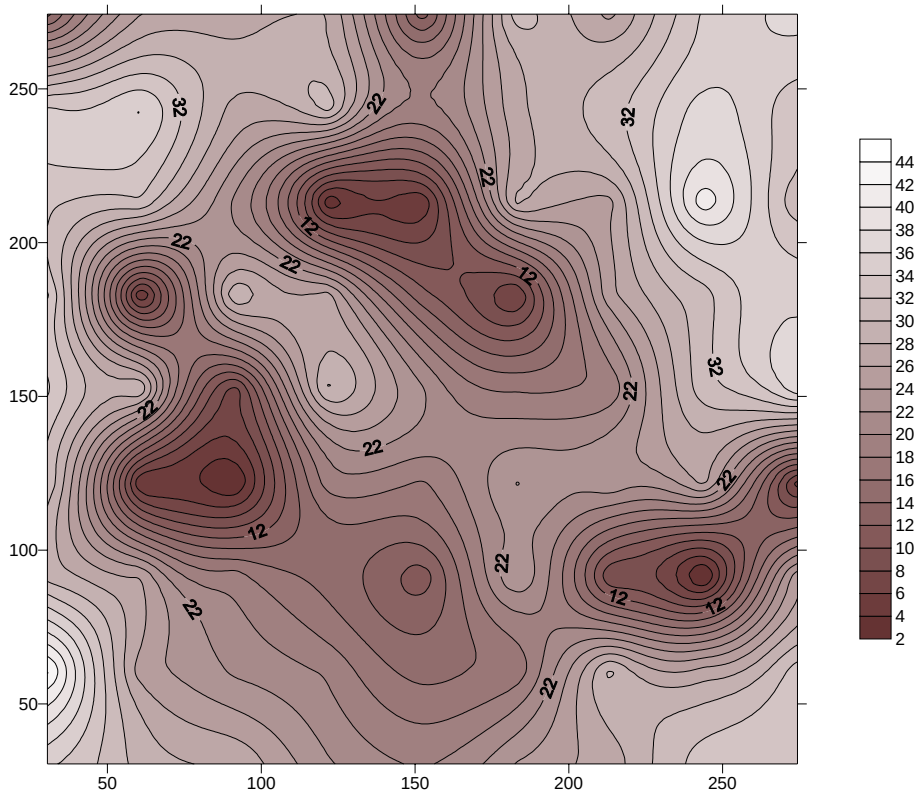
250
200
150
100
50
50
100
150
200
250
44
42
40
38
36
34
32
30
28
26
24
22
20
18
16
14
12
10
8
6
4
2

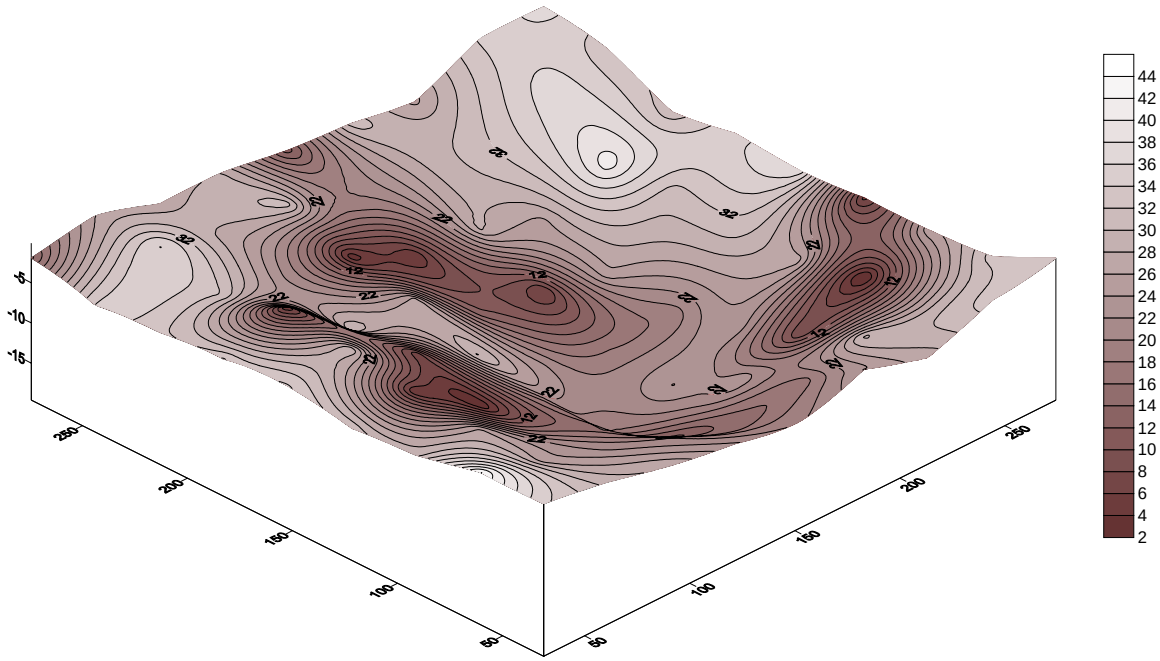
44
42
40
38
36
34
32
30
28
26
24
22
20
18
16
14
12
10
8
6
4
2
-5
-10
-15
250
200
150
100
50

CBSH1

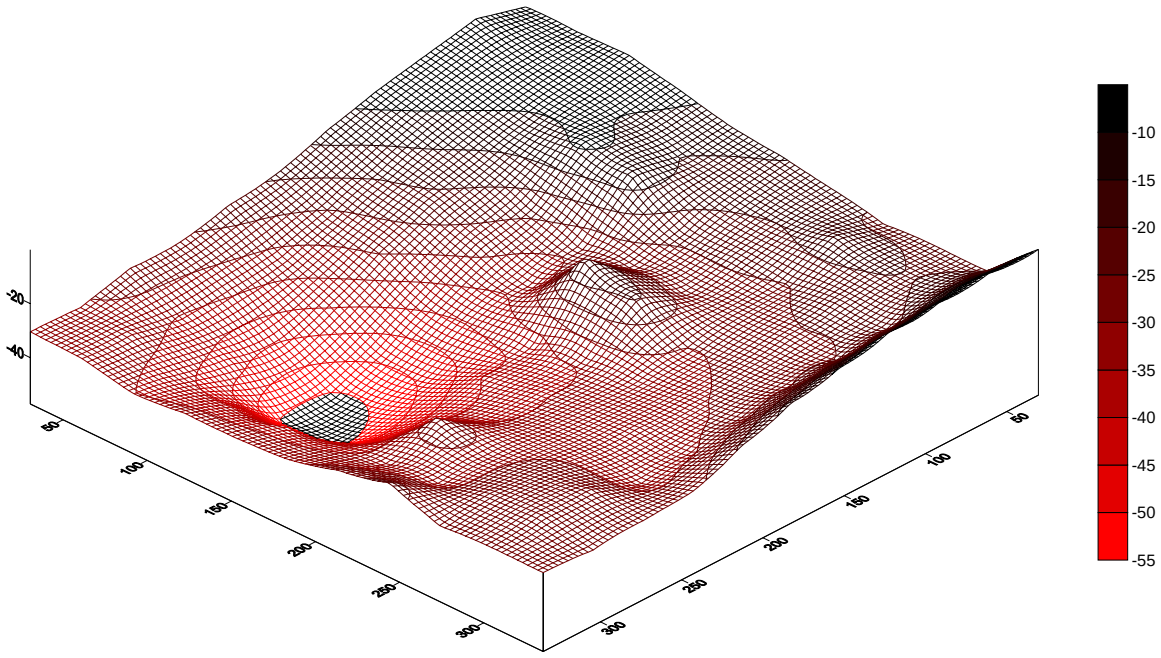
-10
-15
-20
-25
-30
-35
-40
-45
-50
-55

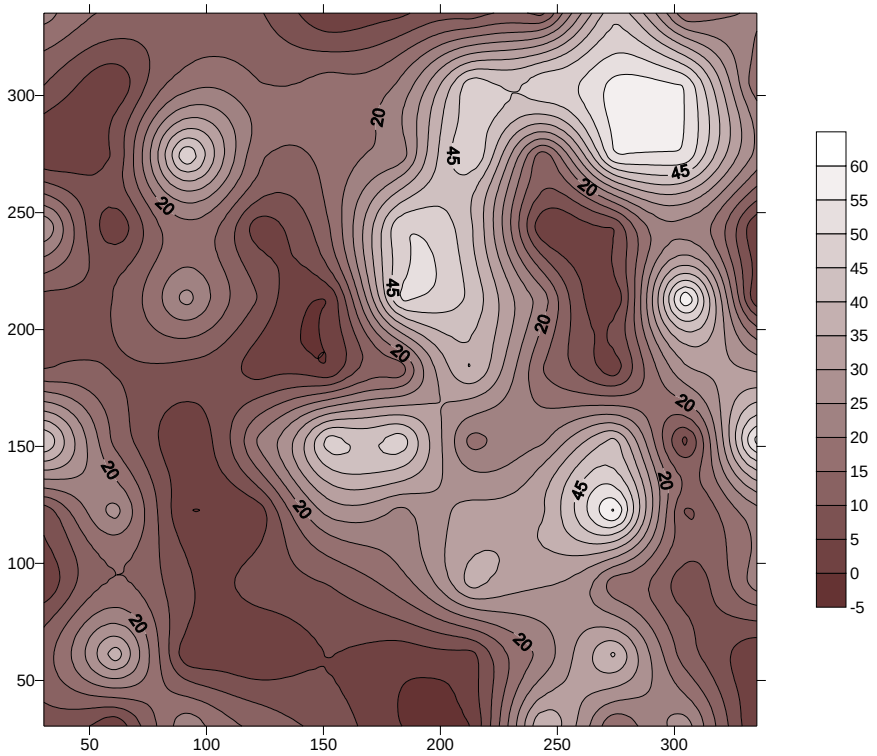
300
250
200
150
100
50
50
100
150
200
250
300
20
45
60
55
50
45
40
35
30
25
20
15
10
5
0
-5

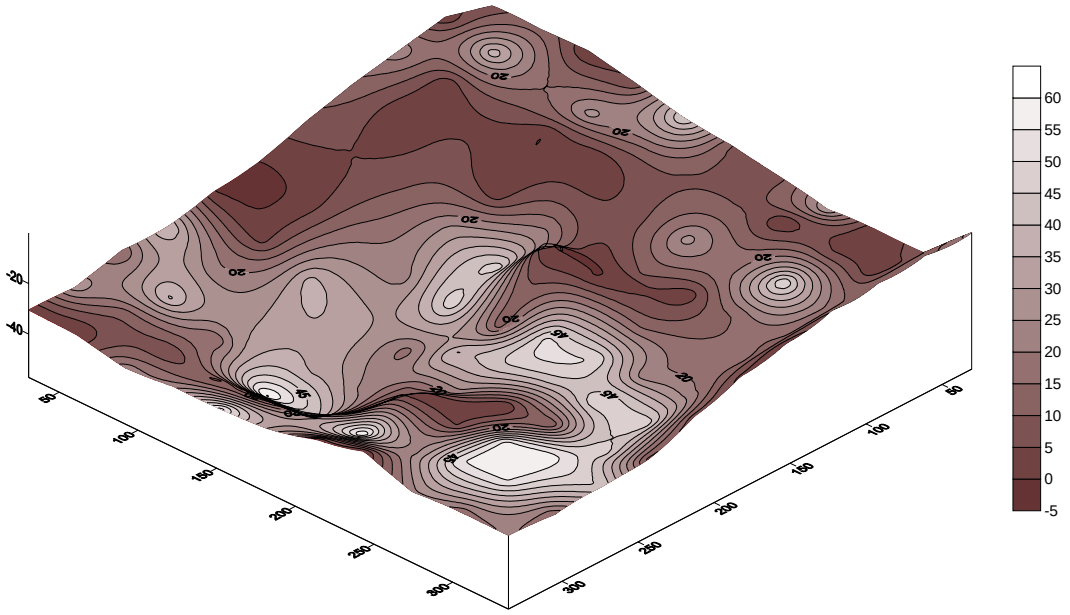
60
55
50
45
40
35
30
25
20
15
10
5
0
-5

HCSH1

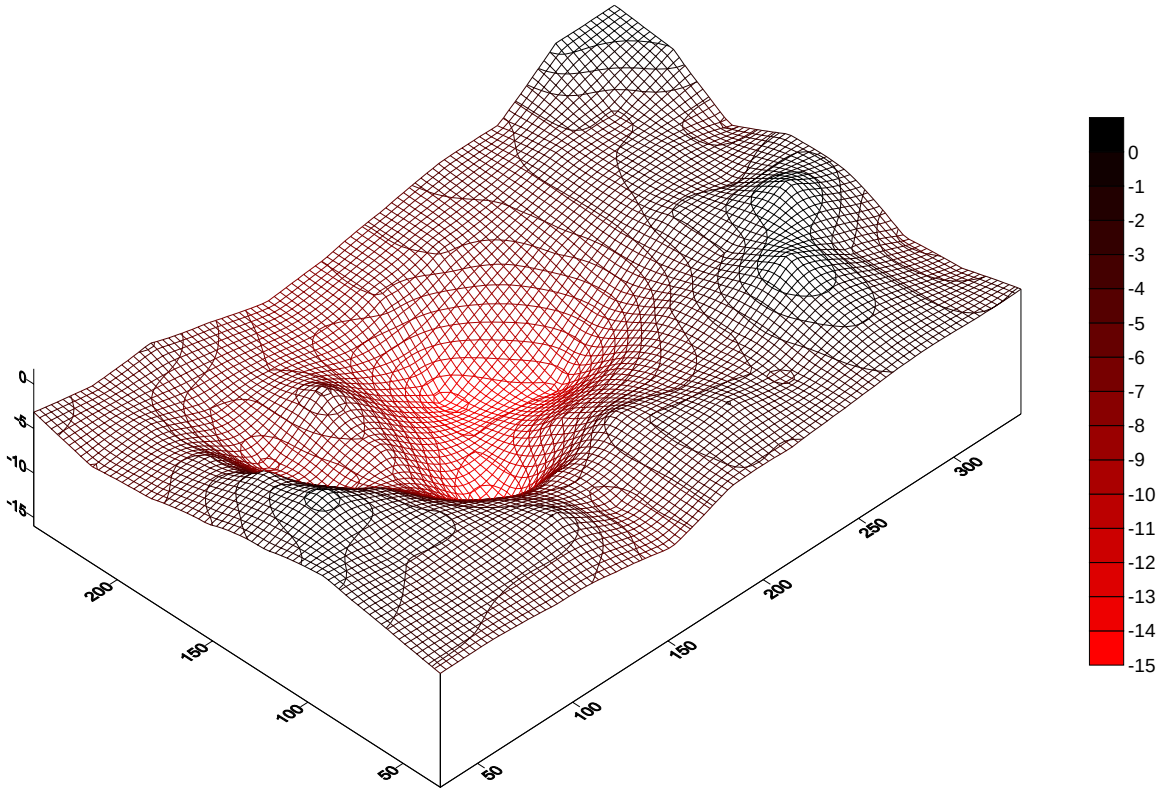
0
-1
-2
-3
-4
-5
-6
-7
-8
-9
-10
-11
-12
-13
-14
-15
50
100
150
200
250
300

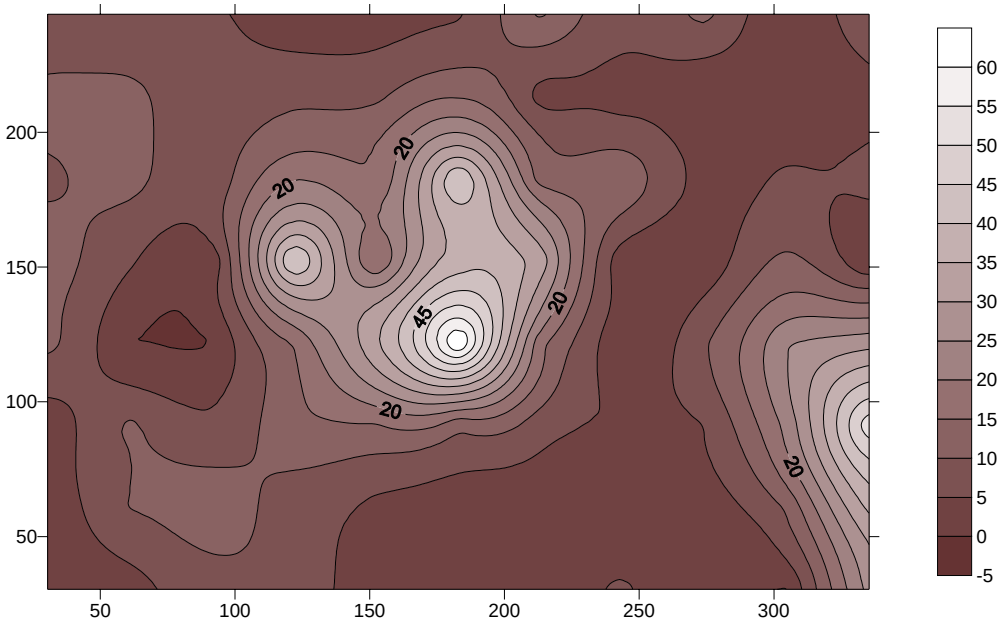
60
55
50
45
40
35
30
25
20
15
10
5
0
-5
20
45
50
100
150
200
250
300

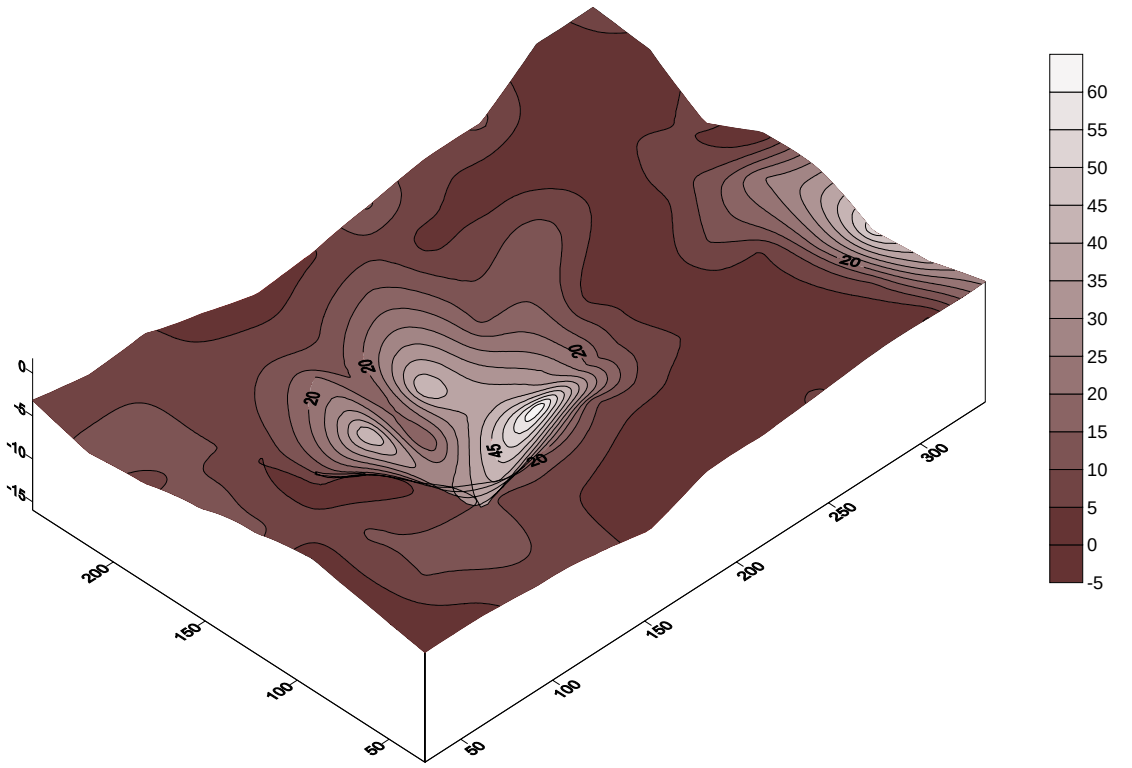
60
55
50
45
40
35
30
25
20
15
10
5
0
-5
0
-5
-10
-15
50
100
150
200
50
100
150
200
250
300
20
20
20
20
20
20
20

CONTROL PLOTS

J17BG1

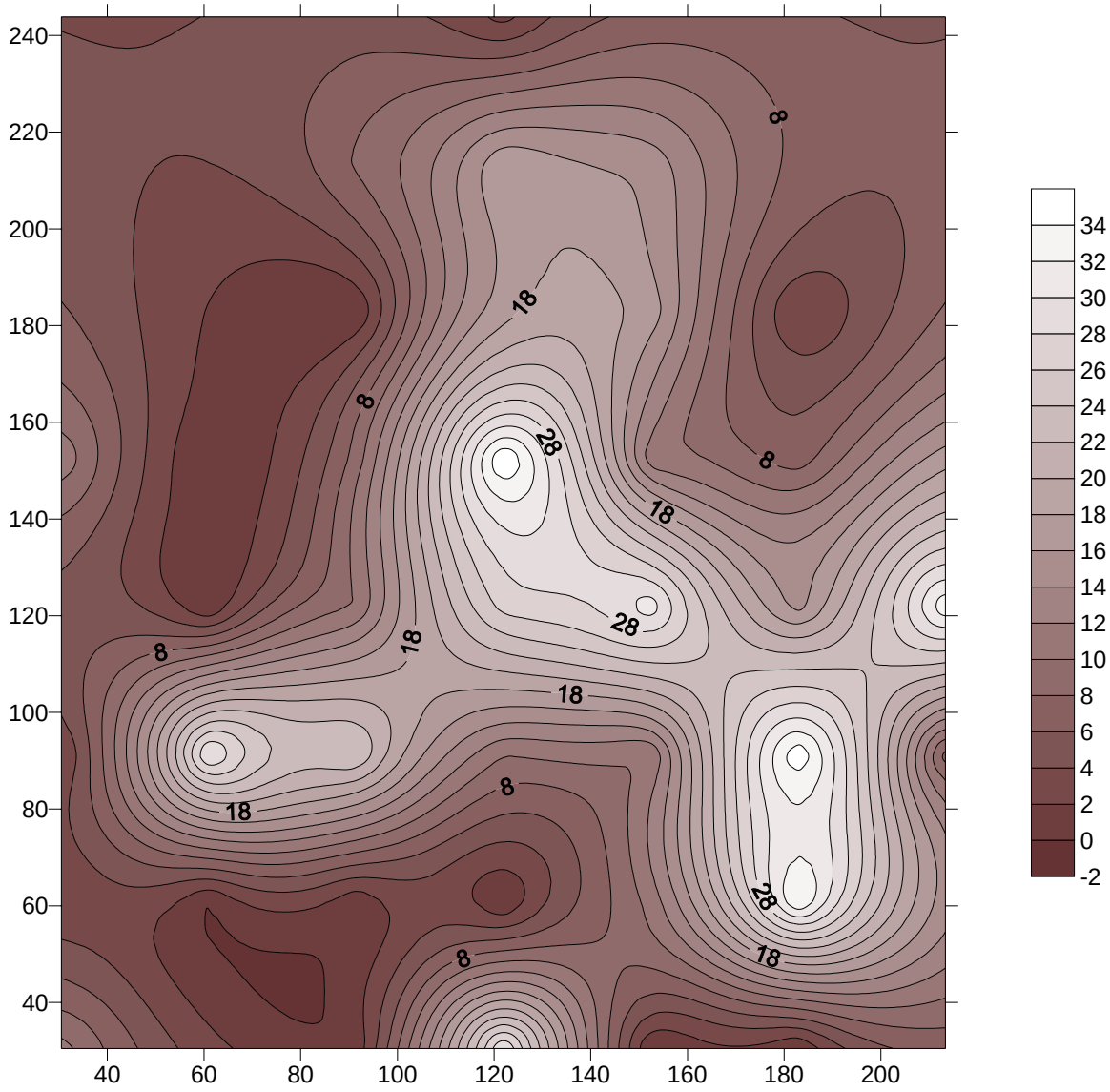

J17BG2

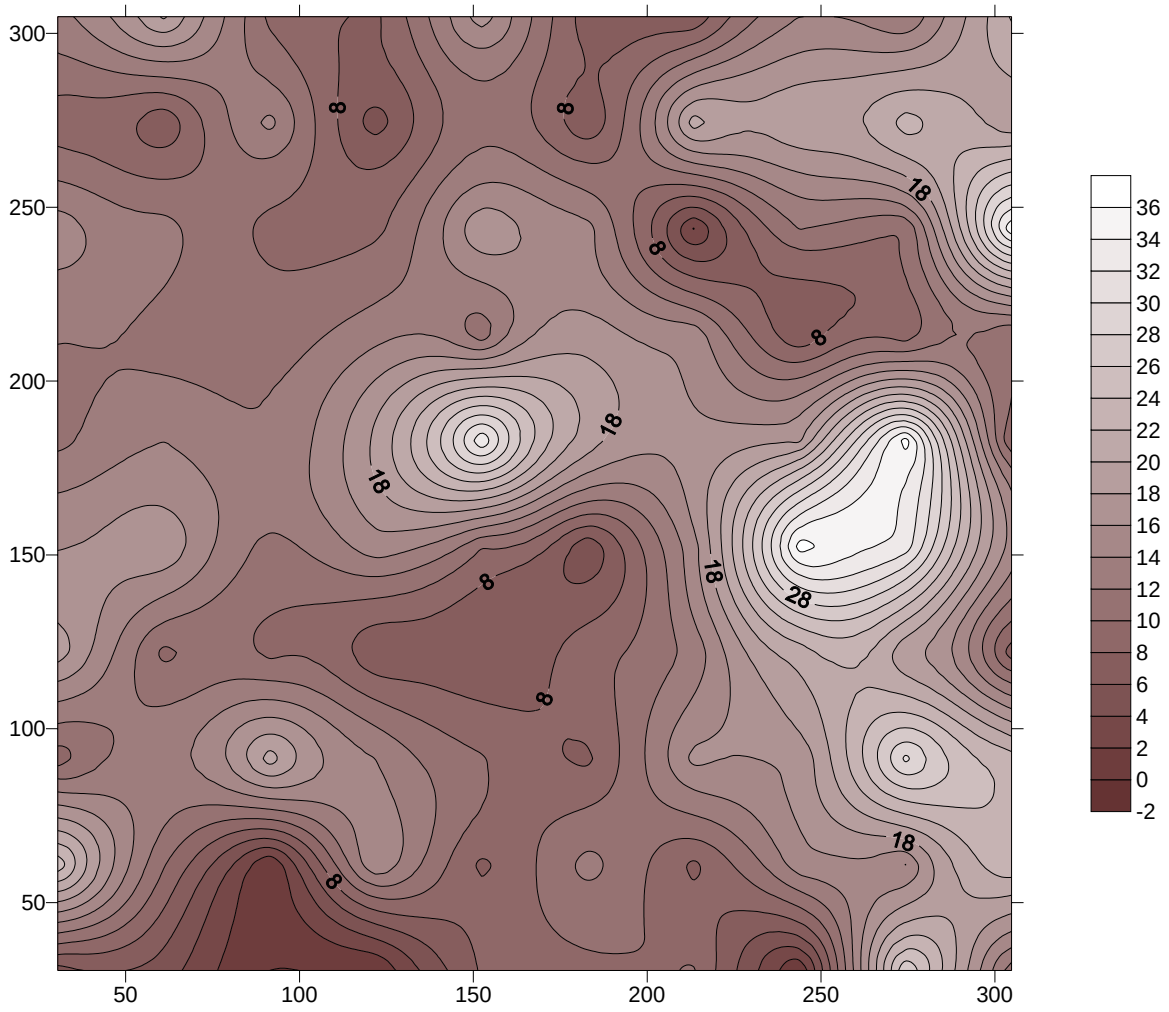
300
250
200
150
100
50
50
100
150
200
250
300
8
8
18
8
8
18
18
8
18
28
8
18
8
36
34
32
30
28
26
24
22
20
18
16
14
12
10
8
6
4
2
0
-2

J17BG3

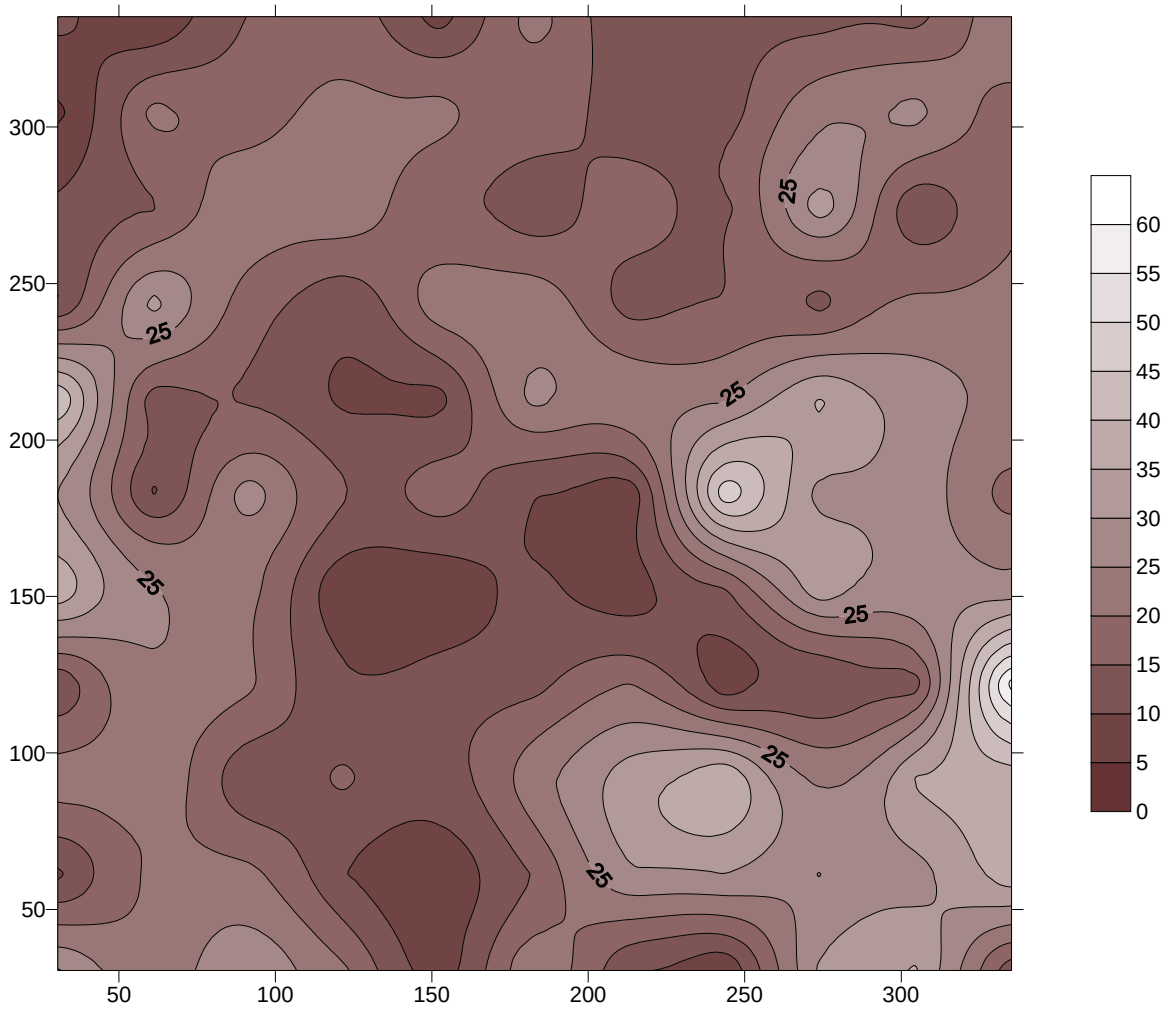
300
250
200
150
100
50
50
100
150
200
250
300
25
25
25
25
25
25
60
55
50
45
40
35
30
25
20
15
10
5
0

J17BG4

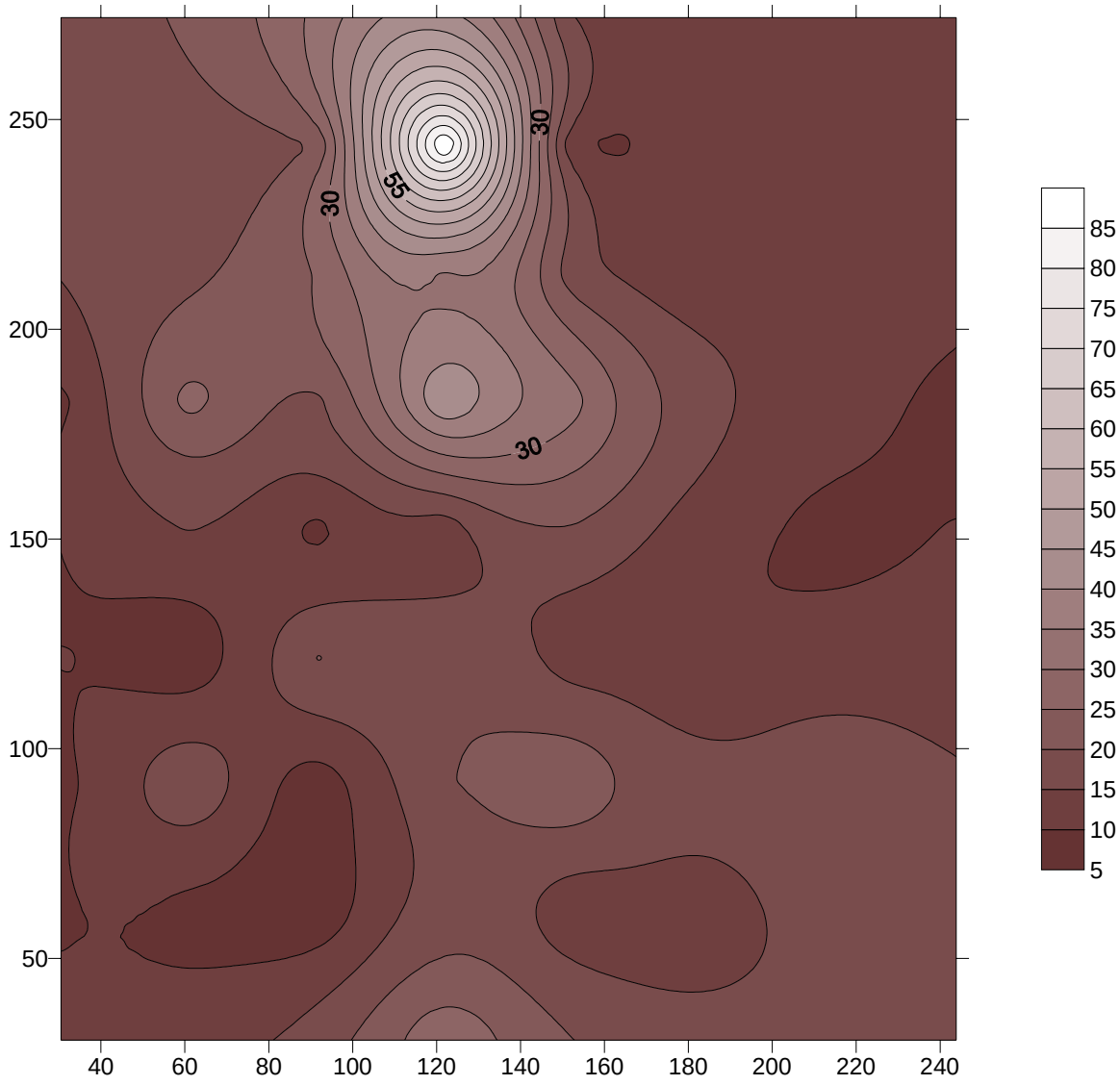
250
200
150
100
50
40
60
80
100
120
140
160
180
200
220
240
30
55
30
30
85
80
75
70
65
60
55
50
45
40
35
30
25
20
15
10
5

RRBG1

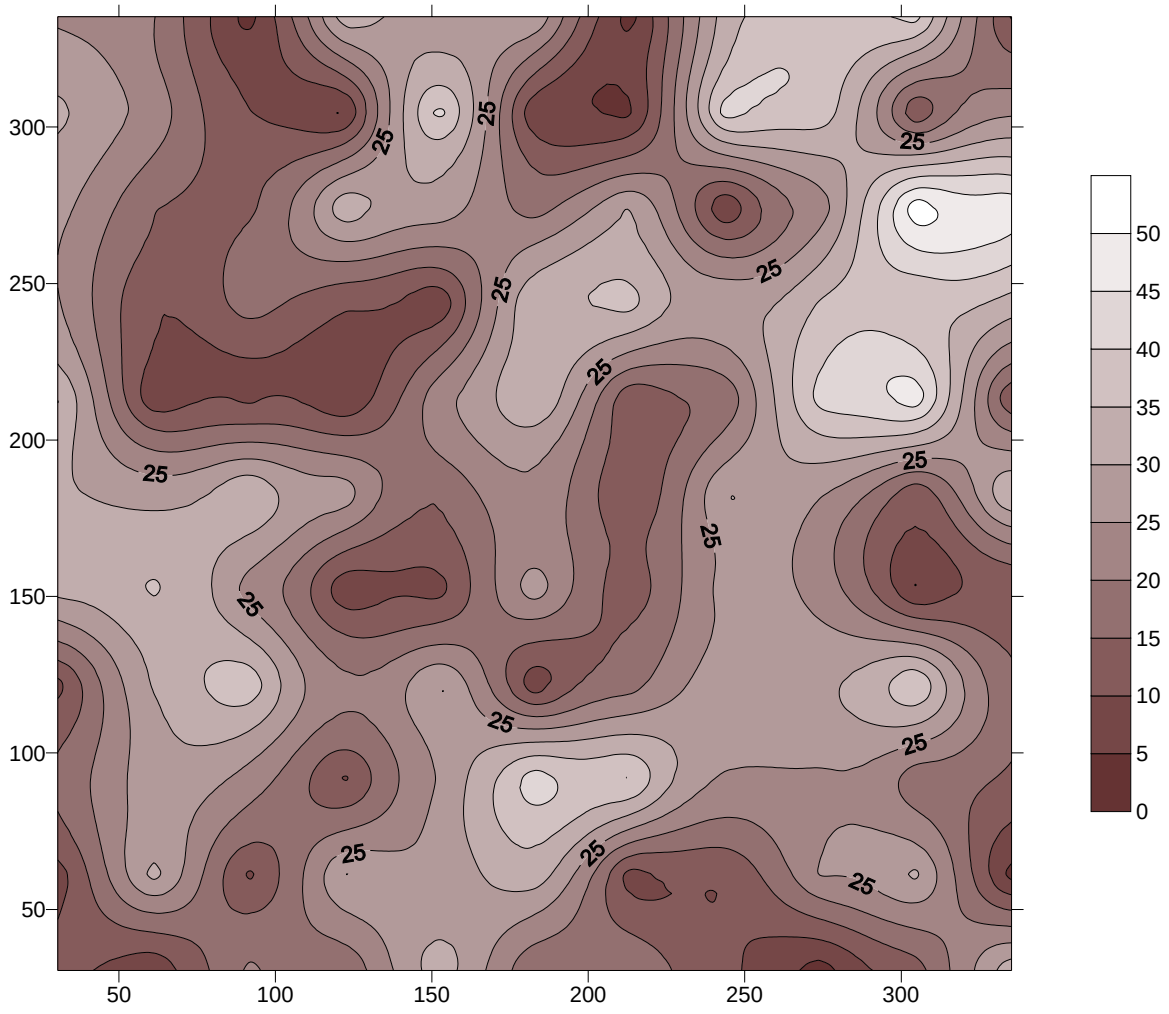
300
250
200
150
100
50
50
100
150
200
250
300
25
50
45
40
35
30
25
20
15
10
5
0

RRBG2

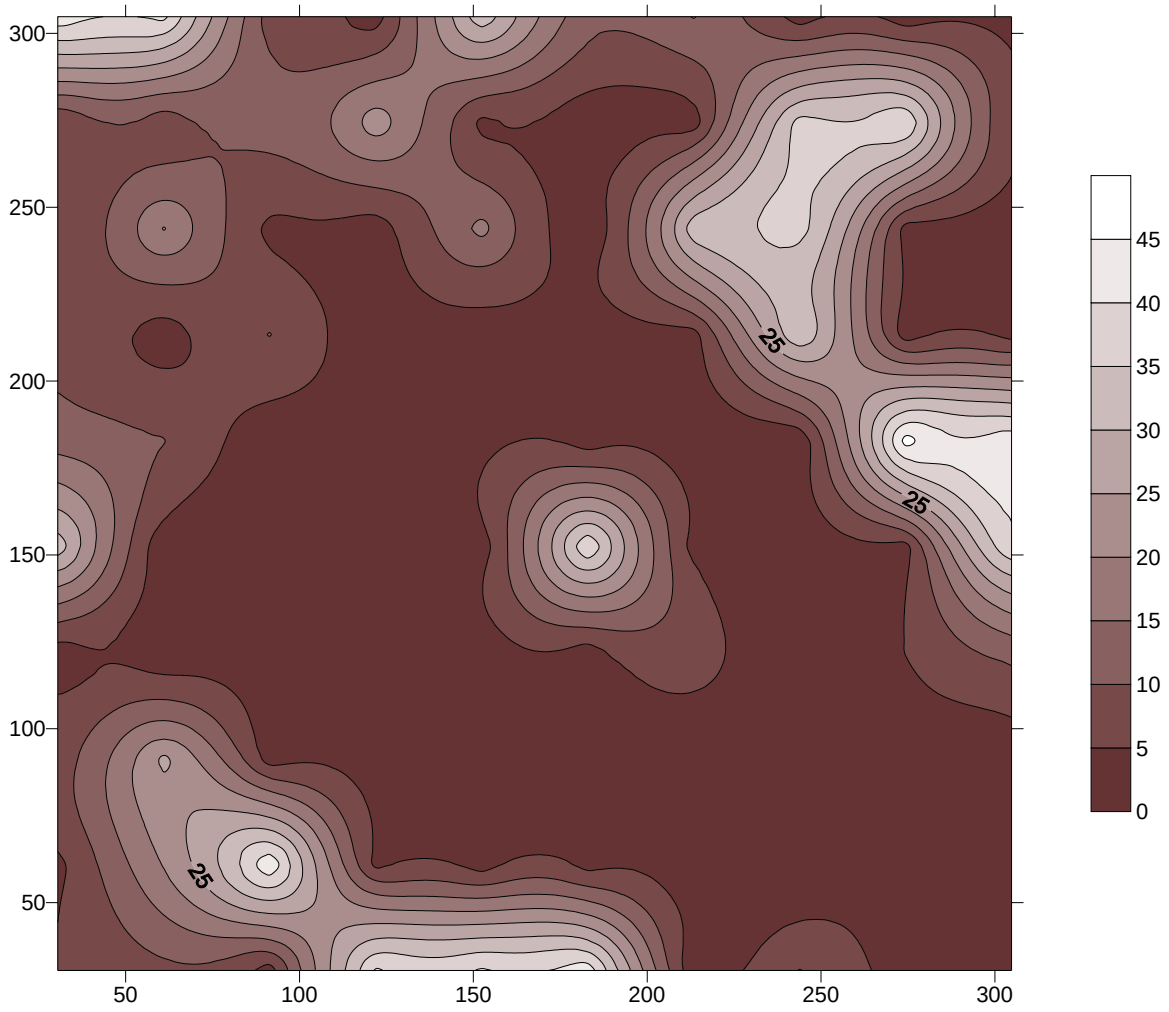
300
250
200
150
100
50
50
100
150
200
250
300
25
25
25
45
40
35
30
25
20
15
10
5
0

RRBG3

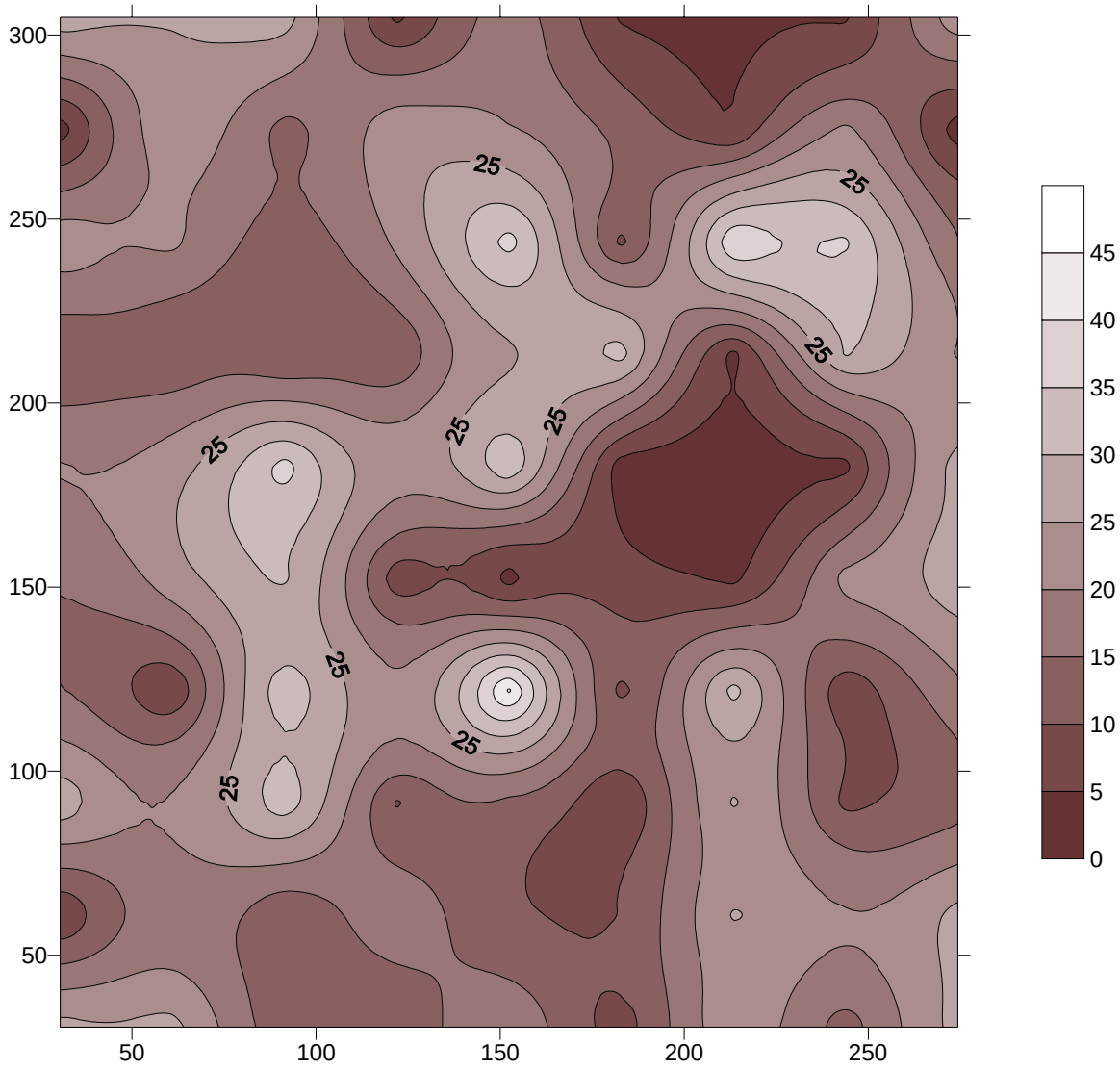
300
250
200
150
100
50
50
100
150
200
250
25
25
25
25
25
25
25
25
45
40
35
30
25
20
15
10
5
0

RRBG4

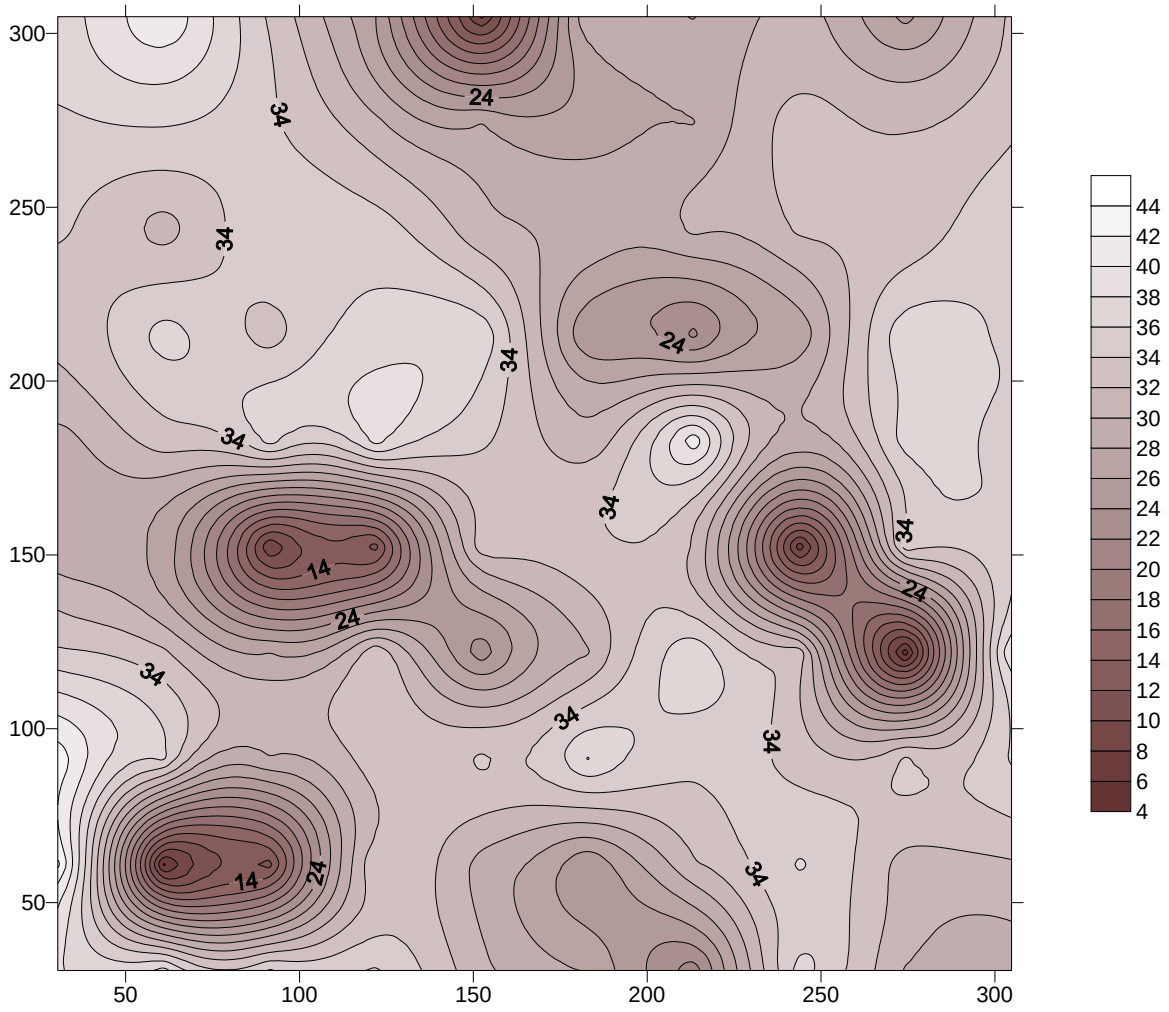
300
250
200
150
100
50
50
100
150
200
250
300
24
34
34
24
34
34
34
14
24
34
24
34
34
14
24
34
44
42
40
38
36
34
32
30
28
26
24
22
20
18
16
14
12
10
8
6
4

CBBG1

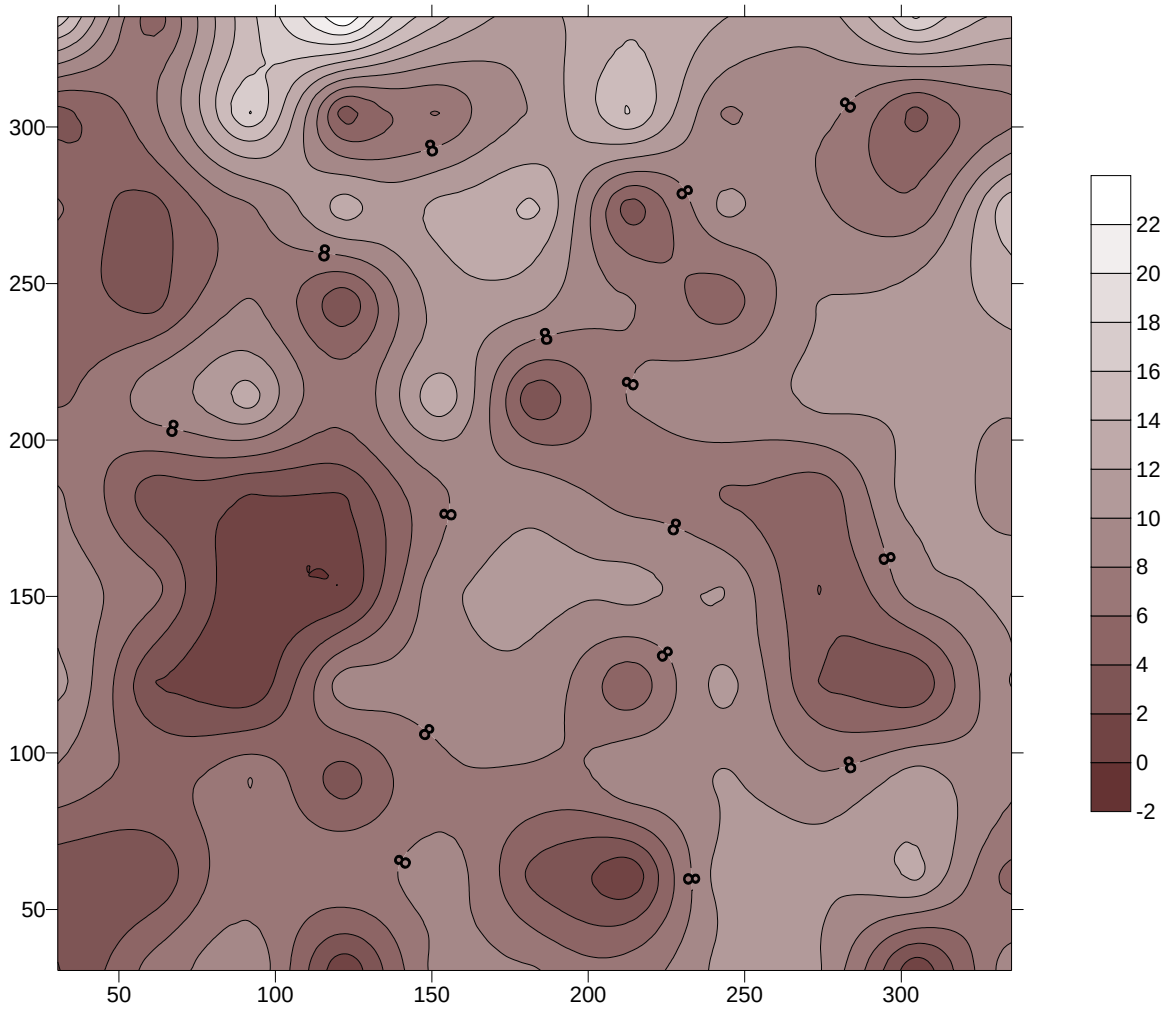
300
250
200
150
100
50
50
100
150
200
250
300
8
22
20
18
16
14
12
10
8
6
4
2
0
-2

HCBG1

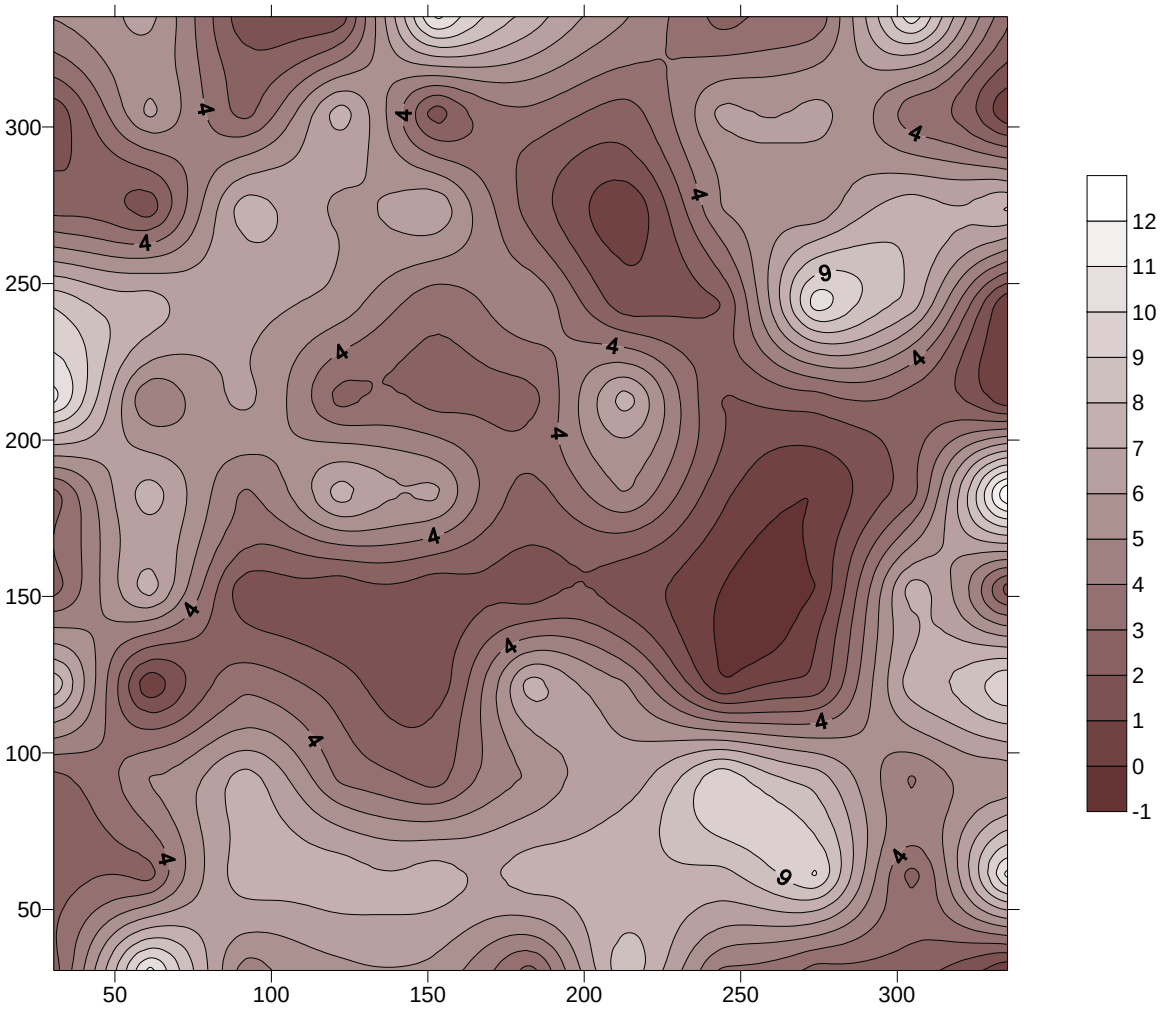
300
250
200
150
100
50
50
100
150
200
250
300
4
9
12
11
10
9
8
7
6
5
4
3
2
1
0
-1

Appendix B

The following are images representing the contrast in dielectric obtained using a ground penetrating radar (GPR) unit, SIR3000. The raw GPR data was processed using two software packages, Seismic Processing Workshop and RADAN. Data processed by Seismic Processing Workshop can be recognized by the red and blue color transform applied, while data processed using RADAN uses a multicolored color transform.

J17SH6

W – E

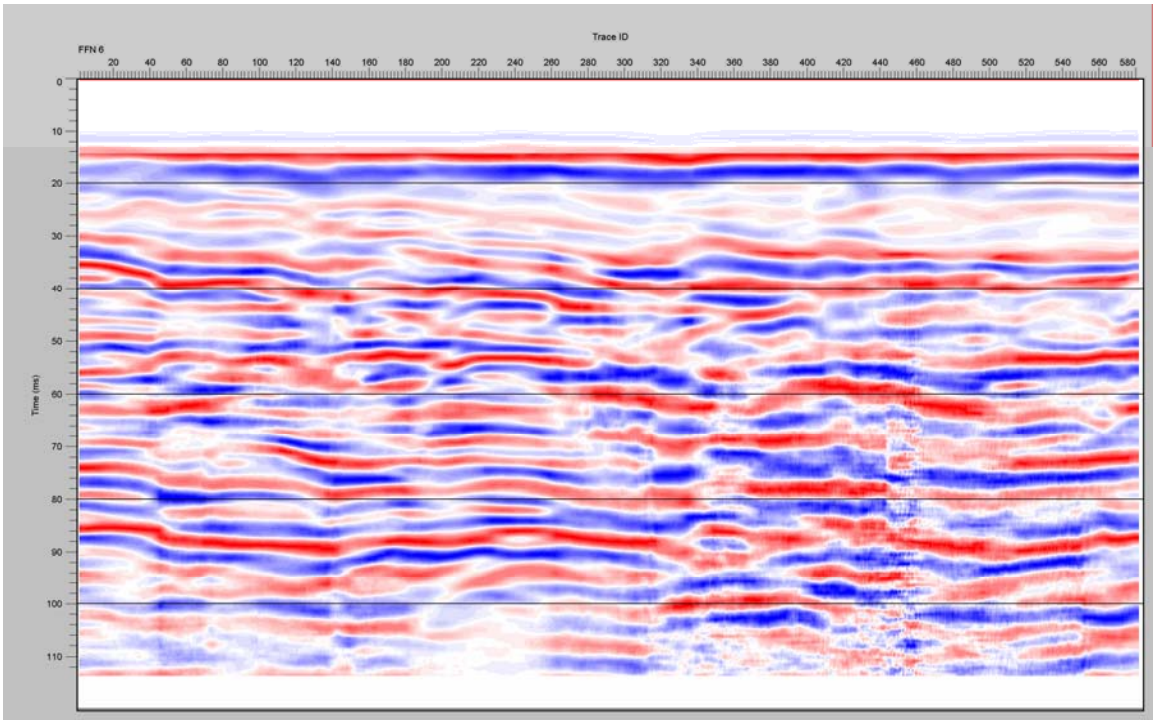

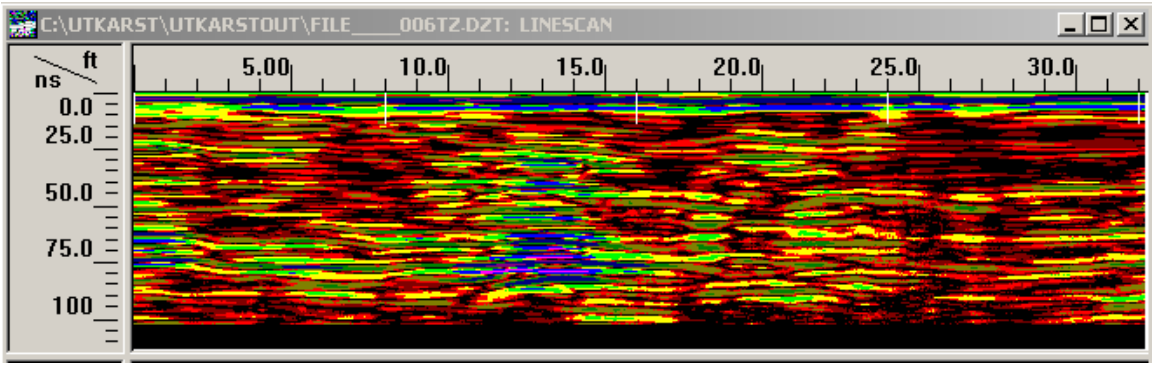
C:\UTKARST\UTKARSTOUT\FILE____006TZ.DZT: LINESCAN
ft
ns
5.00
10.0
15.0
20.0
25.0
30.0
0.0
25.0
50.0
75.0
100

S – E

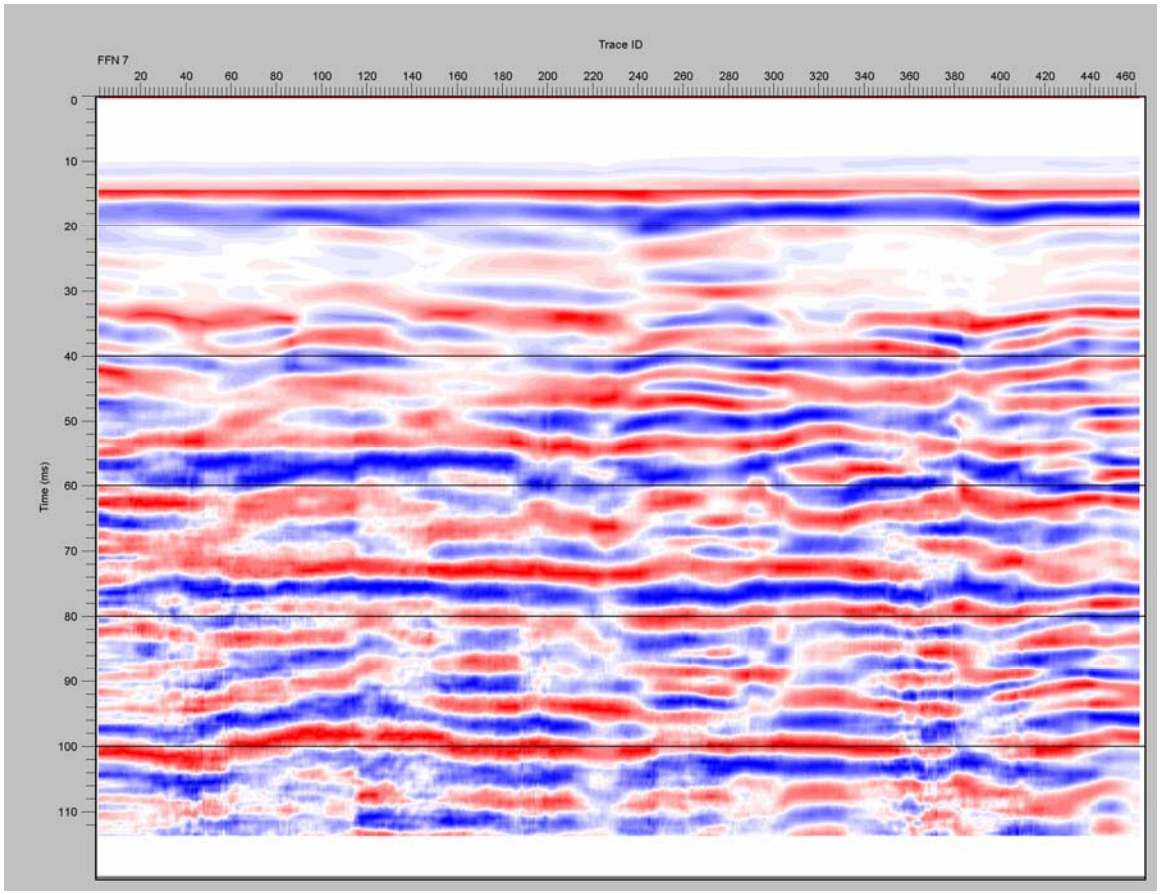
Trace ID
FFN 7
20 40 60 80 100 120 140 160 180 200 220 240 260 280 300 320 340 360 380 400 420 440 460
0 10 20 30 40 50 60 70 80 90 100 110
Time (ns)

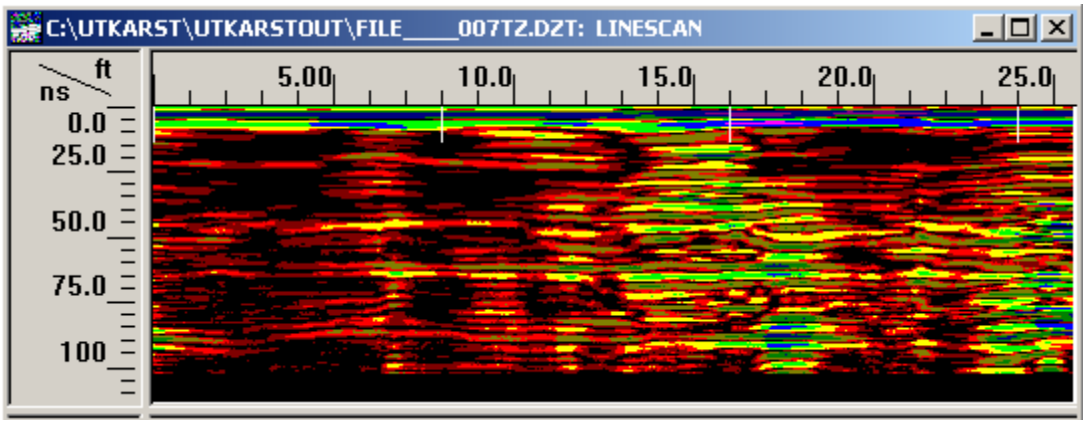
C:\UTKARST\UTKARSTOUT\FILE____007TZ.DZT: LINESCAN
ft
ns
0.0
25.0
50.0
75.0
100
5.00
10.0
15.0
20.0
25.0

J17BG2

S – N

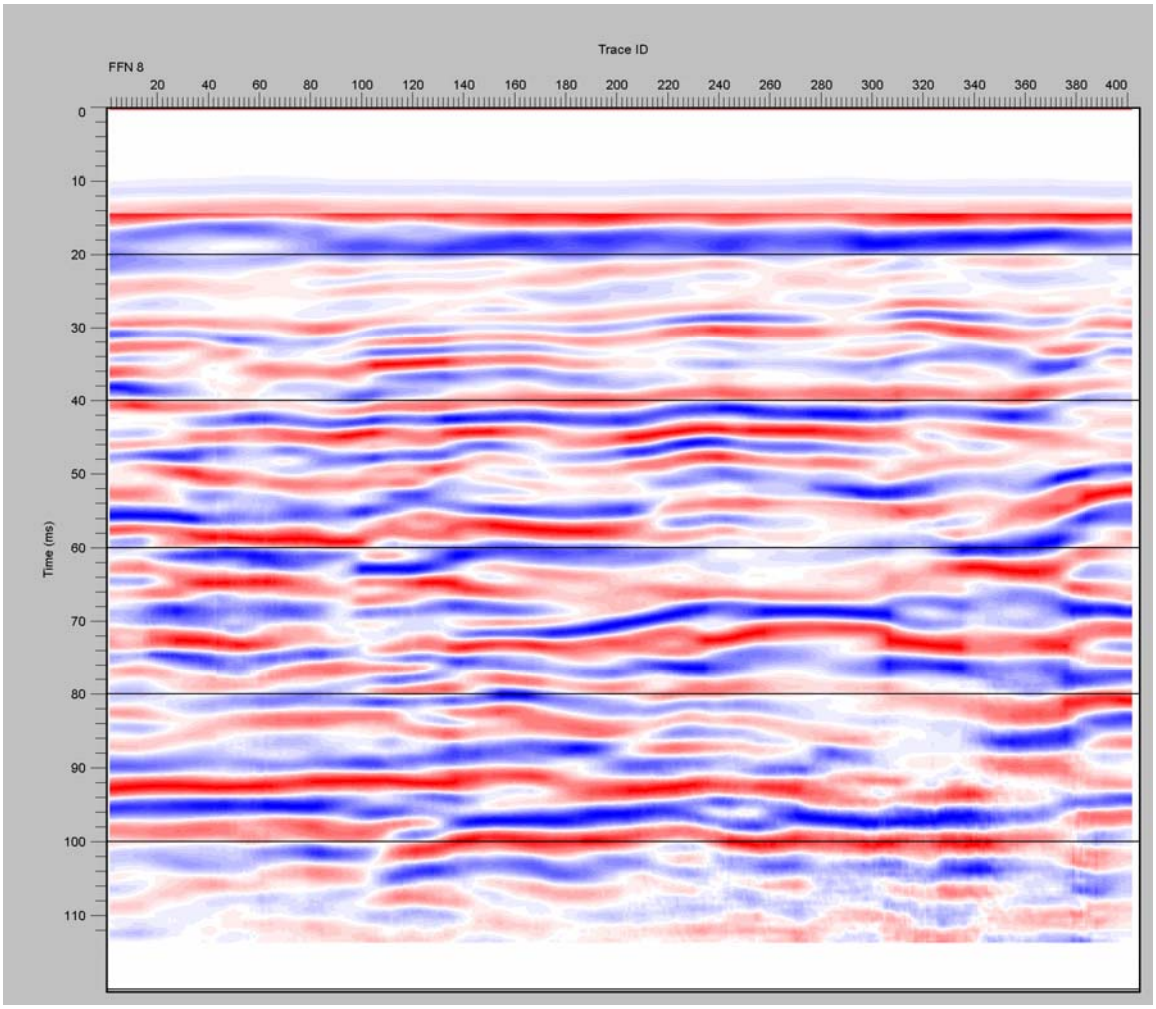
Trace ID
FFN 8
20 40 60 80 100 120 140 160 180 200 220 240 260 280 300 320 340 360 380 400
Time (ms)
0 10 20 30 40 50 60 70 80 90 100 110

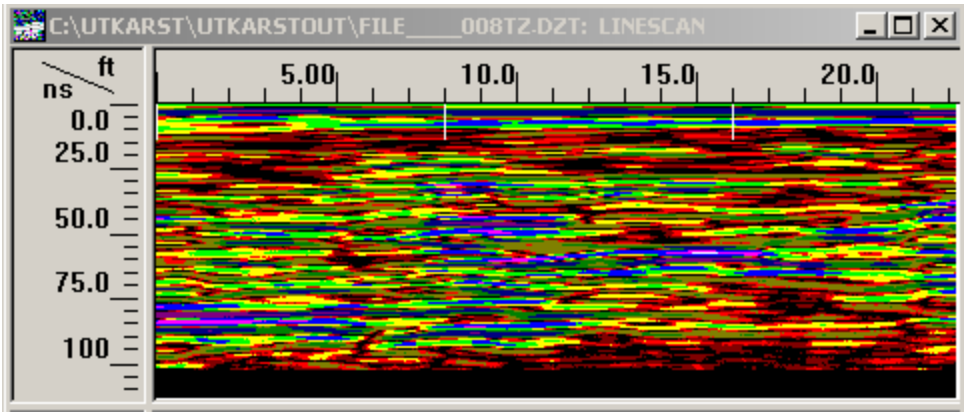

J17SH2

WSW – ENE

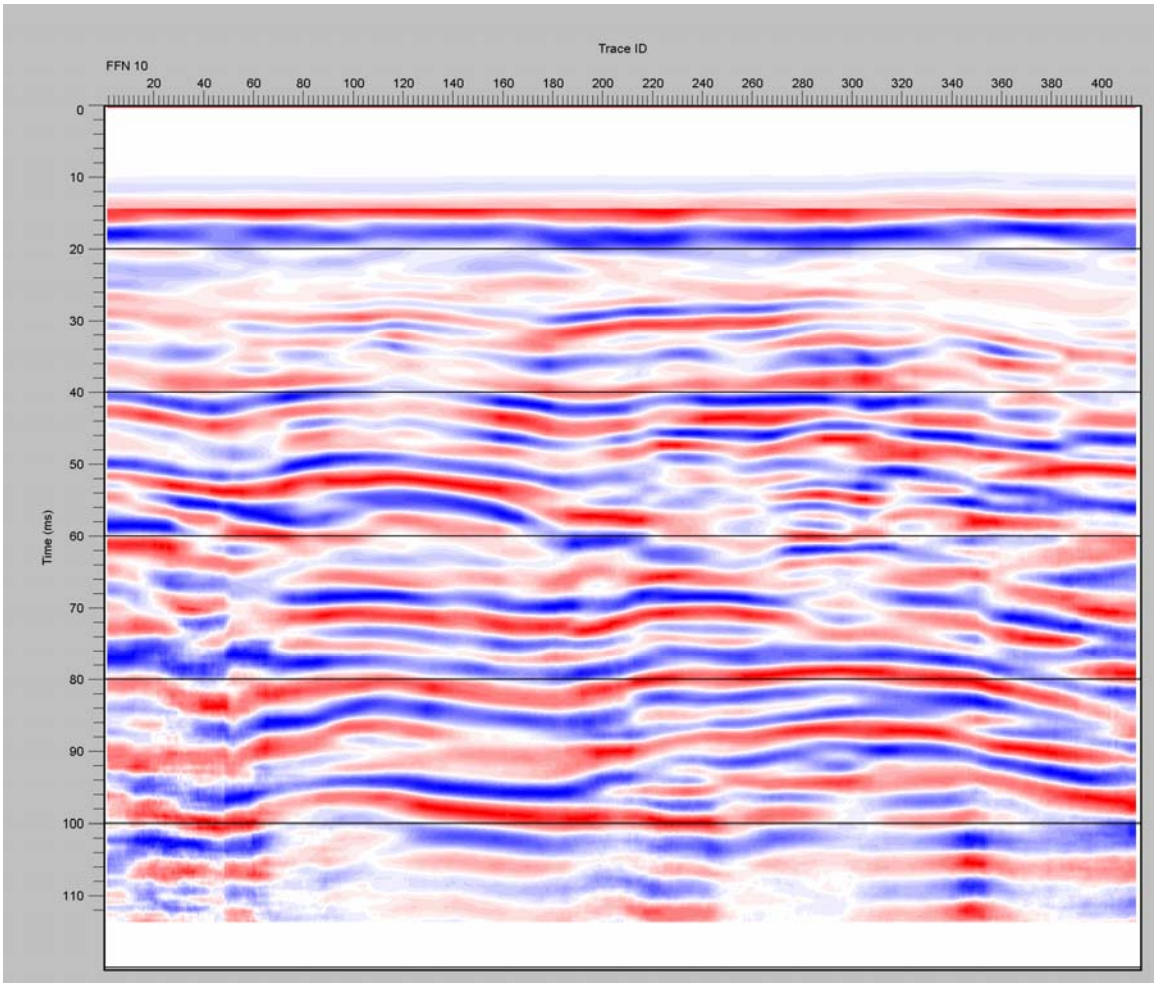

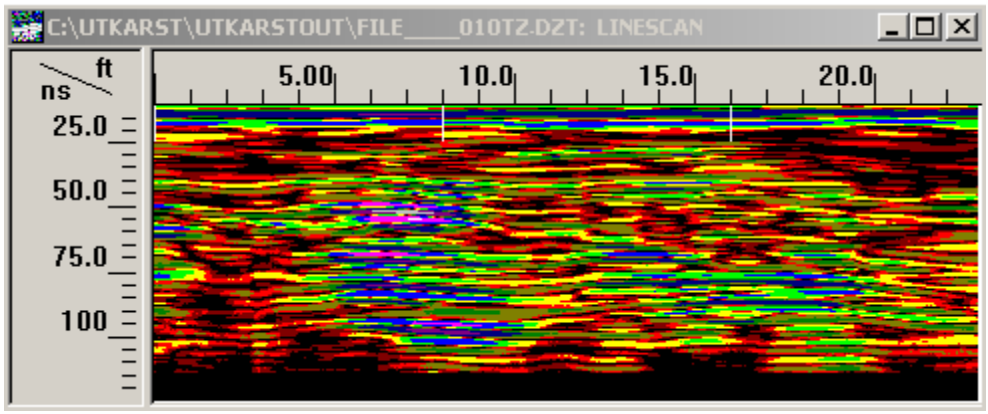
C:\UTKARST\UTKARSTOUT\FILE____010TZ.DZT: LINESCAN
ft
ns
5.00
10.0
15.0
20.0
25.0
50.0
75.0
100

NNW – SSE

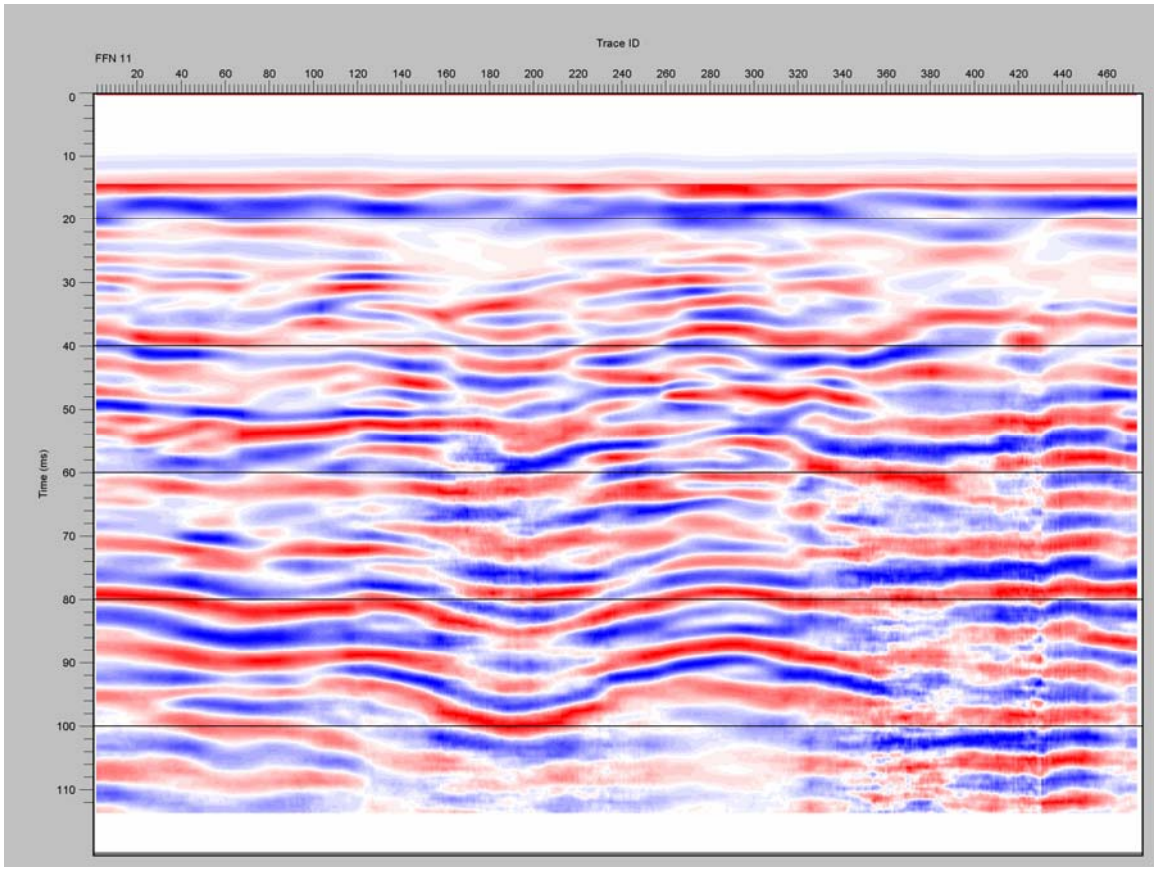
Trace ID
FFN 11
20 40 60 80 100 120 140 160 180 200 220 240 260 280 300 320 340 360 380 400 420 440 460
0 10 20 30 40 50 60 70 80 90 100 110
Time (ns)

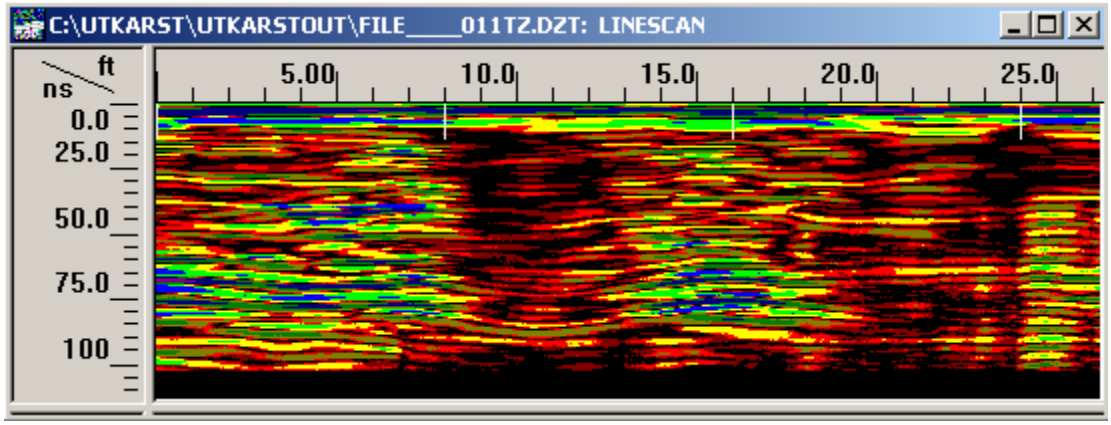
C:\UTKARST\UTKARSTOUT\FILE____011TZ.DZT: LINESCAN
ft
ns
5.00
10.0
15.0
20.0
25.0
0.0
25.0
50.0
75.0
100

J17SH3

S – N

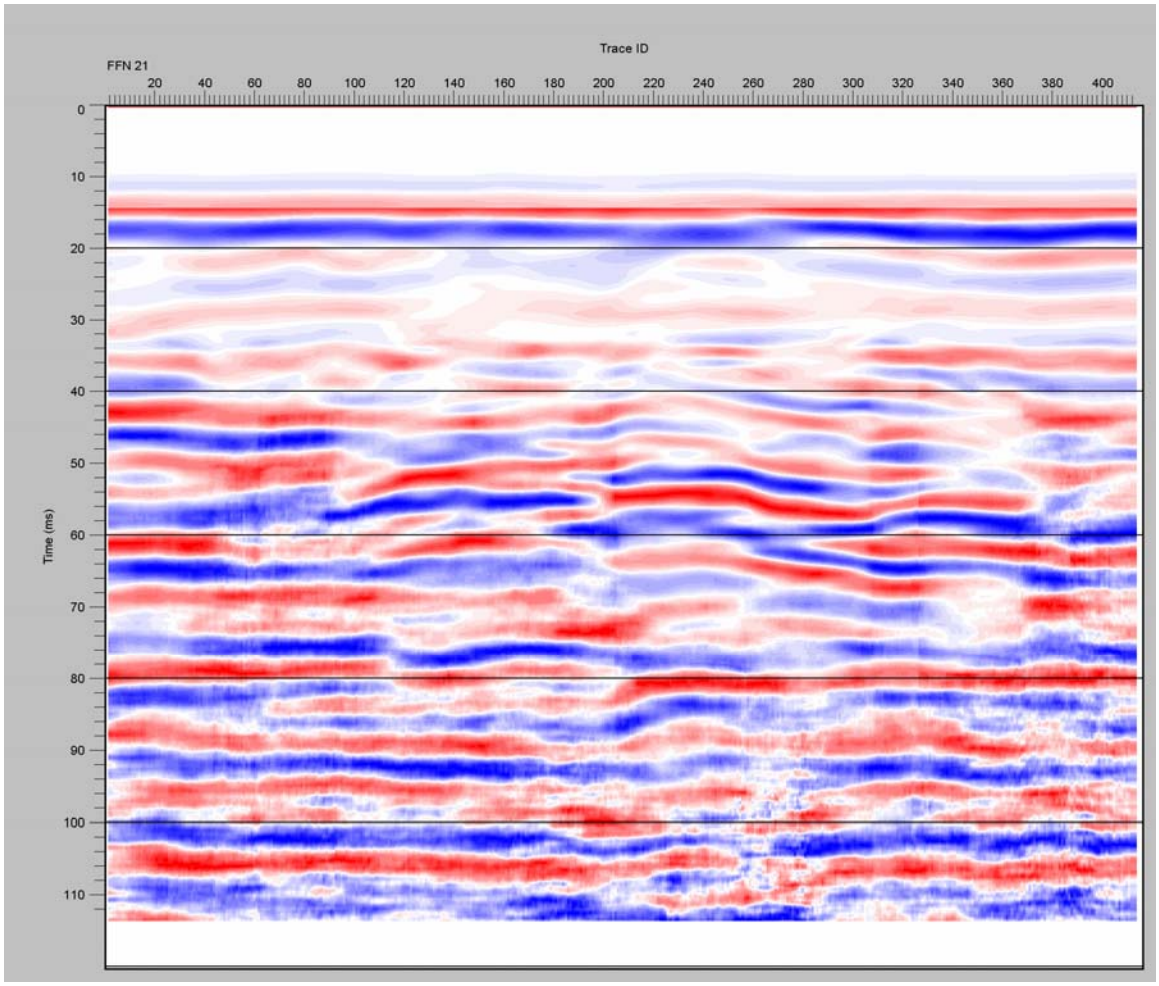
Trace ID
FFN 21
20 40 60 80 100 120 140 160 180 200 220 240 260 280 300 320 340 360 380 400
0 10 20 30 40 50 60 70 80 90 100 110
Time (ms)

NE - SW

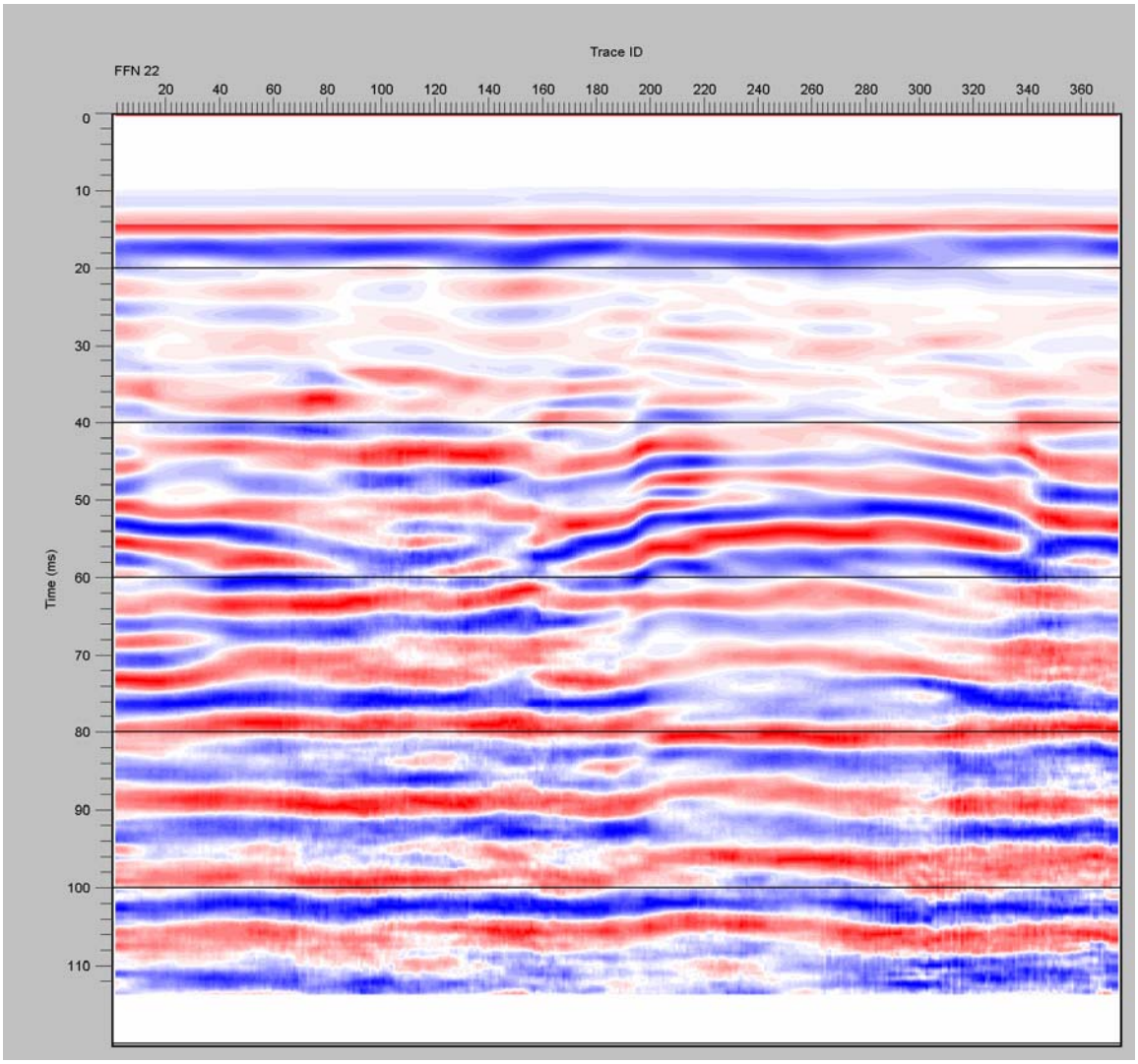
Trace ID
FFN 22
20 40 60 80 100 120 140 160 180 200 220 240 260 280 300 320 340 360
0 10 20 30 40 50 60 70 80 90 100 110
Time (ms)

J17BG3

SE - NW

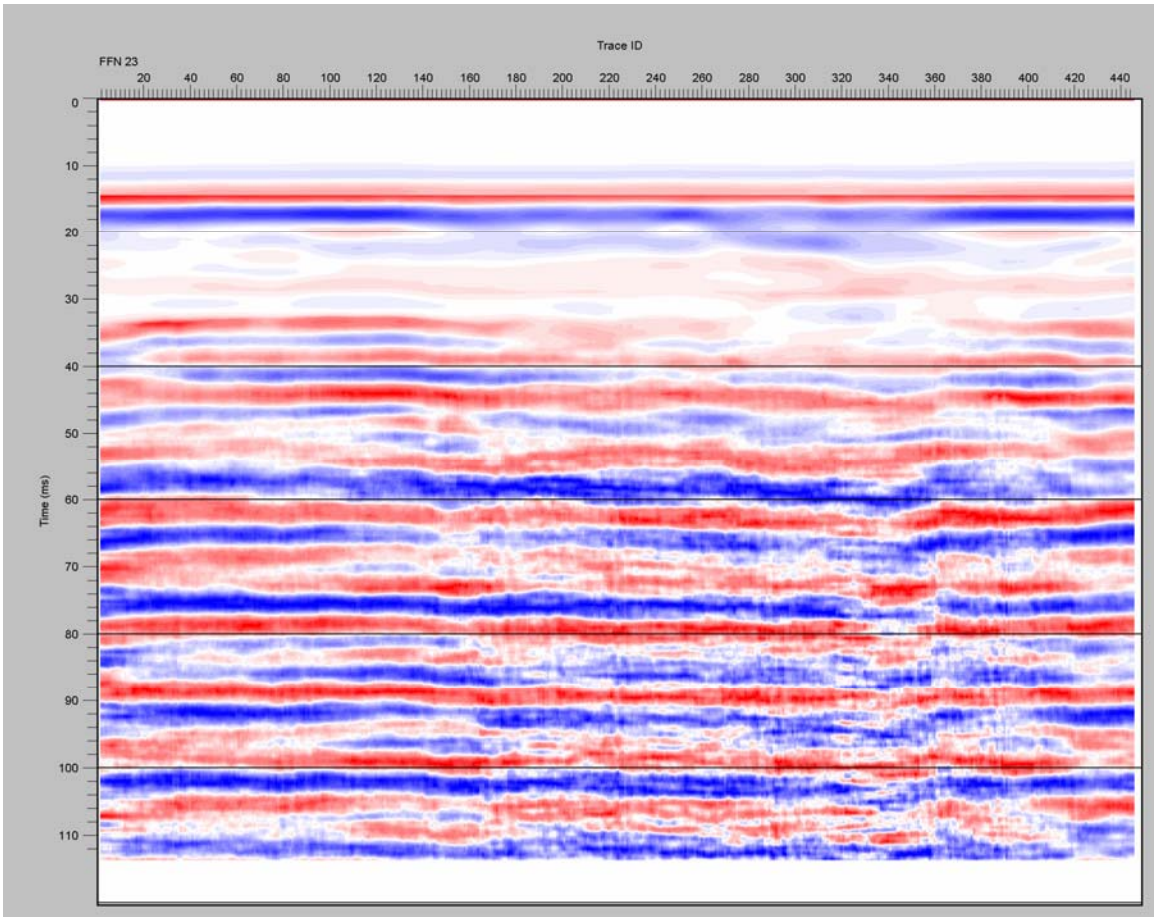
Trace ID
FFN 23
20 40 60 80 100 120 140 160 180 200 220 240 260 280 300 320 340 360 380 400 420 440
0 10 20 30 40 50 60 70 80 90 100 110
Time (ms)

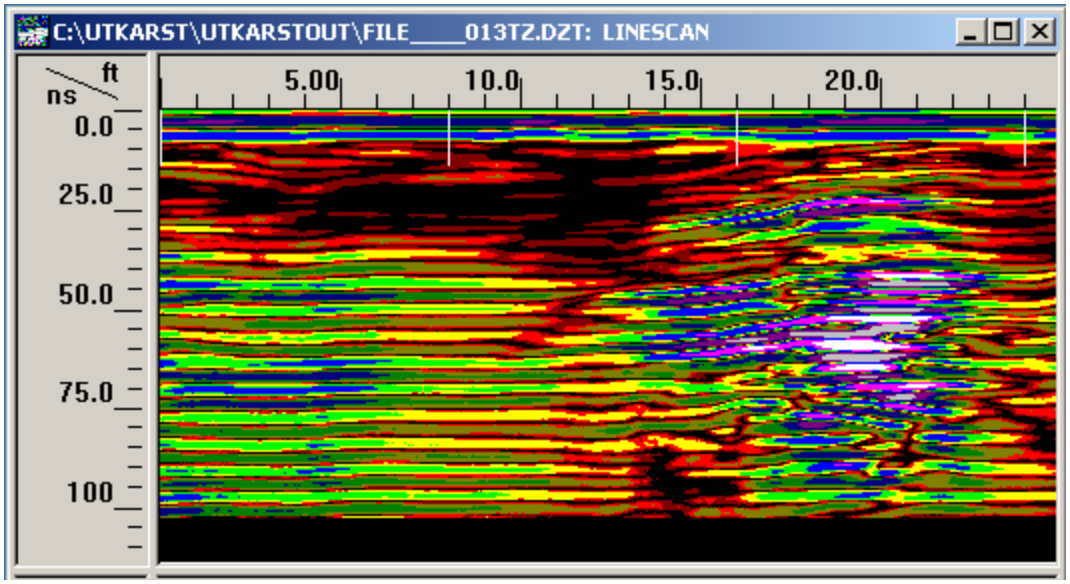
C:\UTKARST\UTKARSTOUT\FILE____013TZ.DZT: LINESCAN
ft
ns
5.00
10.0
15.0
20.0
0.0
25.0
50.0
75.0
100

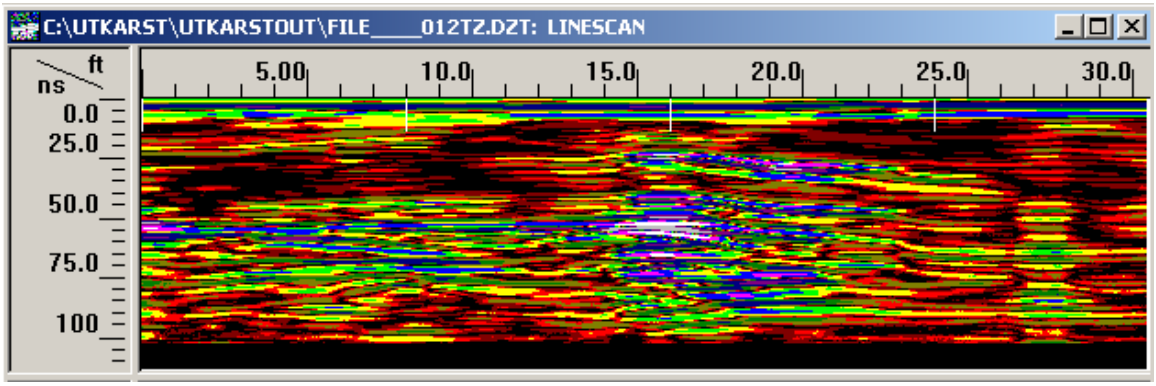
C:\UTKARST\UTKARSTOUT\FILE____012TZ.DZT: LINESCAN
ft
ns
5.00
10.0
15.0
20.0
25.0
30.0
0.0
25.0
50.0
75.0
100

References

Bakalowicz, M., 2004: The epikarst, the skin of karst. In Jones, W. K., Culver, D. C., and Herman, J. S. eds. *Epikarst*, Karst Waters Institute, Inc. Special Publication 9, Charles Town, West Virginia, p. 16-22.

Barr, G. L., 1993: Application of ground-penetrating radar methods in determining hydrogeologic conditions in a karst area, West-Central Florida. USGS Water Resources Investigations Report. 92-4141, p. 26.

Batte, C., 1984: Soil Survey of Comal and Hays Counties Texas. United States Department of Agriculture, Soil Conservation Service in Cooperation with Texas Agricultural Experiment Station, 136 p.

Benson, R. C., Yuhr, L., B., 1987: Assessment and long term monitoring of localized subsidence using ground penetrating radar. *In* Beck, B. F. and Wilson, W. L., eds., *Karst Hydrogeology: Engineering and Environmental Applications*. Proceedings of the Second Multidisciplinary Conference on Sinkholes and the Environmental Impacts of Karst. A. A. Balkema Publishers, Rotterdam, The Netherlands, 467 pp.

Chamberlain, A. T., Sellers, W., Proctor, C., Coard, R., 2000: Cave detection in limestone using ground penetrating radar. Journal of Archaeological Science, v. 27, p. 957-964.

Corbel, J., 1957: *Les karsts du Nord-Ouest de l'Europe*. Institut des Estudes Rhodaniennes de l'Universite de Lyon, 12. [1] Corbel, J., 1957: *Les karsts du Nord-Ouest de l'Europe*. Institut des Estudes Rhodaniennes de l'Universite de Lyon,12.

Collins, E. W., 1987: Characterization of fractures in limestones, northern segment of the Edwards aquifer and Balcones Fault Zone, central Texas: Gulf Coast Association of Geological Societies Transactions, v. 37, p. 43-54.

Collins, E. W., and Hovorka, S. D., 1997: Structure map of the San Antonio segment of the Edwards aquifer and Balcones Fault Zone, South-central Texas: Structural framework of a major limestone aquifer: Kinney, Uvalde, Medina, Bexar, Comal and Hays Counties: University of Texas at Austin, Bureau of Economic Geology, Miscellaneous map 38.

Collins, M. E., Crum, M., Hanninen, P., 1994: Using ground-penetrating radar to investigate subsurface karst landscape in North-Central Florida. Geoderma, v. 61, p. 1-15.

Cvijic, J., 1893: *Das Karstphanomen. In* Geog. Abhandlungen 5:225-276. Fargher, M. *trans. In* Sweeting, M. M. ed. 1981: *Karst Geomorphology*, Benchmark Papers in Geology, v. 59. Hutchinson Ross Publishing Company, Stroudsburg, Pennsylvania, 427 pp.

Dingman, L. S., 2002: *Physical Hydrology*. Prentice Hall, Upper Saddle River. New Jersey, 646 pp.

Drew, D., 1985: Karst Processes and Landforms. *In* Clayton, K. and Johnson, J. H. eds. Aspects of Geology. Macmillan Education, London, England, 63 pp.

Edwards Aquifer Authority, 2005. www.edqardsaquifer.org

Eckhardt, G., 2005: The Edwards Aquifer Homepage. http://www.edwardsaquifer.net.

Ferrell, D. A. and Morris, A. P., 2003: Dilatational normal faults: Journal of Structural geology, p. 183-196.

Field, M. S., 2002: *A Lexicon of Cave and Karst Terminology With Special Reference to Environmental Karst Hydrology*. The United States Environmental Protection Agency, Office of Research and Development, EPA/600/R-02/003, 221 pp.

Gregory, L., July 2005: personal communication.

Gregory, L., Veni, G., Shade, B., Wilcox, B., Munster, C., and Owens, K., 2005: Quantifying Recharge via Fractures in an Ashe Juniper Dominated Landscape. *In* Beck, B. F., and P. E. LaMoreaux & Associates, Inc. *eds. Sinkholes and the Engineering and Environmental Impacts of Karst*, Proceedings of the Tenth Multidisciplinary Conference: American Society of Civil Engineers, Geotechnical Special Publication No. 114, p. 216 - 223.

Halihan, Todd, Mace, R. E., Sharp, J. M, 2000, Flow in the San Antonio segment of the Edwards aquifer; matrix, fractures, or conduits?: *in* Sasowsky, I. D. and Wicks, C. M., Groundwater flow and contaminant transport in carbonate aquifers, p. 129-146.

Halihan, T., Mace, R. E., and Sharp, J. M., 2000: Flow in the San Antonio segment of the Edwards aquifer: matrix, fractures, or conduits? *in:* Sasowsky, I. D., and Wicks, C. M., eds., Groundwater Flow and Contaminant Transport in Carbonate Aquifers, A. A. Balkema, Rotterdam, p. 129-146.

Hanson, J. A., and Small, T. A., 1995: Geologic framework and hydrogeologic characteristics of the Edwards aquifer outcrop, Hays county, Texas. U.S. Geological Survey, Water-Resources Investigations Report, 95-4265, 10 p.

Hauwert, N. M., Litvak, M. E., and Sharp, J., M., 2005: Characterization and Water Balance of Internal Drainage Sinkholes. *In* Beck, B. F., and P. E. LaMoreaux & Associates, Inc. *eds.* Sinkholes and the Engineering and Environmental Impacts of Karst, Proceedings of the Tenth Multidisciplinary Conference: American Society of Civil Engineers, Geotechnical Special Publication No. 114, p.188-200.

Hill, 1901: Geography and geology of the Black and Grand Prairies of Texas. *21st Annual Report*, U.S. Geol. Survey, pt.7, 666 p.

Hovorka, S. D., Mace, R. E., and Collins, E. W., 1998: Permeability structure of the Edwards aquifer, South Texas—implications for aquifer management: The University of Texas at Austin, Bureau of Economic Geology Report of Investigations No. 250, 55 p.

Hovorka, S. D., Dutton, A. R., Ruppel, S. T., Yeh, J. S., 1996: Edwards aquifer ground-water resources: geologic controls on porosity development in platform carbonates: The University of Texas at Austin, Bureau of Economic Geology Report of Investigations No. 238, 75 p.

Jennings, J. N., 1971: *Karst*. The M.I.T. Press, Cambridge, Massachusetts.

Jennings, J. N., 1987: *Karst Geomorphology*. Basil Blackwell Ltd., New York, New York, 293 p.

Kiraly, L., 2002: Karstification and Groundwater Flow. In. Gabrovsek, F. ed. *Evolution of Karst: From Prekarst to Cessation.* Postojna-Ljubljana: Institut za raziskovanje krasa, ZRC SAZU, Zalozba ZRC, p 155-190.

Klimchouk, A., 2004: Towards defining, delimiting and classifying epikarst: it's origin, processes and variants of geomorphic evolution. In Jones, W. K., Culver, D. C., and Herman, J. S. eds. *Epikarst*, Karst Waters Institute, Inc. Special Publication 9, Charles Town, West Virginia, p. 23-35.

Klimchouk, A. and Ford, D., 2000: Types of Karst and Evolution of Hydrogeologic Setting. In Klimchouk, A. B., Ford, D. C., Palmer, A., N.,and Dreybrodt, W. eds. *Speleogenesis: Evolution of Karst Aquifers.* National Speleological Society, Inc., Huntsville, Alabama, p. 45-53.

Klimchouk, A., and Ford, D., 2000: Lithologic and Structural Controls on Cavern Development. In Klimchouk, A. B., Ford, D. C., Palmer, A., N.,and Dreybrodt, W. eds. *Speleogenesis: Evolution of Karst Aquifers.* National Speleological Society, Inc., Huntsville, Alabama, p. 54-76.

Mace, R. E., Chowdhury, A. H., Anaya, R., and Way, S. C., 2000: Groundwater availability of the Trinity Aquifer, Hill Country Area, Texas: numerical simulations through 2050. Texas Water Development Board Report 353, 117 p.

Maclay, R. W., and Small, T., A., 1976: Progress report on the Edwards aquifer, San Antonio area, Texas, and preliminary interpretation of borehole geophysical and laboratory data on carbonate rocks. U.S. Geological Survey Open-File Report 76-627, 65 p.

Natural Resources Conservation Service (NRCS), 2005: Web Soil Survey http://websoilsurvey.nrcs.usda.gov/app.

Palmer, A. N., 2002: Speleogenesis in Carbonate Rocks. In. Gabrovsek, F. ed. *Evolution of Karst: From Prekarst to Cessation.* Postojna-Ljubljana: Institut za raziskovanje krasa, ZRC SAZU, Zalozba ZRC, p 43-59.

Rettman, Paul L., 1991, Worlds largest flowing well: Twichell hydrology symposium; American Water Resources Association, Texas Section, Fort Worth, TX, p. 64.

Rose, P. R., 1972: Edwards Group, surface and subsurface, central Texas, v. 1, Stratigraphy: Austin, University of Texas, *Report of Investigations,* Bureau of Economic Geology, No. 74, 198 p.

Scanlon, B., Langford, R., and Goldsmith, R., 1999: Relationship between geomorphic settings and unsaturated flow in an arid setting. Water Resources Research, v. 35, no. 4, p983 – 999.

Sharp, J. M., Jr., 1990: Stratigraphic, geomorphic, and structural controls on the Edwards aquifer, Texas, U.S.A.: In Simpson, E. S., and Sharp, J. M., Jr. *eds*. Selected Papers on Hydrogeology, International Association of Hydrogeologists, Heise, Hannover, v. 1, p. 67-82.

Sweeting, M. M., 1972: *Karst Landforms*. The MacMillan Press, Ltd., London, England.

Small T, Hanson J, Hauwert N, 1996: Geologic framework and hydrogeologic characteristics of the Edwards aquifer outcrop (Barton springs segment), northeastern Hays and southwestern Travis counties. U.S. Geological Survey, Water-Resources Investigations Report, 96-4306, 15 p.

Taucer, P. T., Munster, C. L., Wilcox, B. P., Shade, B., Dasgupta, S., Owens, M. K., and Mohanty, B., 2005: Large plot tracing of subsurface flow in the Edwards aquifer epikarst. *In* Beck, B. F., and P. E. LaMoreaux & Associates, Inc. *eds*. Sinkholes and the Engineering and Environmental Impacts of Karst, Proceedings of the Tenth Multidisciplinary Conference: American Society of Civil Engineers, Geotechnical Special Publication No. 114, p.207-215.

Wermund, E. G., Cepeda, J. C., and Luttrell, P. E., 1978: Regional distribution of fractures in the southern Edwards Plateau and their relationship to tectonics and caves: The University of Texas at Austin, Bureau of Economic Geology Geological Circular, no. 2, 14 p.

Werchan, L., Lowther, A. and Ramsey, R., 1974: Soil Survey of Travis County Texas. United States Department of Agriculture, Soil Conservation Service in Cooperation with Texas Agricultural Experiment Station, 123 p.

White, William B., and White, Elizabeth L., 2001, Conduit fragmentation, cave patterns, and the localization of karst ground water basins: the Appalachians as a test case; Theoretical and Applied Karstology, 13-14, 9-24.

White, W. B., 1988: *Geomorphology and Hydrology of Karst Terrains*. Oxford University Press, London, England, 464 pp.

White, W. B., 2002: Karst Hydrology: recent developments and open questions. Engineering Geology, v. 65, p. 85-105.

White, W. B., 2003: Conceptual models for karst aquifers: Speleogenesis and Evolution of Karst Aquifers, 1(1), 6 p.

Williams, P. W., 2004: The epikarst: evolution of understanding. In Jones, W. K., Culver, D. C., and Herman, J. S. eds. *Epikarst*, Karst Waters Institute, Inc. Special Publication 9, Charles Town, West Virginia, p. 8-15.

Williams, P. W., 1983: The role of the subcutaneous zone in karst hydrology. Journal of Hydrogeology, v. 61, p. 45-67.

Woodruff, C. M., Jr., 1984: Water budget analysis for the area contributing recharge to the Edwards Aquifer, Barton Springs segment. *In* Woodruff, C. M., Jr. and Slade, R. M. Jr., *eds. Hydrology of the Edwards Aquifer-Barton Springs Segment*. Austin Geological Society Guidebook No. 6, Austin, Texas.

Woodruff, C. M., and Abbott, P. L., 1986: Stream piracy and evolution of the Edwards Aquifer along the Balcones Escarpment, Central Texas; in Abbot, P. L. and Woodruff, C. M., Jr. eds., The Balcones Escarpment, central Texas: Geological Society of America Annual Meeting, p 77-100.

The vita has been removed from the reformatted version of this document.